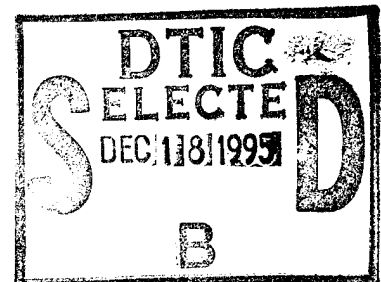PL-TR-95-2057

GLOBAL IONOSPHERIC WEATHER

Dwight T. Decker
Patricia H. Doherty

Boston College
Institute for Space Research
Chestnut Hill, MA 02167

DTIC
SELECTED
DEC 18 1995
B

28 February 1995

19951215 030
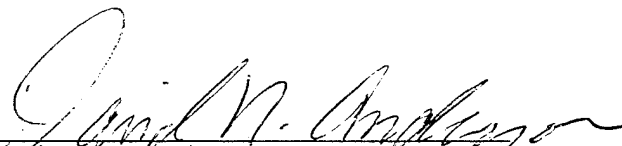
Scientific Report No. 2
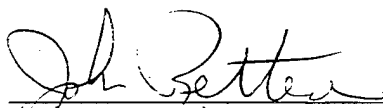
PHILLIPS LABORATORY
Directorate of Geophysics
AIR FORCE MATERIEL COMMAND
HANSCOM AIR FORCE BASE, MA 01731-3010
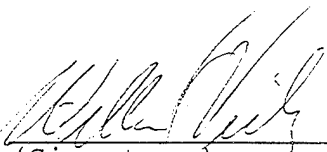
DTIC QUALITY INSPECTED

"This technical report has been reviewed and is approved for publication"

_____
(Signature)
JOHN RETTERER
Contract Manager

_____
(Signature)
DAVID ANDERSON
Branch Chief

_____
(Signature)
WILLIAM VICKERY
Division Director

This report has been reviewed by the ESC Public Affairs Office (PA) and is releasable to the National Technical Information Service (NTIS).

Qualified requestors may obtain additional copies from the Defense Technical Information Center (DTIC). All others should apply to the National Technical Information Service (NTIS).

If your address has changed, if you wish to be removed from the mailing list, of if the addressee is no longer employed by your organization, please notify PL/IM , 29 Randolph Road, Hanscom AFB, MA 01731-3010. This will assist us in maintaining a current mailing list.

Do not return copies of this report unless contractual obligations or notices on a specific document require that it be returned.

REPORT DOCUMENTATION PAGE

Form Approved
OMB No. 0704-0188

Public reporting burden for this collection of information is estimated to average 1 hour per response, including the time for reviewing instructions, searching existing data sources, gathering and maintaining the data needed, and completing and reviewing the collection of information. Send comments regarding this burden estimate or any other aspect of this collection of information, including suggestions for reducing this burden, to Washington Headquarters Services, Directorate for Information Operations and Reports, 1215 Jefferson Davis Highway, Suite 1204, Arlington, VA 22202-4302, and to the Office of Management and Budget, Paperwork Reduction Project (0704-0188), Washington, DC 20503.

1. AGENCY USE ONLY (Leave blank)	2. REPORT DATE	3. REPORT TYPE AND DATES COVERED
	28 February 1995	Scientific #2

4. TITLE AND SUBTITLE

GLOBAL IONOSPHERIC WEATHER

5. FUNDING NUMBERS

PE 63707F
PR 4643
TA GL
WU AA

Contract:
F19628-93-K-0001

6. AUTHOR(S)

Dwight T. Decker and Patricia H. Doherty

7. PERFORMING ORGANIZATION NAME(S) AND ADDRESS(ES)

Boston College
Institute for Space Research
140 Commonwealth Avenue
Chestnut Hill, MA 02167

8. PERFORMING ORGANIZATION REPORT NUMBER

9. SPONSORING/MONITORING AGENCY NAME(S) AND ADDRESS(ES)

Phillips Laboratory
29 Randolph Road
Hanscom AFB, MA 01731-3010
Contract Manager: John Retterer/GPIM

10. SPONSORING/MONITORING AGENCY REPORT NUMBER

PL-TR-95-2057

11. SUPPLEMENTARY NOTES

12a. DISTRIBUTION/AVAILABILITY STATEMENT

Approved for public release; distribution unlimited

12b. DISTRIBUTION CODE

13. ABSTRACT *(Maximum 200 words)*

In the last year, we have studied several issues that are critical for understanding ionospheric weather. Work on global F-region modeling has consisted of participation in the Phillips Laboratory Low-Latitude Ionospheric Tomography Campaign, testing of the Global Theoretical Ionospheric Model (GTIM), and testing of the Parameterized Ionospheric Model (PIM). Analysis of TEC data and comparisons with other ionospheric models have been successfully conducted and are ongoing. Analysis of GPS observations are also ongoing. Studies have been made concerning limitations in determining TEC from dual-frequency GPS measurements as well as the statistics of time rate of change of TEC. Software has been developed to process RINEX formatted GPS data into TEC. Work comparing our electron-proton-H atom model to both observations and other models has been very successful. We have also successfully modeled the creation of boundary blobs using time varying convection to first create patches in the polar cap and then to transport and distort them into boundary blobs in the auroral region.

14. SUBJECT TERMS

ionospheric weather, global F-region modeling, total electron content (TEC), GPS, tomography, aurora, electron transport, proton-H atom transport, plasma structure, blobs

15. NUMBER OF PAGES

72

16. PRICE CODE

17. SECURITY CLASSIFICATION OF REPORT	18. SECURITY CLASSIFICATION OF THIS PAGE	19. SECURITY CLASSIFICATION OF ABSTRACT	20. LIMITATION OF ABSTRACT
UNCLASSIFIED	UNCLASSIFIED	UNCLASSIFIED	SAR

NSN 7540-01-280-5500

Standard Form 298 (Rev. 2-89)
Prescribed by ANSI Std. Z39-18
298-102

TABLE OF CONTENTS

1. INTRODUCTION

The objective of this research is to improve our ability to observe and theoretically model the ionospheric "weather". In this second year, we have studied five issues where we have had the tools and experience to make significant progress. Those issues include: 1) Global F region modeling, 2) GPS observations, 3) electron backscatter, 4) proton precipitation, and 5) modeling high-latitude F-region structures.

2. GLOBAL F REGION MODELING

In this year, we participated in the Phillips Laboratory Low-Latitude Ionospheric Tomography Campaign and the initial processing of all the Total Electron Content (TEC) measurements made during the campaign. In order to develop the needed data for testing ionospheric models, we have analyzed three solar cycles of TEC data to illustrate the solar cycle dependencies of mid-latitude TEC. There was also ongoing work comparing the Global Theoretical Ionospheric Model (GTIM) to other theoretical models as part of the PRIMO (Problems Related to Ionospheric Modeling and Observations) workshop that has been held at the last four annual CEDAR meetings. A study comparing the Parameterized Ionospheric Model (PIM) to the International Reference Ionosphere Model (IRI90) at low latitudes was also performed.

2.1. 1994 South American Ionospheric Tomography Campaign

From 28 March 94 to 15 April 94, Patricia Doherty participated in a major field data collection campaign. Participation included the installation, maintenance and operation of a Magnavox MX1502 Satellite Receiver System in Bermuda for the duration of the campaign. The prime purpose of the campaign was to observe the day-to-day variability of the *equatorial anomaly* using ionospheric tomography techniques. The anomaly region, typically between ±25 degrees of the magnetic equator, is that part of the world where the highest values of electron density and TEC occur. Fluctuations in the anomaly can be very intense and can affect high-frequency radio propagation.

This experiment was successful in collecting simultaneous measurements of ionospheric Total Electron Content data from six identical satellite receiver systems from a series of stations in the American Sector. The stations included:

> Hanscom AFB, MA
> Bermuda
> Puerto Rico
> Merida, Venezuela
> La Paz, Bolivia
> Tucuman, Argentina.

The data will be used to create tomographic reconstructions of electron density and TEC over a large section of the ionosphere. In addition to providing information on the equatorial anomaly, the campaign results will be useful in validating current techniques for ionospheric tomography.

All measurements made during the campaign have now been processed. General processing of the data included combining relative TEC measurements from all stations, converting them to equivalent vertical TEC and determining absolute TEC values using a visual, multi-station software package that enables the calculation of absolute TEC. This report also includes the initial TEC results from that campaign.

1

A chain of receiving stations was set up along the ~70° West longitude meridian to measure relative TEC values from differential carrier phase on the 150 and 400 MHz carriers from the NNSS satellites. Figure 1 illustrates the locations of the stations in the receiving chain. The station at Tabatinga, Brazil was not operated due to logistical difficulties and resulted in a data gap. The data gap did not profoundly affect the measurements of equivalent vertical TEC, but severely limited two-dimensional tomographic reconstructions over locations near the geomagnetic equator.

Figure 2 shows a plot of the Kp values during the campaign period. The first few days of the campaign experienced relatively quiet geomagnetic activity. A major magnetic storm began on April 1st, and the remainder of the period of observations had at least moderate geomagnetic activity. This storm allowed the opportunity to study the behavior of storm effects on the development and strength of the equatorial anomaly. Unfortunately, some of the stations in the chain were not operational during the quiet period before the onset of the magnetic storm.

An example of equivalent vertical TEC from the full chain of six stations is shown in Figure 3. The TEC is plotted from ~50° North to 40° South, a latitude span of 90° which encompasses both sides of the equatorial anomaly region. At this longitude sector the magnetic equator is located at ~11° geographic latitude. Note in Figure 3 that the two stations from which the southern anomaly peak in equivalent vertical TEC is inferred give somewhat different TEC values, though they both show the peak at the same latitude. The reason for this difference in equivalent vertical TEC is that, in the conversion from measured slant TEC to vertical, different values are obtained from stations observing different gradients as a function of elevation angle.

Equivalent vertical TEC versus latitude for the approximate local noon period is illustrated in Figure 4 for three successive days of the campaign. Not all six of the stations were operating for these days, but the general behavior of both sides of the equatorial anomaly can be seen nevertheless in this figure. Differences in the shape of the TEC anomaly among the three days can be clearly seen in this figure. Note that there is little evidence of the northern anomaly on day 94, while there is clear evidence of it on days 95 and 96. Also, the ratio of the latitudinal TEC peaks in the southern and the northern hemispheres changes from day to day over this three day period. Finally, the slope of TEC versus latitude in the latitudes to the north of the northern hemisphere anomaly differ greatly over this three day period. Note that the middle panel, day 95, clearly has larger TEC values, and, in the northern mid-latitudes, a greater slope of TEC versus latitude, than does either day 94 or day 96. To what extent this may be due to the development of the anomaly, and its effect on TEC in the mid-latitudes will be the subject of further work using this two week campaign data set.

Examples of local nighttime values of TEC versus latitude are illustrated in Figure 5. Note that the TEC scale in this figure has a maximum value of only 10 TEC units, as opposed to the maximum of 100 TEC units illustrated in Figure 4 and 80 TEC units in Figure 3. The bottom panel of Figure 5 illustrates the latitudinal dependence of TEC on day 90 at approximately 03 hours local time, over the latitude range from -45° to 60°. This panel shows large maxima in TEC near the geographic equator and near 35° north latitude.

The middle panel of Figure 5 shows behavior of TEC for the next night, day 91, still before the onset of the magnetic storm on day 92, which shows similar behavior to the bottom panel, except for the large difference in TEC in the latitude range from 0° to +30° which is much higher in the middle panel. The top panel illustrates another pass also occurring on day 91, but less than one hour later than the pass shown in the middle panel. Note that within one hour the TEC in the near-equatorial region dropped by a large amount, and there was an increase in TEC in the latitude range near 30° - 35° north over this one hour period. Does this imply large scale transport of ionization from the equatorial region to the lower mid-latitudes during this one hour period? Without corroborating evidence of plasma motion it is difficult to determine what caused these differences in the latitudinal behavior of TEC over this one hour period.

2

FIGURE 1

FIGURE 2

4
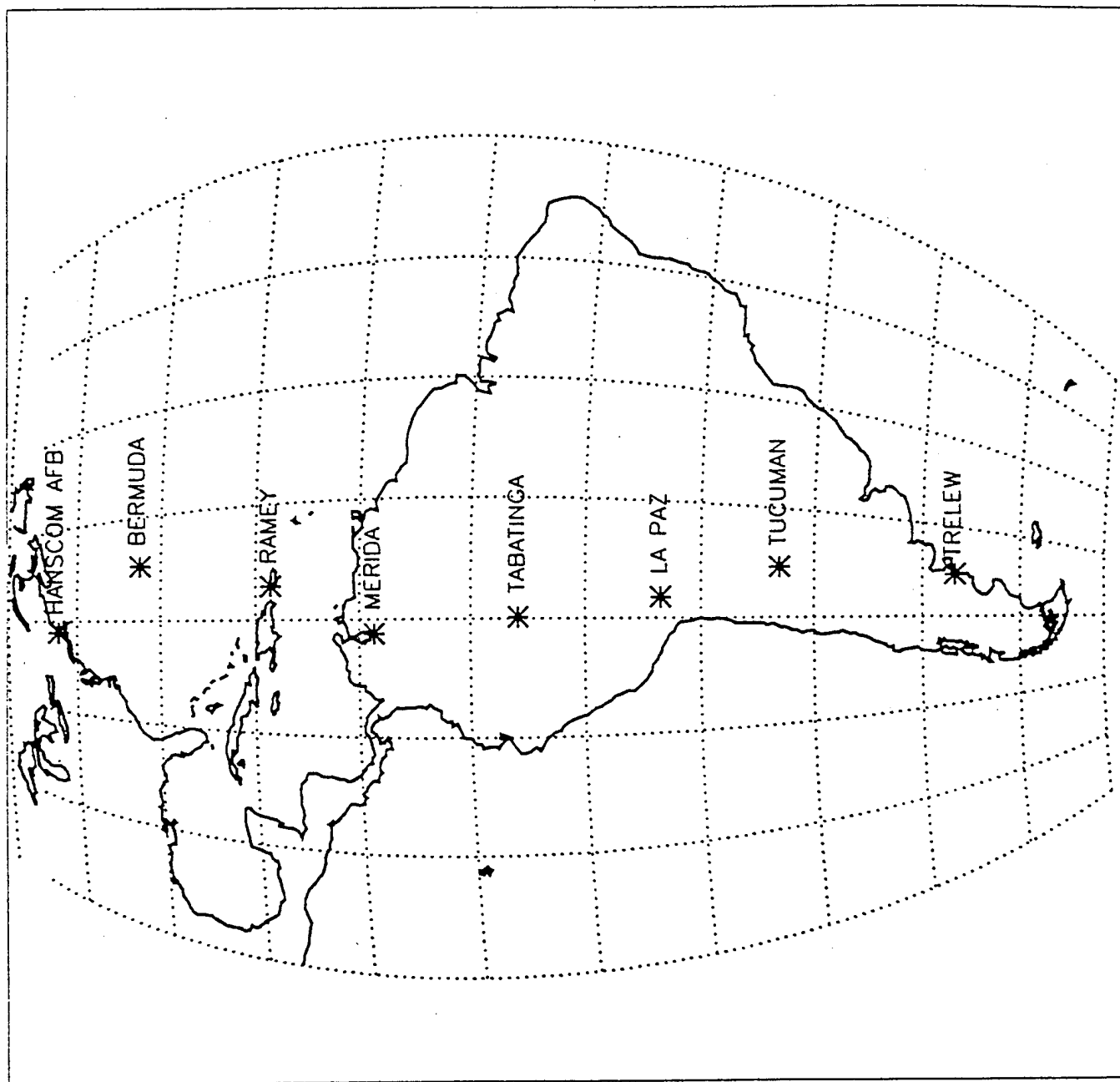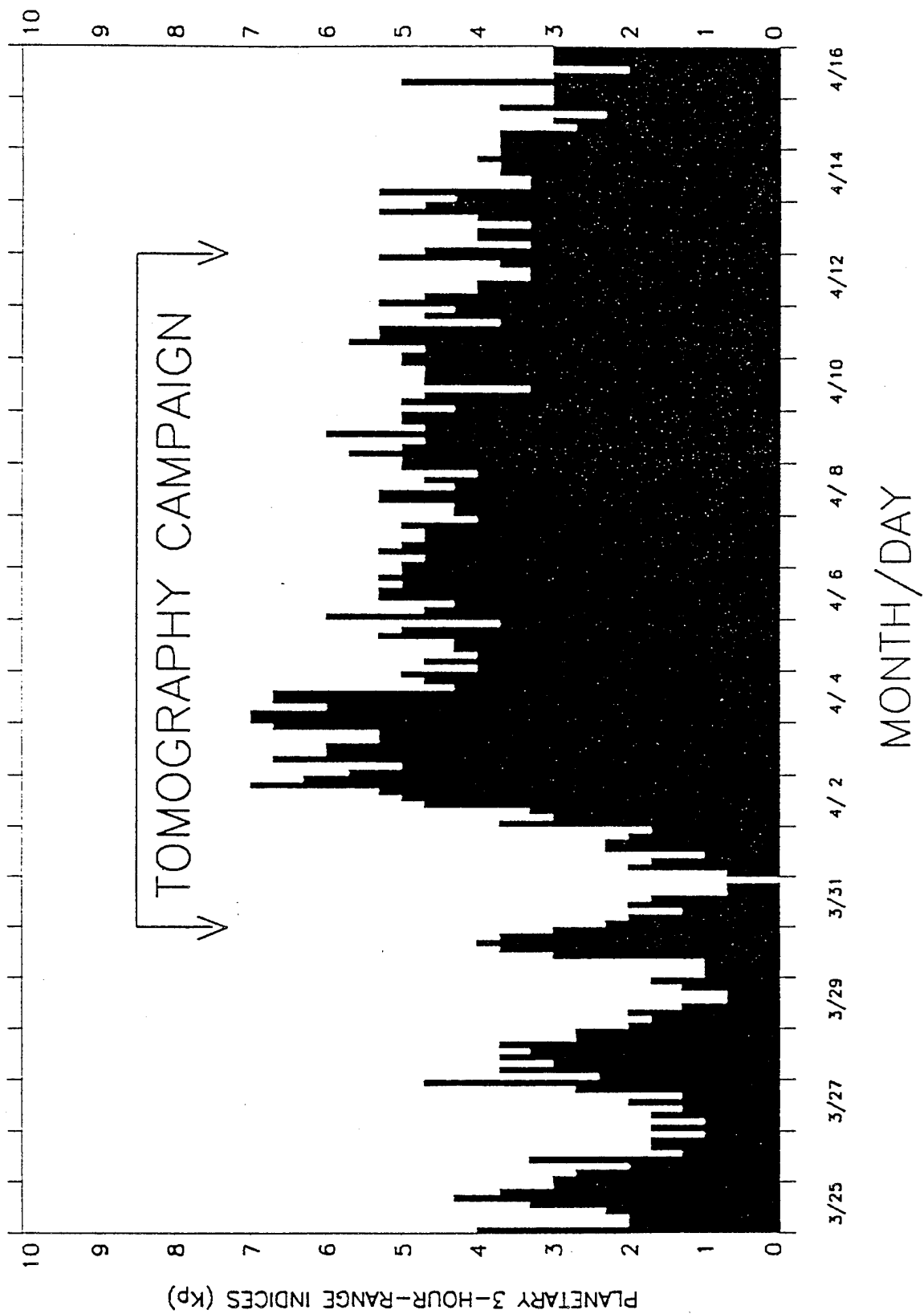
Equivalent Vertical TEC

DAY 96   1600 UT

TEC (10^16 el/sq meter)

Ionospheric Latitude (400 km)

Tucuman, Arg
La Paz, Bol
Merida, Ven
Puerto Rico
Bermuda, UK
Hanscom AFB

max elev = 82

FIGURE 3

FIGURE 4

6

Equivalent Vertical TEC

DAY 91   0840 UT

max elev = 75

Equivalent Vertical TEC

DAY 91   0740 UT

max elev = 55

Equivalent Vertical TEC

DAY 90   0740 UT

max elev = 77

Ionospheric Latitude (400 km)

TEC (10⁶ el/sq meter)

FIGURE 5

7
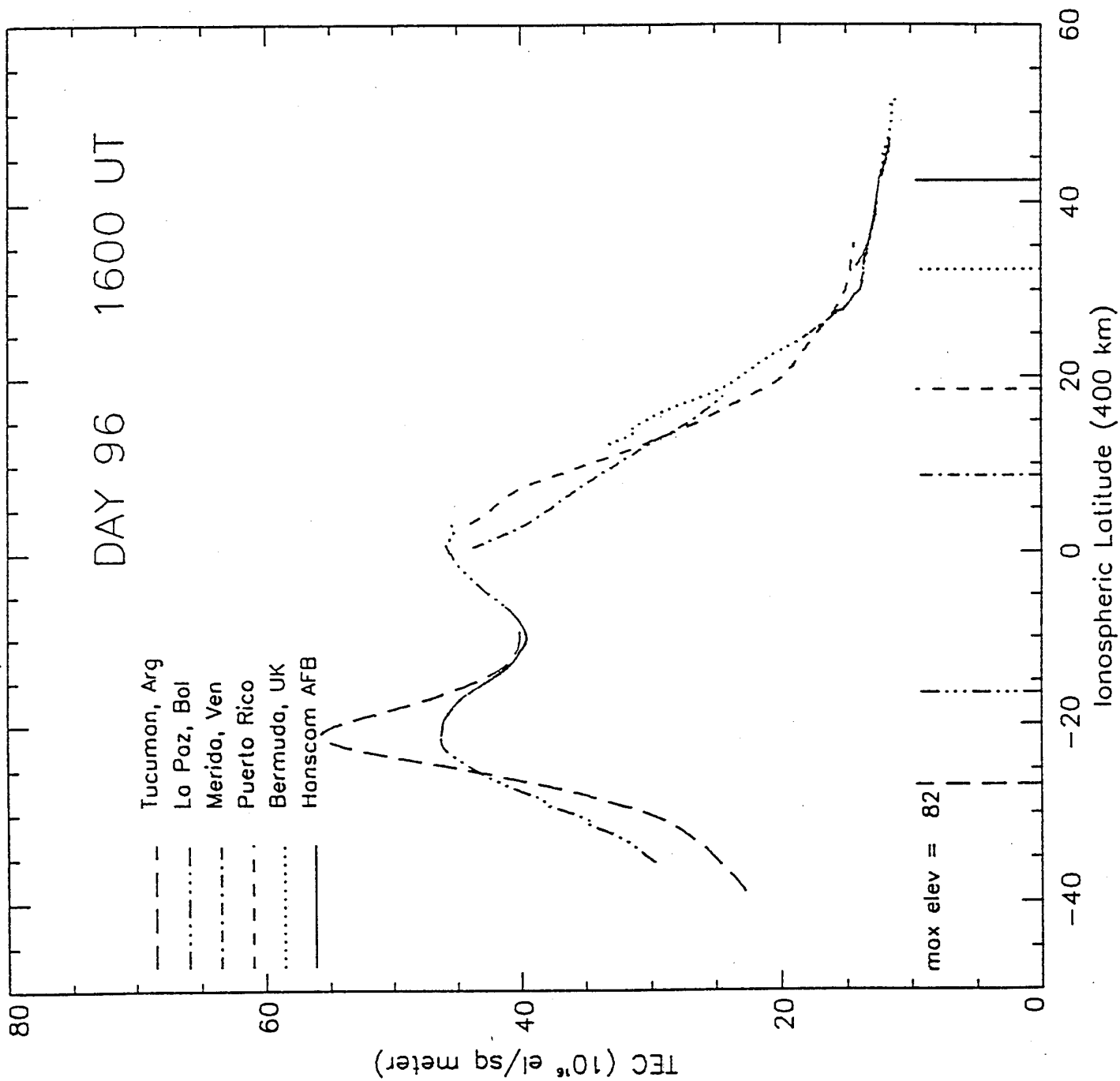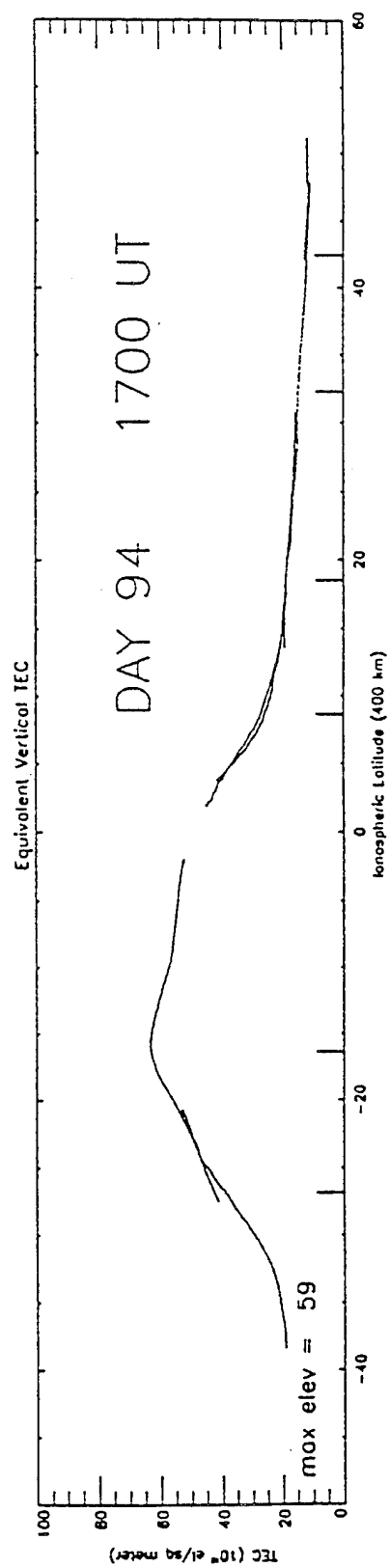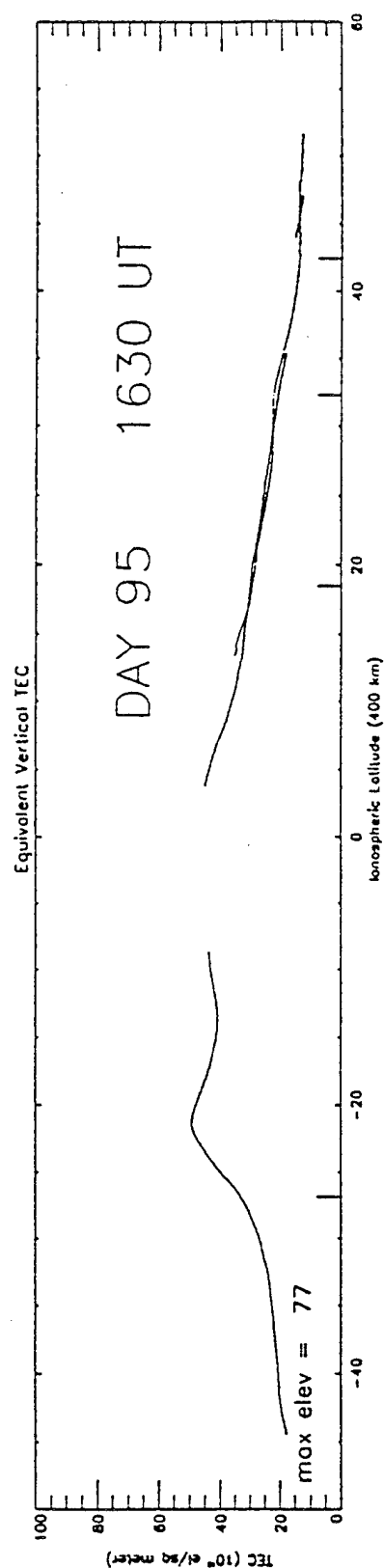
Future work with this data set includes the reconstruction of electron density profiles using tomographic reconstruction techniques, and then, comparisons of these reconstructions with theoretical models of the low latitude ionosphere models. The initial results show that the day-to-day variability of the ionosphere can be measured by the ionospheric tomography technique.

2.2. Solar Cycle Dependencies in Mid-Latitude Total Electron Content

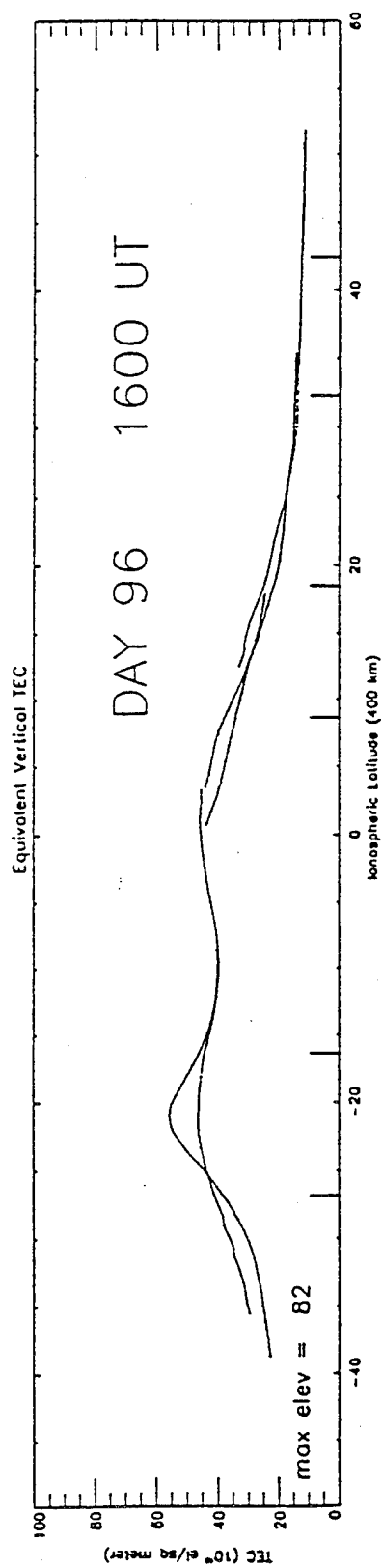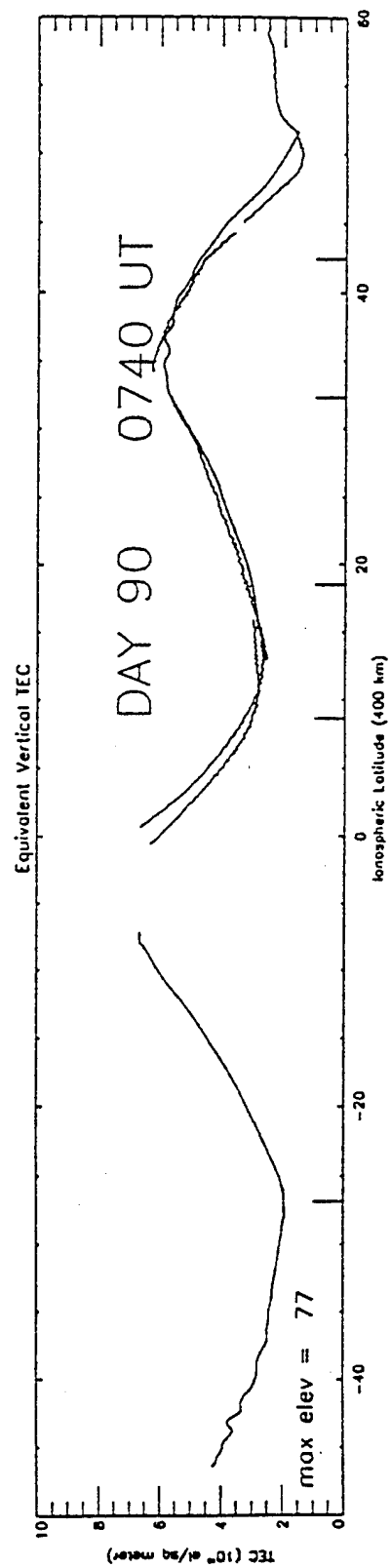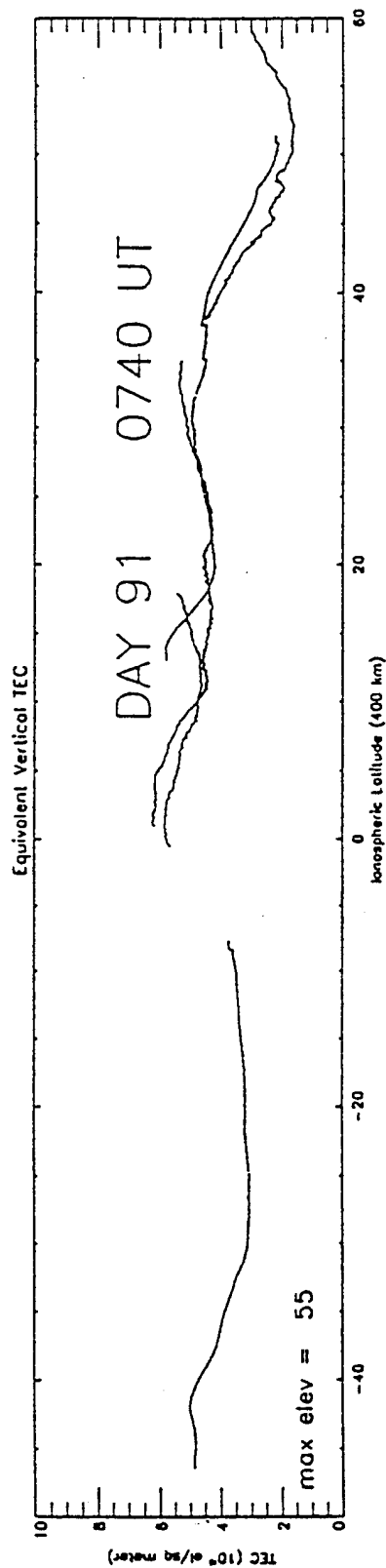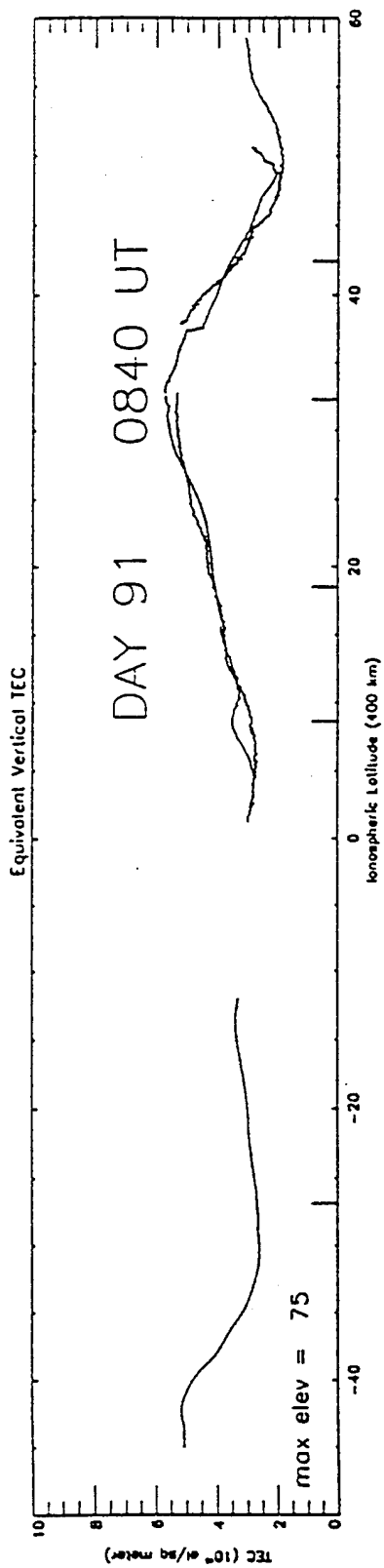Total Electron Content data recorded at Hamilton, MA over the last three solar cycles has been analyzed to illustrate short and long term effects of solar activity.

Variations in TEC are essentially controlled by the F2 region of the ionosphere, where electron densities and scale heights are the highest. The primary source of energy in the F region is the solar extreme ultraviolet (EUV) flux with wavelengths less than 1026 Angstroms. Solar EUV irradiances in this range are difficult to measure because they are absorbed in the earth's atmosphere. Since reliable time series of EUV are not available, researchers have traditionally relied upon the extensive, ground based series of 10.7 cm solar radio flux (F10.7) measurements as an index of solar activity.

### Short Term Response to Solar Activity

The short term fluctuations seen in solar flux are caused by the approximate 27 day rotation period of the sun. Figure 6 is a sample of an attempt to determine how well the short term fluctuations in solar flux correlate with short term changes in TEC. In this figure, TEC vs. F10.7 is plotted with values of the correlation coefficient, the 95% confidence interval and the number of days used in the calculations printed at the top. All days with AP values greater than 25 were not used so that only geomagnetically quiet days were used in the calculations. The correlations are irregular with some months showing a fair amount of positive correlation and other months showing poor or negative correlations. Results of this study using 5 day running means of the solar flux did not significantly improve the statistics. Similar figures have been generated for seven locations during 1981 and 1986. In general, the results were inconsistent indicating that short term changes in TEC are not reflective of short term fluctuations in F10.7.

Long Term Response to Solar Activity

Prior studies have shown that TEC increases with long term solar activity and their variations are fairly well correlated with variations in F10.7. These studies were limited to periods during solar cycle 20, a relatively low solar cycle as compared with solar cycles 21 and 22.

Recent research has shown surprising evidence that TEC saturates at extremely high levels of F10.7 [Balan et al., 1993, 1994]. This research infers that the saturation in TEC is related to a similar saturation between F10.7 and solar EUV irradiances during intense solar cycles.

Figure 7 summarizes our effort to support or dispel the existence of saturation at high levels of 10.7 cm flux. In this plot, the entire Hamilton TEC data base covering almost three solar cycles was used with the exception of days affected by geomagnetic storm activity. Sudden commencement storms cause an enhancement in daytime TEC that lasts for several hours. This enhancement is often followed by depletions in both daytime and nighttime TEC that may last for one or two days. In order to eliminate all storm effects from this study, we have excluded disturbed days (when Ap > 10) and the day that follows a disturbed day. For the remaining quiet time data, daily averages of TEC between 11 and 17 hours local time were calculated. The results are plotted versus daily F10.7 for each of the three seasons, winter (November through February), summer (May through August) and the combined equinoxes (March, April, September and October). This figure clearly illustrates the long term linear relationship between TEC and solar

8
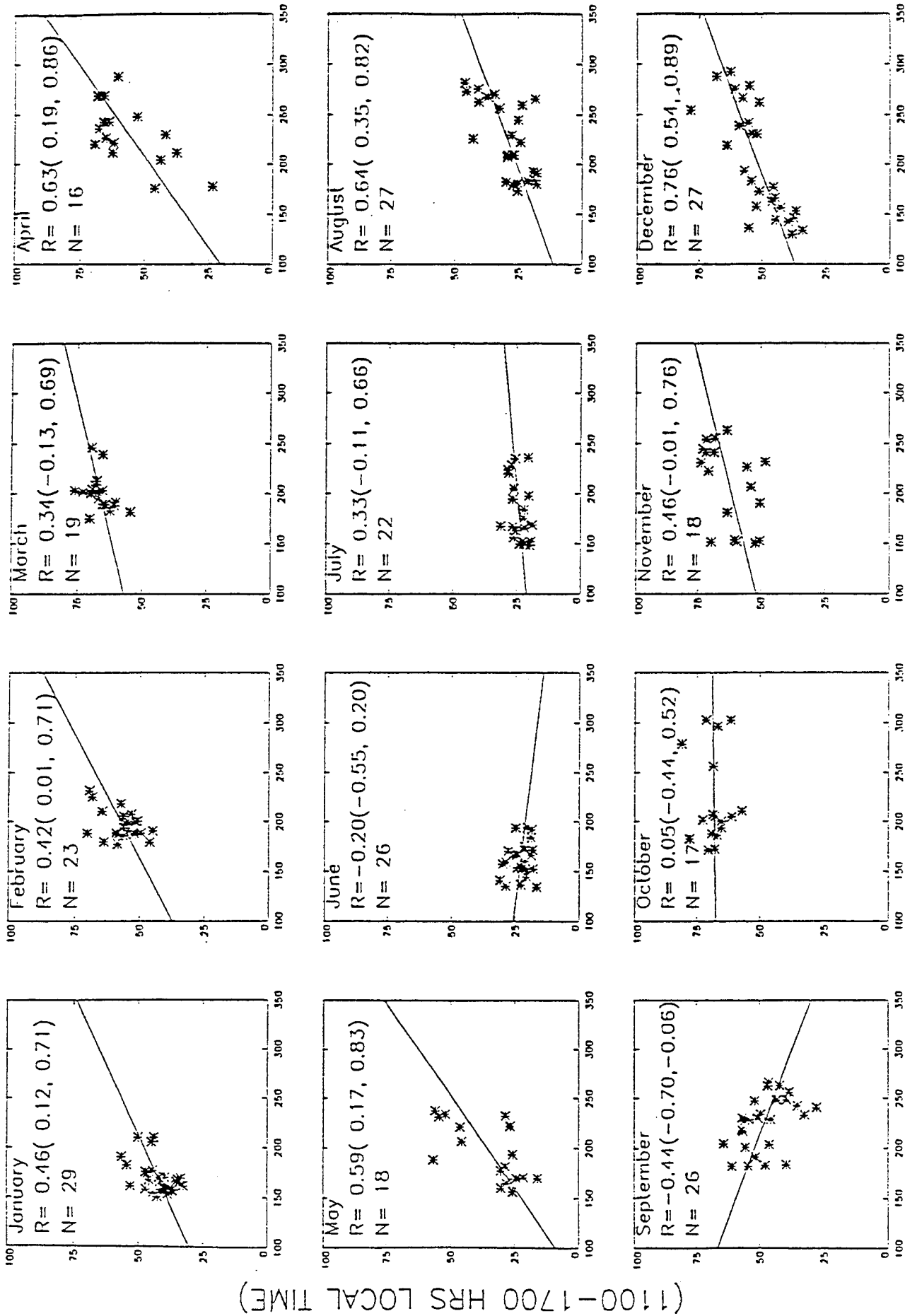
MEAN DAILY OBSERVED SOLAR FLUX

1981 HAMILTON, MA (DAYS WITH AP>25 EXCLUDED)

FIGURE 6

MEAN TEC(10**16 EL/M**2)
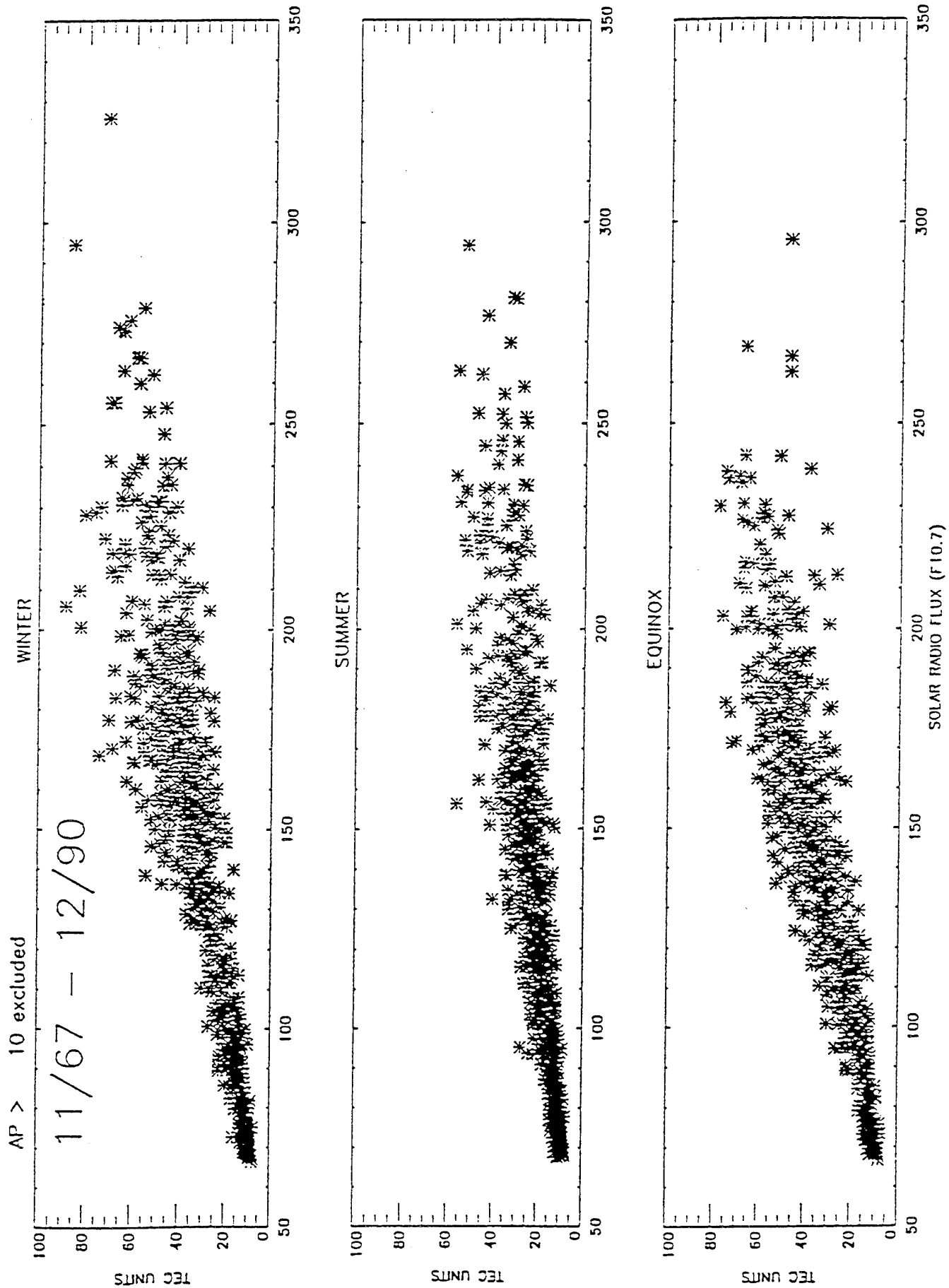(1100-1700 HRS LOCAL TIME)

9

FIGURE 7

radio flux. Although there is a greater amount of scatter in TEC with increasing values of solar flux, strong signs of saturation are not apparent. In particular, winter and summer show no clear signs of saturation. Equinox displays subtle saturation effects when F10.7 values exceed 200. On further investigation of the equinox data, it was found that the deviant points at F10.7 values greater that 200 are attributed to sets of consecutive days in early September 1980 and 1981. Early September is a period of transition from summer to equinox and this could account for the low measured values of TEC. It is important to note that all variations in TEC cannot be attributed to solar irradiance. Neutral winds, drifts, temperature and chemical composition also contribute to TEC variations.

Since all solar cycles exhibit different behavior, Figures 8 and 9 are included to observe possible saturation during separate solar cycles. Figure 8 includes data collected during solar cycle 21, June 1976 through September 1986, a period characterized by very high values of 10.7 cm flux. During the winter and summer, saturation effects are definitely not observed. Equinox shows some hint of saturation at high levels of solar flux. The work presented by *Balan et al.* [1993, 1994] focused on the second half of this solar cycle period and included the days following a geomagnetically disturbed day. Using his technique, we were able to reproduce his results at Hamilton and Palehua, Hawaii. Figure 3, however, illustrates that the saturation effect apparent in his work, becomes less apparent when data from the entire solar cycle is included and when days following magnetically disturbed days are excluded. Figure 9 includes data collected during the increasing and maximum phases of solar cycle 22, October 1986 through December 1990. This was a period of similarly high solar flux levels as solar cycle 21. The results again show no signs of saturation during winter and summer. The equinox period also appears to show no signs of saturation as was hinted in the solar cycle 21 data.

The results of this investigation are puzzling. There is certainly more scatter in daytime TEC at high levels of F10.7, but the existence of saturation over three solar cycles is just not apparent at this mid-latitude location. Although the equinox season shows subtle hints of saturation during solar cycle 21, the source of this effect is questionable. The equinox results could be exhibiting a TEC seasonal effect by showing the highest degree of day to day variability.

2.3. Theoretical Model Comparison at Mid-Latitudes

As part of our effort in global modeling, we have participated in the PRIMO workshops that have been held at the last four annual CEDAR meetings. One outcome of those meetings is that the five modeling groups involved are now working on a paper on the "Intercomparison of Physical Models and Observations of the Ionosphere". For that paper, we are performing a more detailed assessment of the differences between the models than has been done previously. In Scientific Report No. 1 [*Decker et al.*, 1994], we described the initial comparisons between our global theoretical ionospheric model (GTIM) and the Utah State University's time dependent ionospheric model (TDIM). Over the last year, we began comparisons between GTIM and the Space Environment Lab's coupled thermosphere/ionosphere model (CTIM).

As is evident from its name, CTIM couples the neutral and ionized atmospheres and hence calculates ion densities as well as neutral densities, temperatures and winds. In contrast, GTIM calculates ion densities, but the neutral quantities have to be supplied as inputs. Typically those inputs come from empirical models such as MSIS-86 and HWM-87. As a first step in our study, we compared a standard GTIM run to both a CTIM run and observations. In Figures 10 and 11 we show standard runs for 22 December 1990 compared to the median for the month at Millstone. The solid curve is the data, GTIM results are the long dashed curve, and CTIM results are the short dashed curve. Figure 10 shows the density of the peak of the F2 region (NmF2) and Figure 11 shows the altitude of the F2 peak (HmF2). The agreement between models and between models and observations is fairly typical of what we have seen in earlier work.
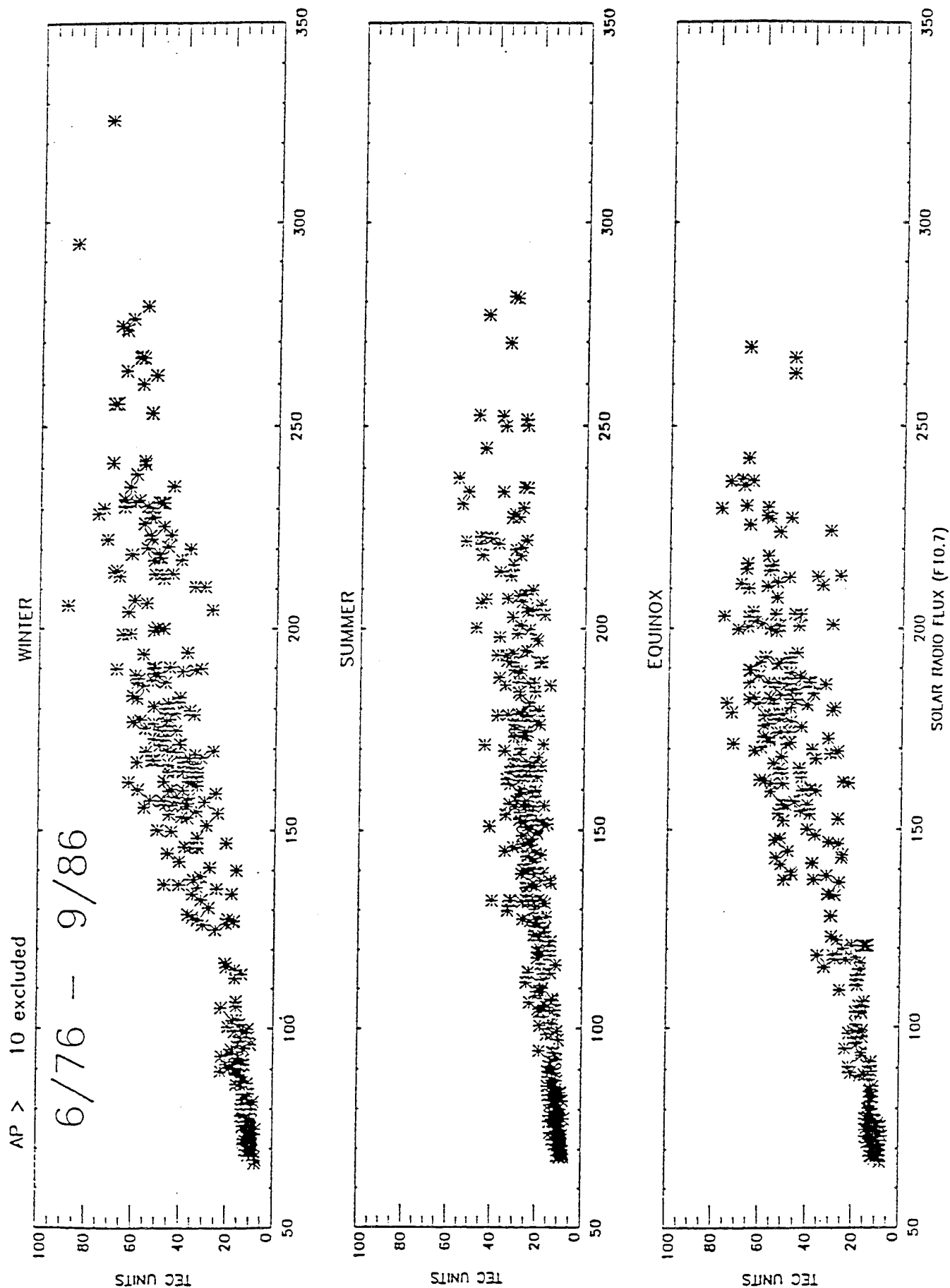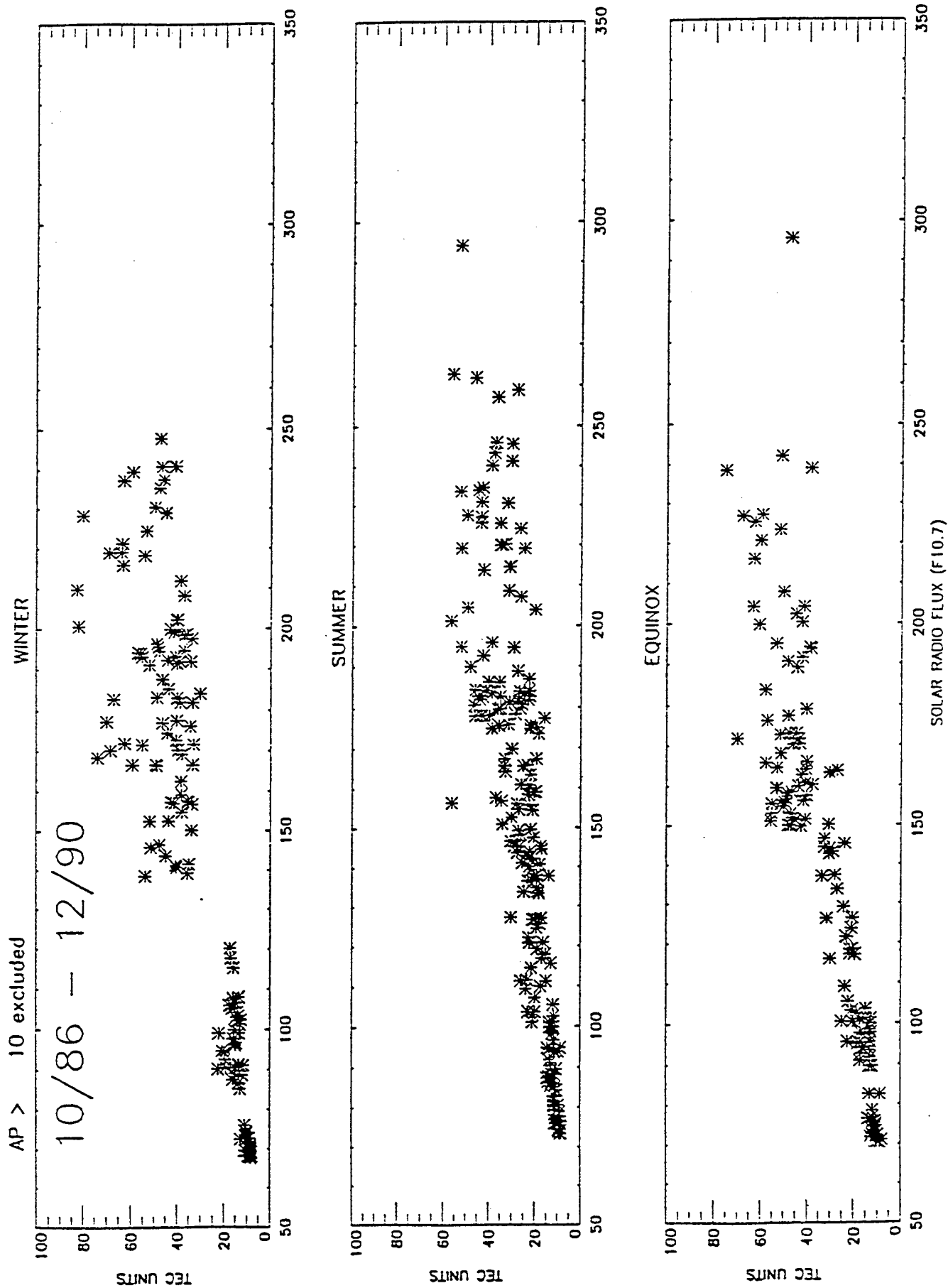
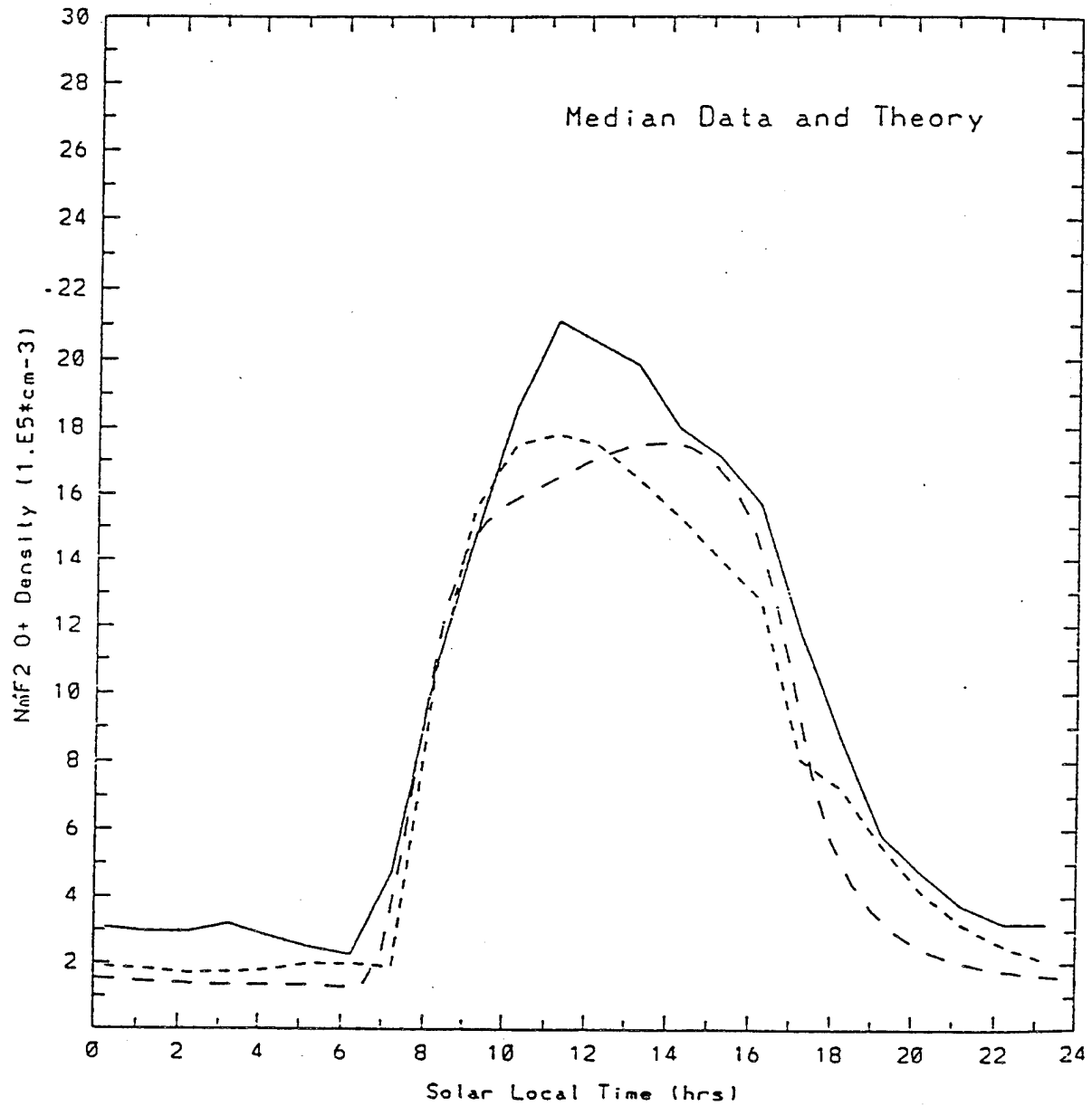FIGURE 8

12

FIGURE 9

13

MILLSTONE December 22 1990

FIGURE 10
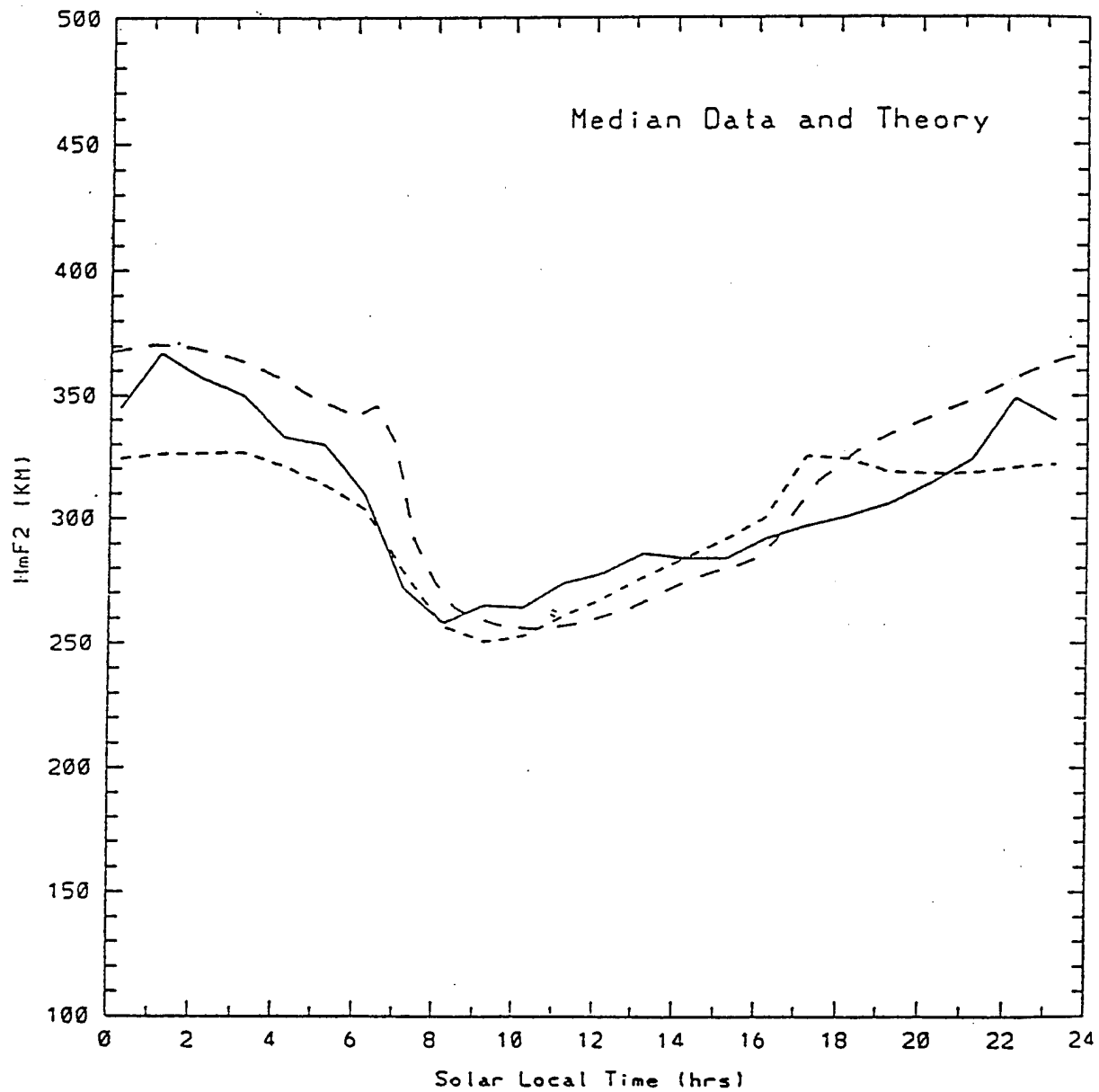
MILLSTONE   December 22 1990

Median Data and Theory

FIGURE 11

In order to make a more precise comparison between the ionospheric calculations of the two models, it is necessary to use the neutral quantities calculated by CTIM as the neutral inputs to GTIM. When we examine the neutral winds, densities, and temperatures calculated by CTIM, we find the winds weaker, the densities lower, and the temperatures cooler than the empirical models used by GTIM. In Figures 12 and 13 we present the results of using the CTIM quantities as the inputs for GTIM. The solid curve gives the CTIM F2 peak results and the dashed curves are the various GTIM results. The longest dashed curve is the standard GTIM calculation where the neutral densities, temperatures, and winds come from empirical models. The curve of shortest dashes is the GTIM results where all the neutral quantities come from CTIM. The intermediate dashed curve is the GTIM calculation that used CTIM neutral winds but MSIS86 neutral densities and temperatures. We see that using the CTIM winds enhances the NmF2 in the afternoon leading to poorer agreement between GTIM and CTIM. However using all the CTIM neutral quantities brings the models back into much better agreement.

While using all the CTIM neutral quantities as inputs for GTIM leads to better agreement, differences do remain between the models especially in the afternoon and early evening. Calculations performed using non-zero fluxes at the top boundary indicate that GTIM F2 peak results are sensitive to this boundary condition. Thus we should use boundary fluxes that are consistent with what is occurring within CTIM. Also, if H^+ is important at the top altitude then either the boundary in GTIM should be lowered or the GTIM boundary flux should include the H^+ flux as well as the O^+ flux. We plan to modify GTIM to accept a time-dependent boundary condition at the top altitude and we hope to obtain the CTIM O^+ and H^+ fluxes as a function of time and altitude for use as the GTIM boundary condition.

2.4. Low Latitude F Region Models

The International Reference Ionosphere Model (IRI90) is a global, climatological model which specifies ionospheric electron density profiles above 80 km representing monthly or "average" electron densities based on past ground-based, rocket and satellite observations. The model, therefore, is only as good as the observed database which was used. Because most of the data was obtained from ground based ionospheric sounders, there is a lack of observations from the low latitude region, from the high latitudes/polar cap and none from the ocean areas. Since most of the database comes from midlatitude stations, IRI90 does an excellent job of specifying this region, climatologically.

There is considerable evidence from past comparisons with both data and theoretical modeling results, that the low latitude portion of IRI90 is not very realistic in specifying the main ionospheric features. First, the observed daytime profile shape in the equatorial region is very broad, with daytime-solar maximum electron densities above 1×10^6 el/cm^3 at 700 km. This broad profile shape is represented in the theoretically-generated model but not in the IRI90 profiles. Figures 14 and 15 illustrate this point.

Secondly, after sunset during solar maximum periods, an enhancement in upward **ExB** drift lifts the F region to altitudes typically above 600 km. These high hmf2 values are observed in the American and Pacific sectors using the Jicamarca and Kwajalein incoherent scatter radars, respectively and are produced theoretically when such drifts are used as inputs to low latitude simulations. This point is also illustrated in Figures 14 and 15.

In IRI90, the F layer peak parameter Nmax and hmf2 are obtained from either of two sets of coefficients, the CCIR or the URSI data base. At low latitudes, these two coefficient data sets are very similar. The bottomside profile shape is determined analytically based on a series of "Lay" functions [*Bilitza and Rawer*, 1990], while the topside shape is determined from *Llewellyn and*

16

MILLSTONE December 22 1990

GTIM and CTIM

FIGURE 12

17

MILLSTONE December 22 1990

GTIM and CTIM

FIGURE 13

18

Comparison of the Measured Profiles and the IRI90 Profiles for (a) 1200 and (b) 1900 LT.
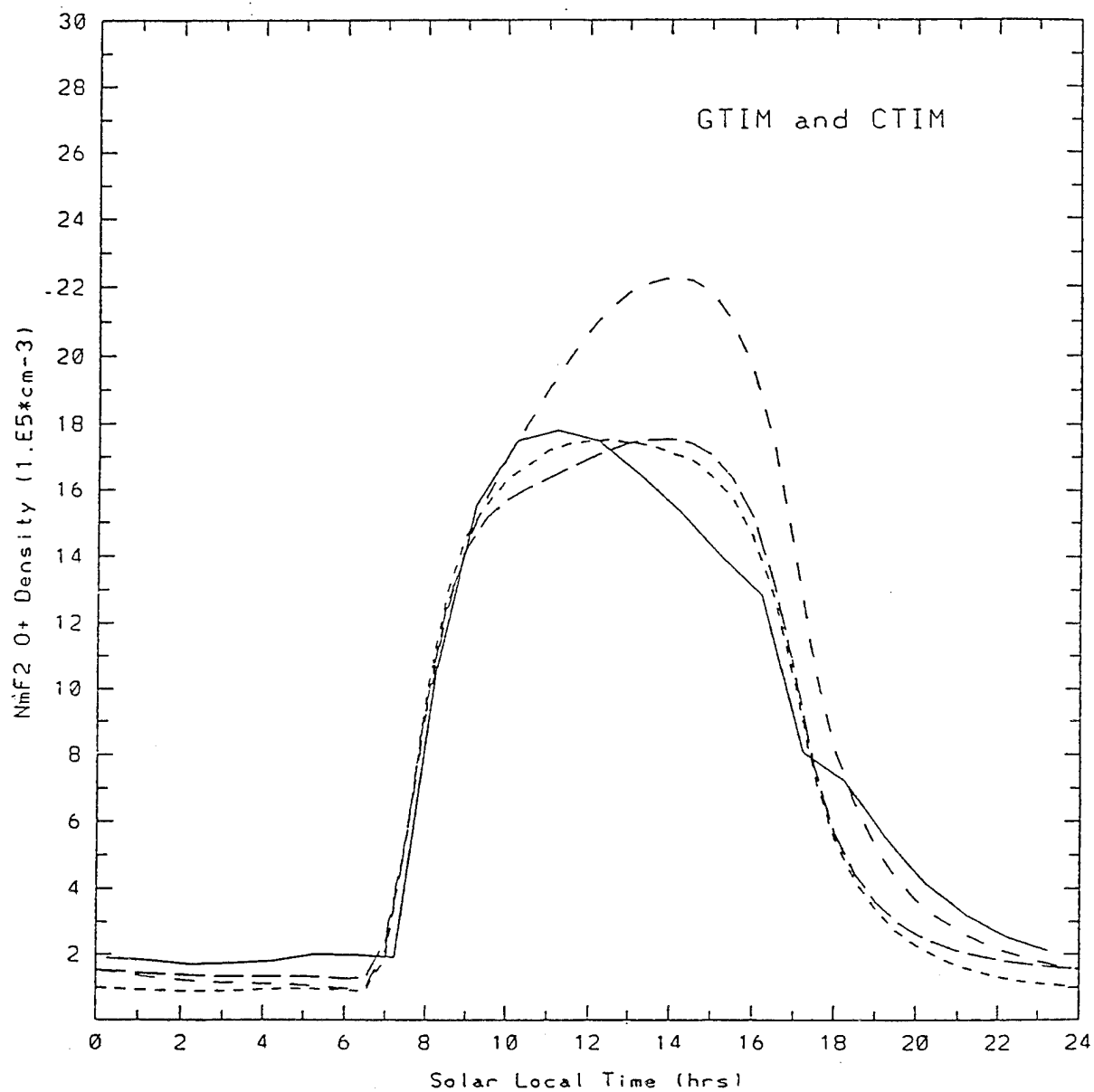
FIGURE 14

Jicamarca   October 1-2, 1970
Model Flux 130, Varied Drifts

1200 LT

△ Observed Drift
○ 1.5°Observed Drift
+ Zero Drift

(a)

1900 LT

(b)

Density (cm^{-3})

Altitude (Km)

20

Comparisons of Measured and Calculated Profiles for (a) 1200 and (b) 1900 LT Showing the Vertical Drift Effects on the Density Profiles.

FIGURE 15

Bent [1973]. We are studying an improvement to IRI90 where a data-set of peak parameters Nmax and hmf2 and profile shapes would be derived from theoretically generated electron density profiles rather than observed density profiles.

Recently, a computationally fast Parameterized Ionospheric Model (PIM) was developed at the Phillips Laboratory Geophysics Directorate as part of a global, real-time ionospheric specification model soon-to-be operational at the Air Force Space Forecast Center in Colorado Springs. PIM is based on many runs of the Global Theoretical Ionospheric Model (GTIM), which calculates electron density profiles as a function of latitude and local time. GTIM solves the coupled continuity and momentum equations for O^+ ions and therefore theoretically models the ionospheric F region. At low latitudes GTIM was run under three solar cycle conditions (low, middle, and high F10.7 cm flux values) and three seasons (fall/spring equinox, summer and winter solstice periods) for four longitude sectors (American, Brazilian, Europe/Indian, and Pacific). Electron density profiles every 2° latitude and every hour local time were parameterized by 9 Empirical Orthonormal Functions (EOFs). At low and mid latitudes these EOFs were analytically fit in latitude and kept in tabular form over the 24 hour period. These tables and functions comprise PIM and reproduce very accurately the electron density profiles generated by GTIM.

A series of comparisons have been performed and are summarized in the following figures. In Figure 14, we present an example of an electron density pro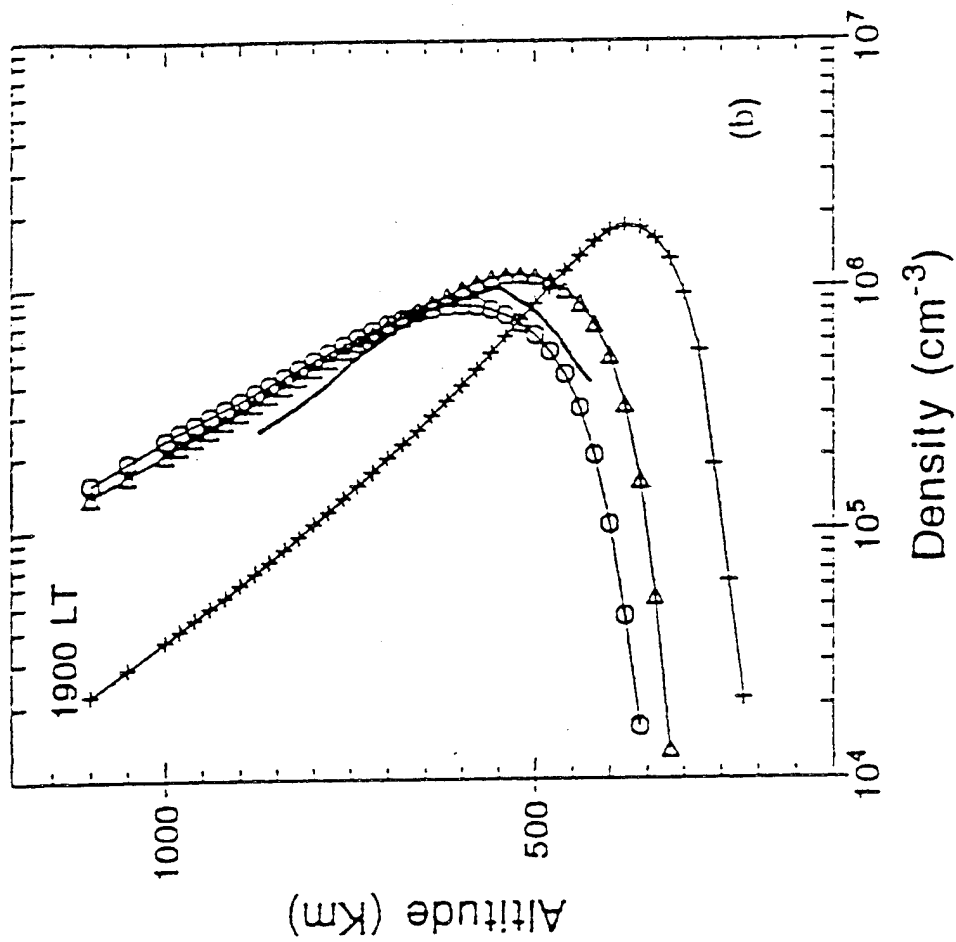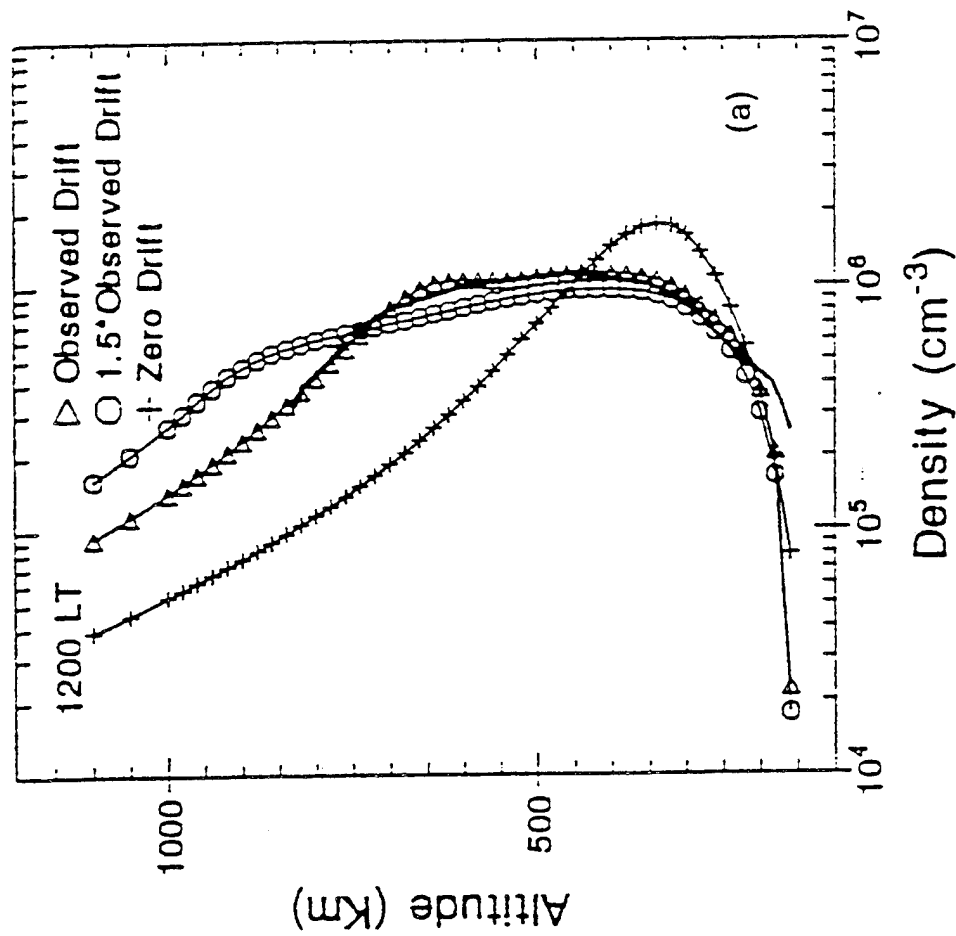file observed by the Jicamarca incoherent radar. Also included in the plot are IRI90 profiles. At 1200 local time the observed profile has a broad shape which is not reproduced by IRI90. At 1900 local time the observed layer has lifted but IRI90 has not. Figure 15 illustrates how a profile produced by GTIM can produce the shape and height of the observed F layer. Also included are calculations using drifts different from what was observed. This illustrates the critical role played by the drifts in determining the height and shape of the F layer. Figure 16 gives average profiles based on several years of Jicamarca data. The point is to illustrate that the broad shape of the daytime profiles and the post sunset lifting of the layer is not a rare event. Rather, it occurs regularly and is seen in averaged data. Figure 17 is the same as Figure 16 except for solar maximum conditions. In Figure 18, we show electron density profiles as observed at Kwajalein by incoherent radar. Here we simply want to illustrate that the low latitude features seen in the American sector are also seen in another longitude sector, the Pacific.

In Figure 19, we directly compare PIM and IRI profiles at 1700 UT in the Jicamarca longitude meridian. The local time is around 1200 and we see that PIM produces a much thicker F layer than does IRI90. The most dramatic differences are seen within about 10 degrees of the magnetic equator. In Figure 20, it is hmf2 that is compared over the entire globe at 0 UT and we see that largest differences between PIM and IRI90 are confined to the post sunset period near the magnetic equator. In Figure 21, it is the topside half thicknesses that are compared and here a sizable difference is seen near the magnetic equator but extended over 180° in longitude. This also points out how the differences in thickness are not confined to just one longitude sector. In Figure 19, a clear difference in layer thickness was seen in the American sector at 1700 UT. At 1200 UT, this difference is seen in the Europe/Indian sector.

At present, there are clear shortcomings in IRI90's description of the low latitude ionosphere. On the other hand, PIM contains many of the features that are not reproduced by IRI90. The present version of IRI90 is designed to accept Nmf2 and hmf2 from outside sources. Thus it would be straightforward to develop a PIM option for these parameters in IRI90. Similarly, an external bottomside half thickness could easily be incorporated into IRI90 given the manner in which IRI90 presently defines its bottomside F region. Unfortunately, the parameter which is most in need of modification is the topside half thickness. Here there is not a trivial way of incorporating a thickness from another source such as PIM into the present IRI. What will be needed will be either
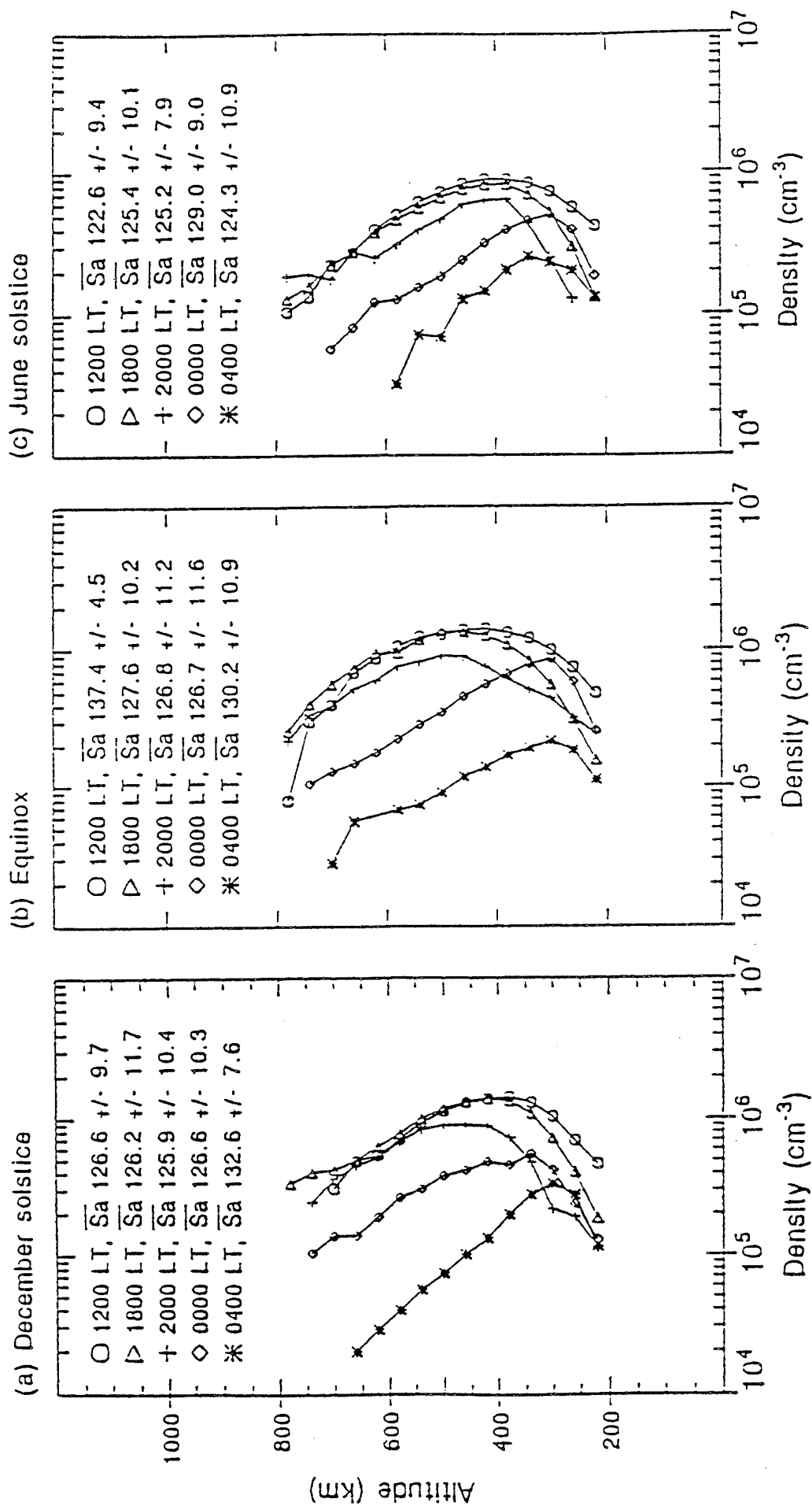
21

Hourly Variations in the Electron Density Profiles for (a) December Solstice, (b) Equinox, and (c) June Solstice, Moderate Solar Conditions. The average flux of each profile is given in the legend.

FIGURE 16
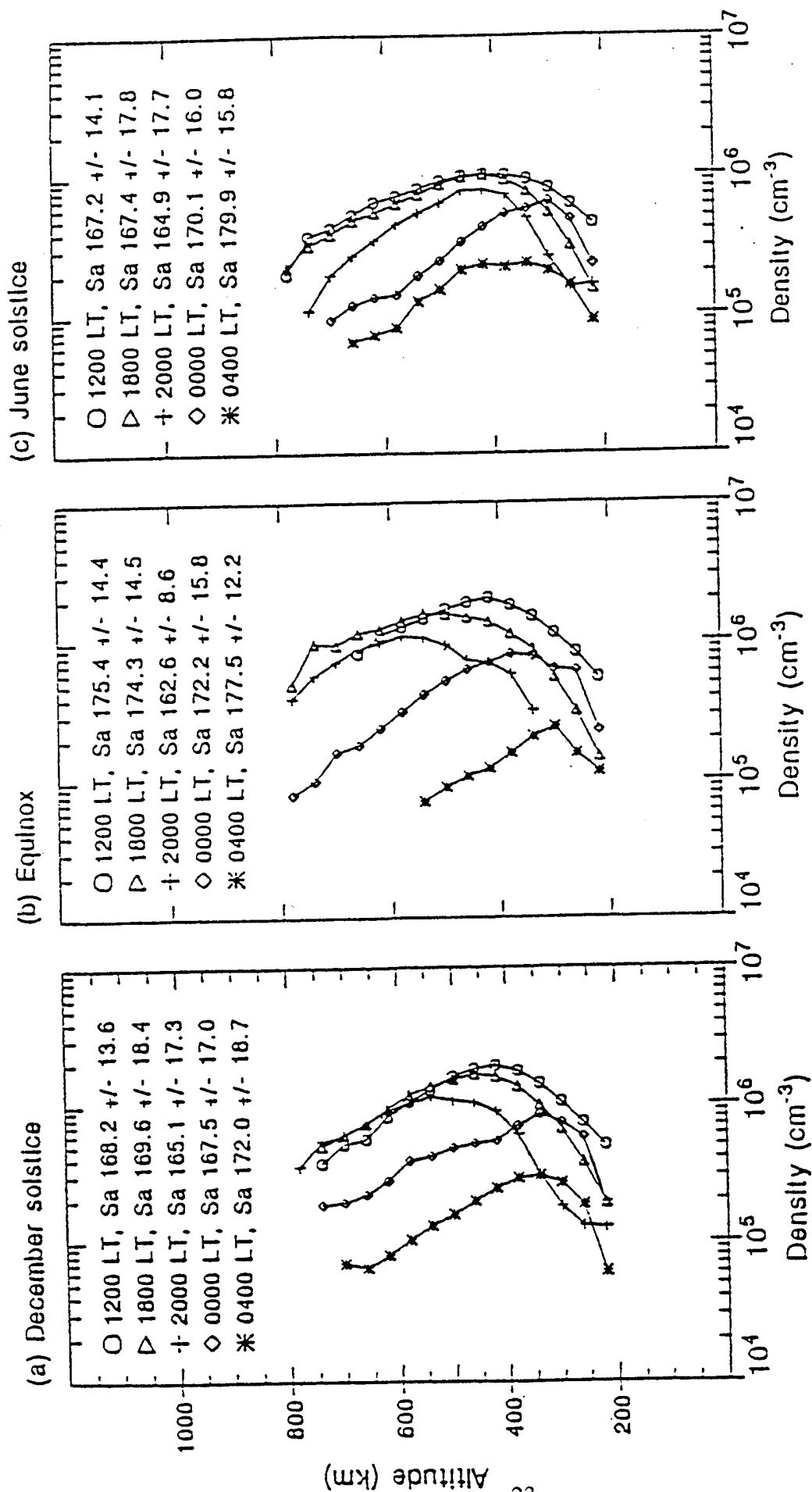
Hourly Variations in the Electron Density Profiles for (a) December Solstice, (b) Equinox, and (c) June Solstice, Solar Maximum Conditions. The average flux of each profile is given in the legend.

FIGURE 17

23

FIGURE 18

24

PIM EDP, 1700 UT, Day 100, Solar Max

IRI EDP, 1700 UT, Day 100, Solar Max

FIGURE 19

25

PIM hmf2, 0 UT, Day 100, Solar Max

IRI hmf2, 0 UT, Day 100, Solar Max

FIGURE 20

26

![PIM Topside Half Thickness, 1200 UT, Day 100, Solar Max and IRI Topside Half Thickness, 1200 UT, Day 100, Solar Max](image)
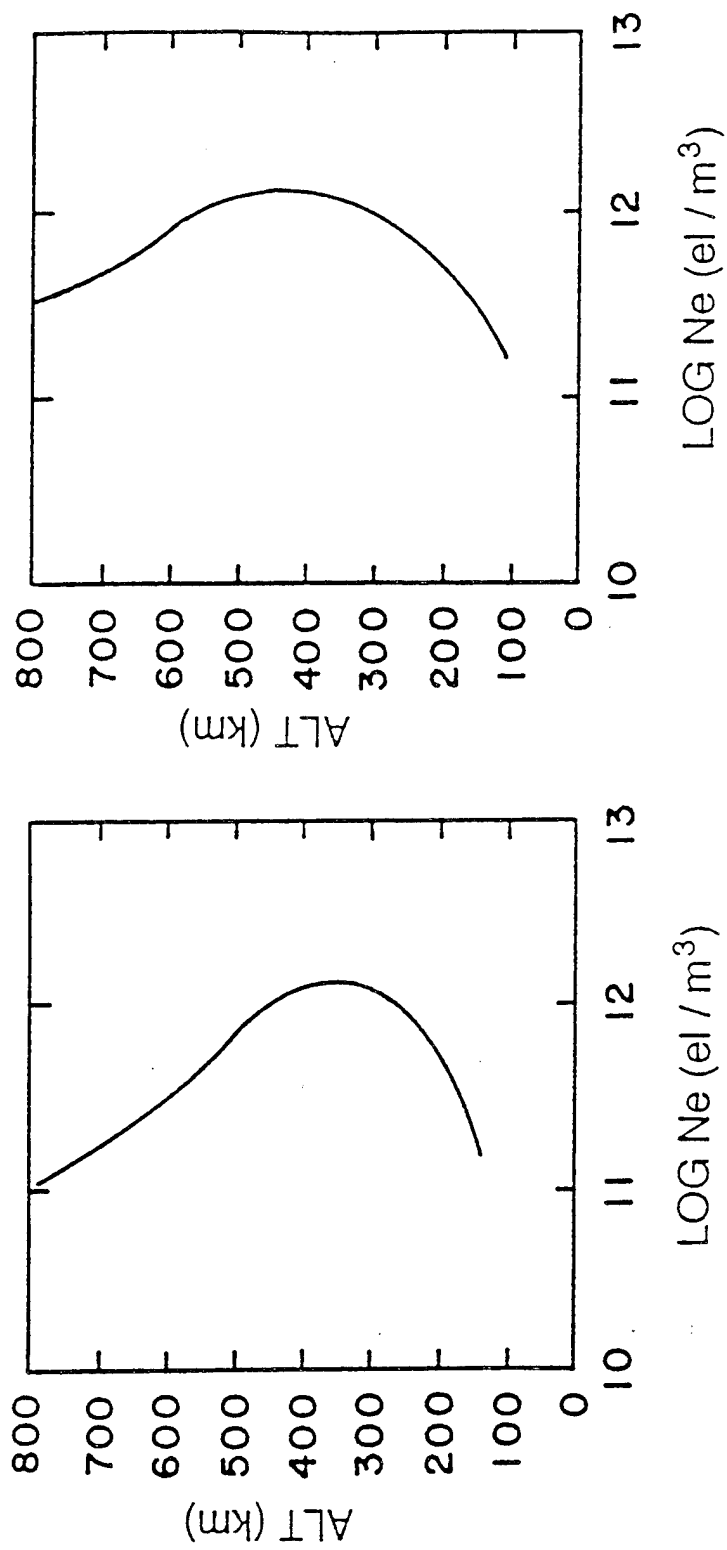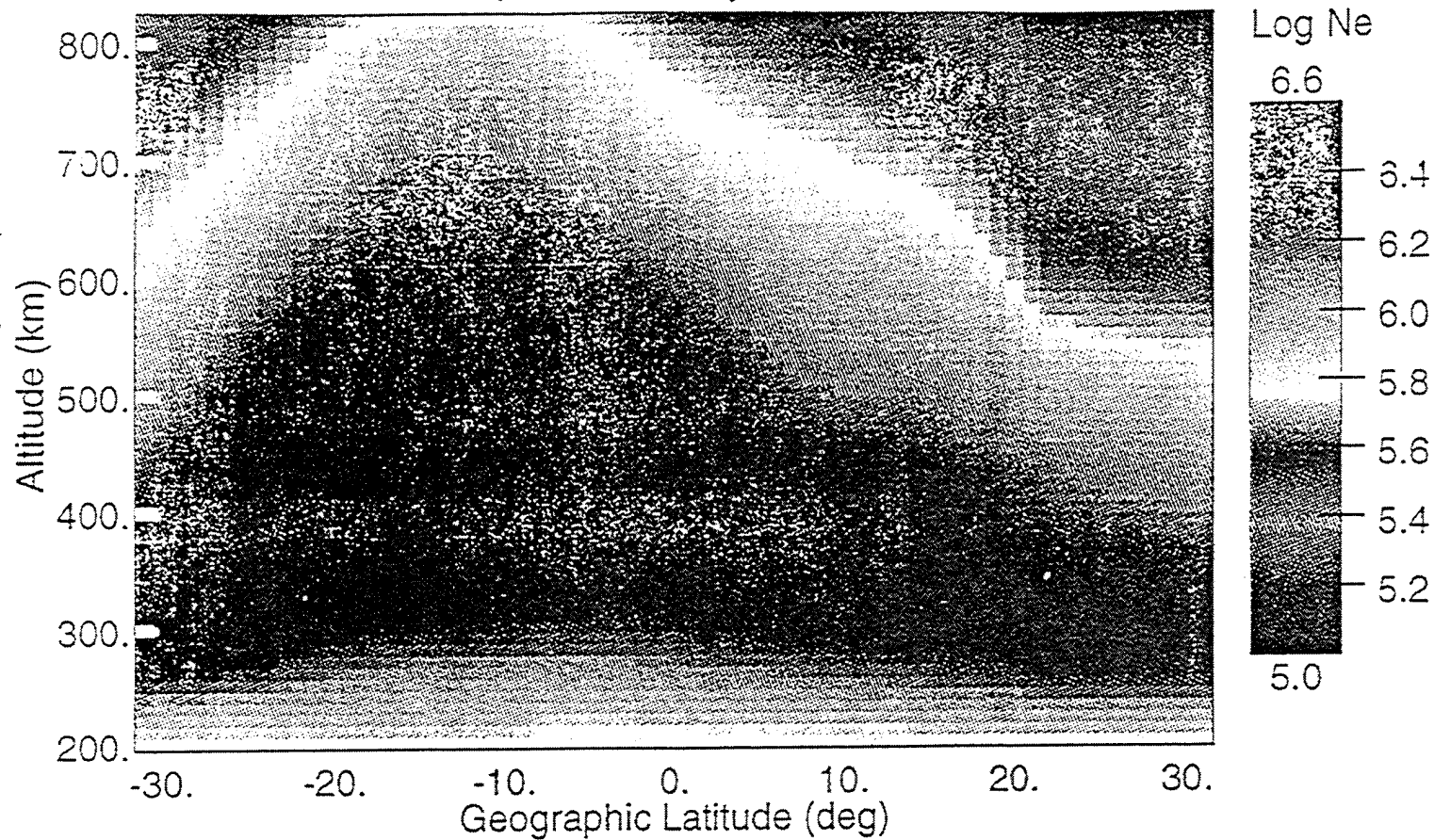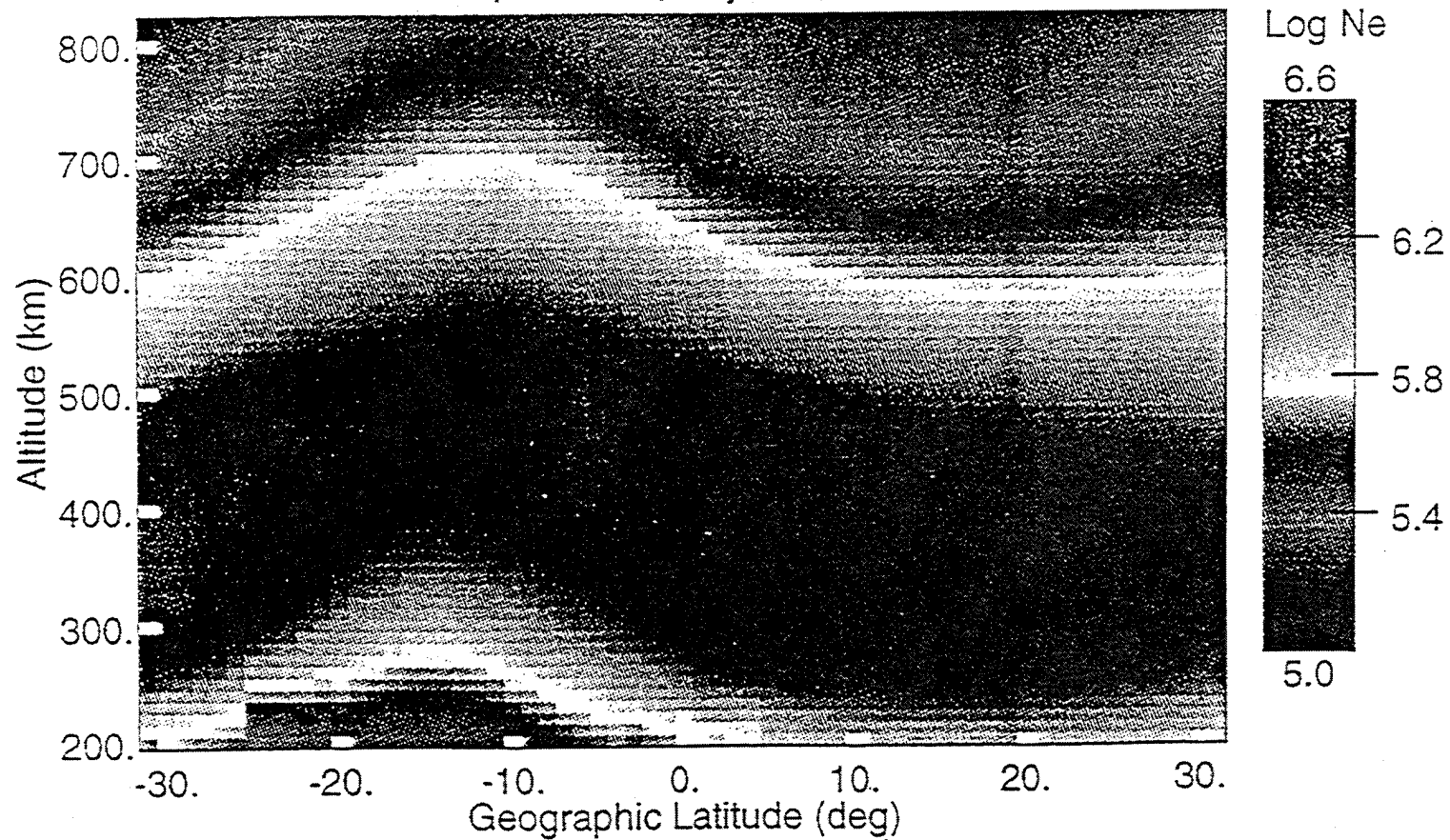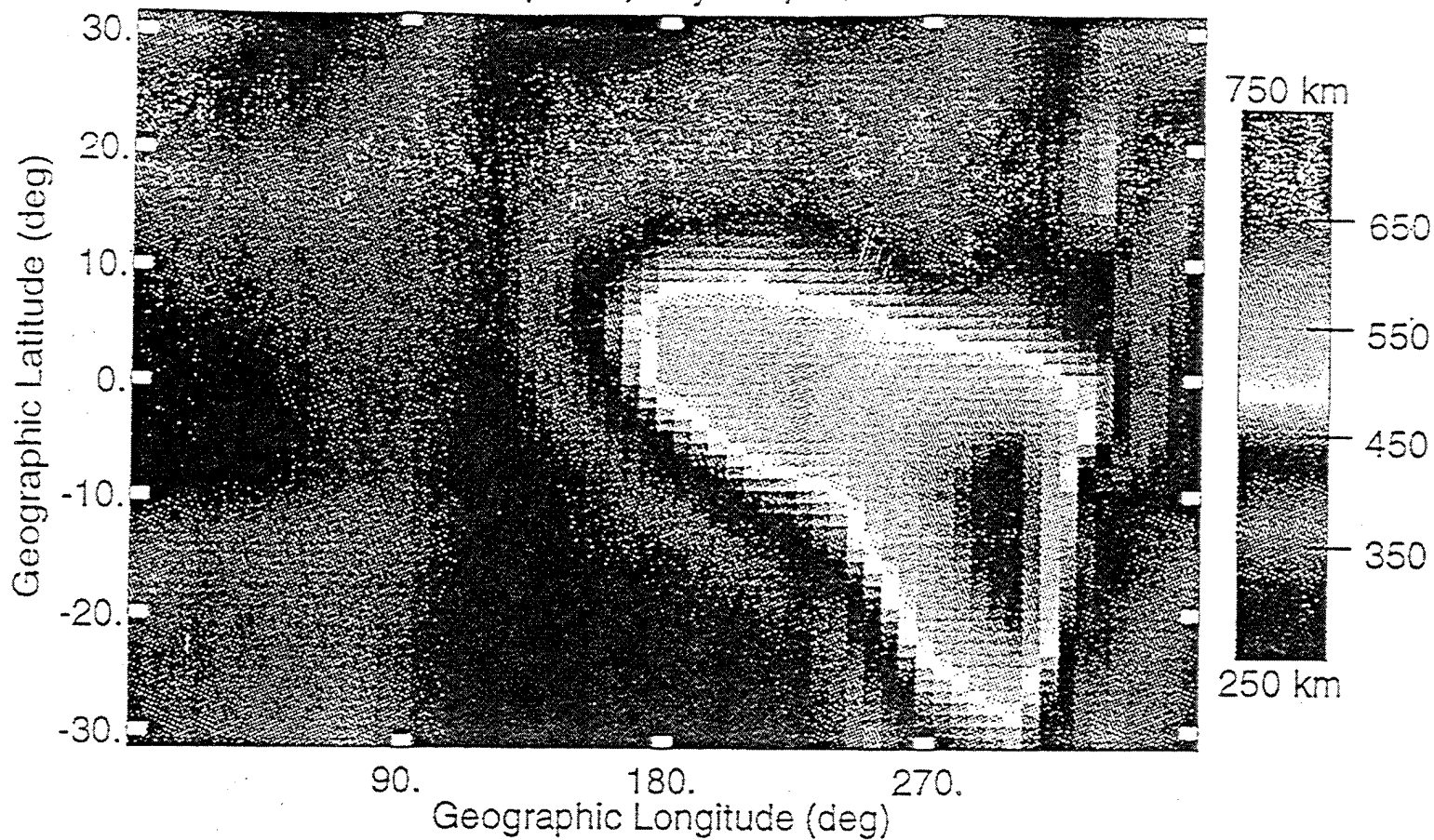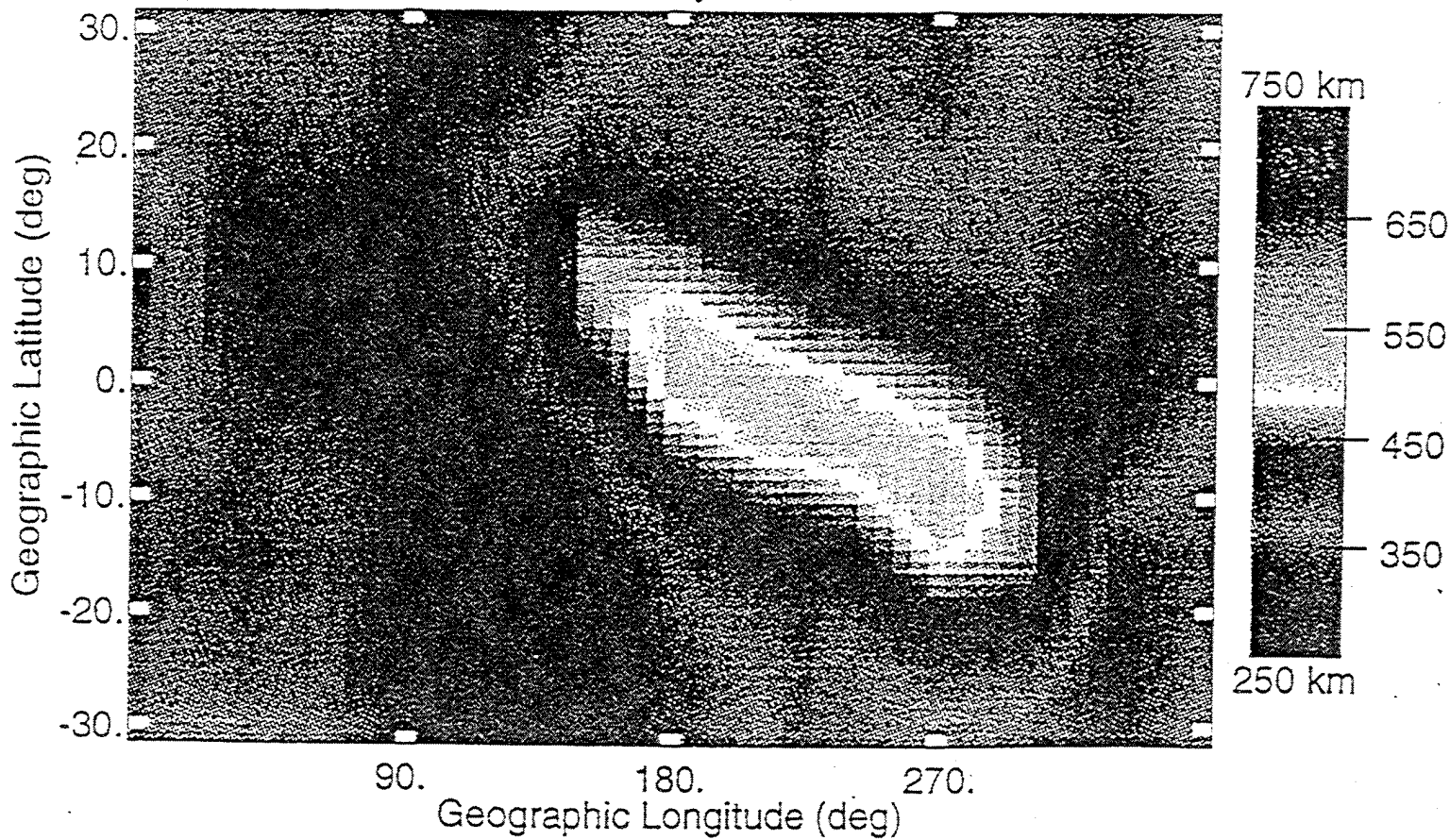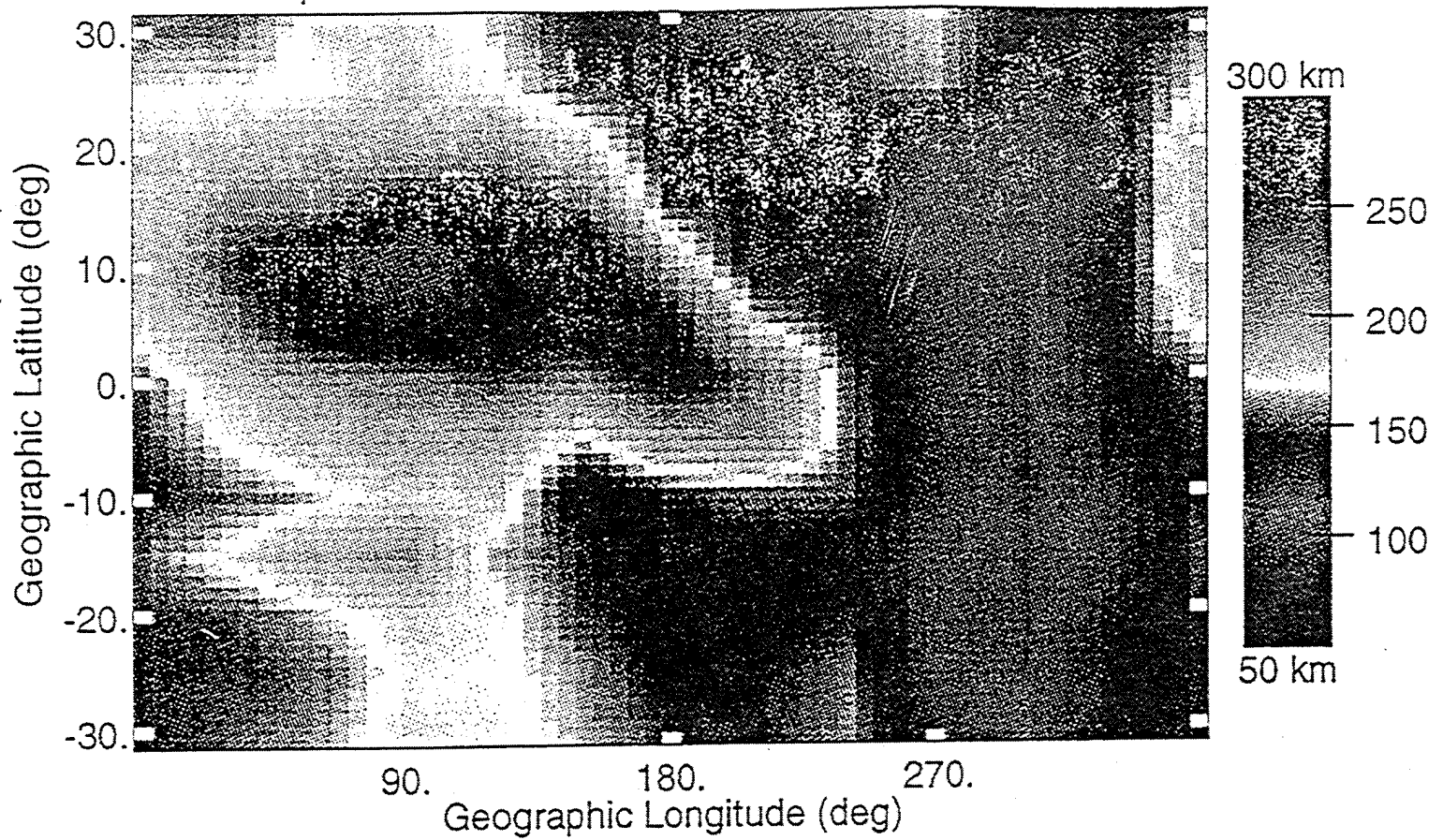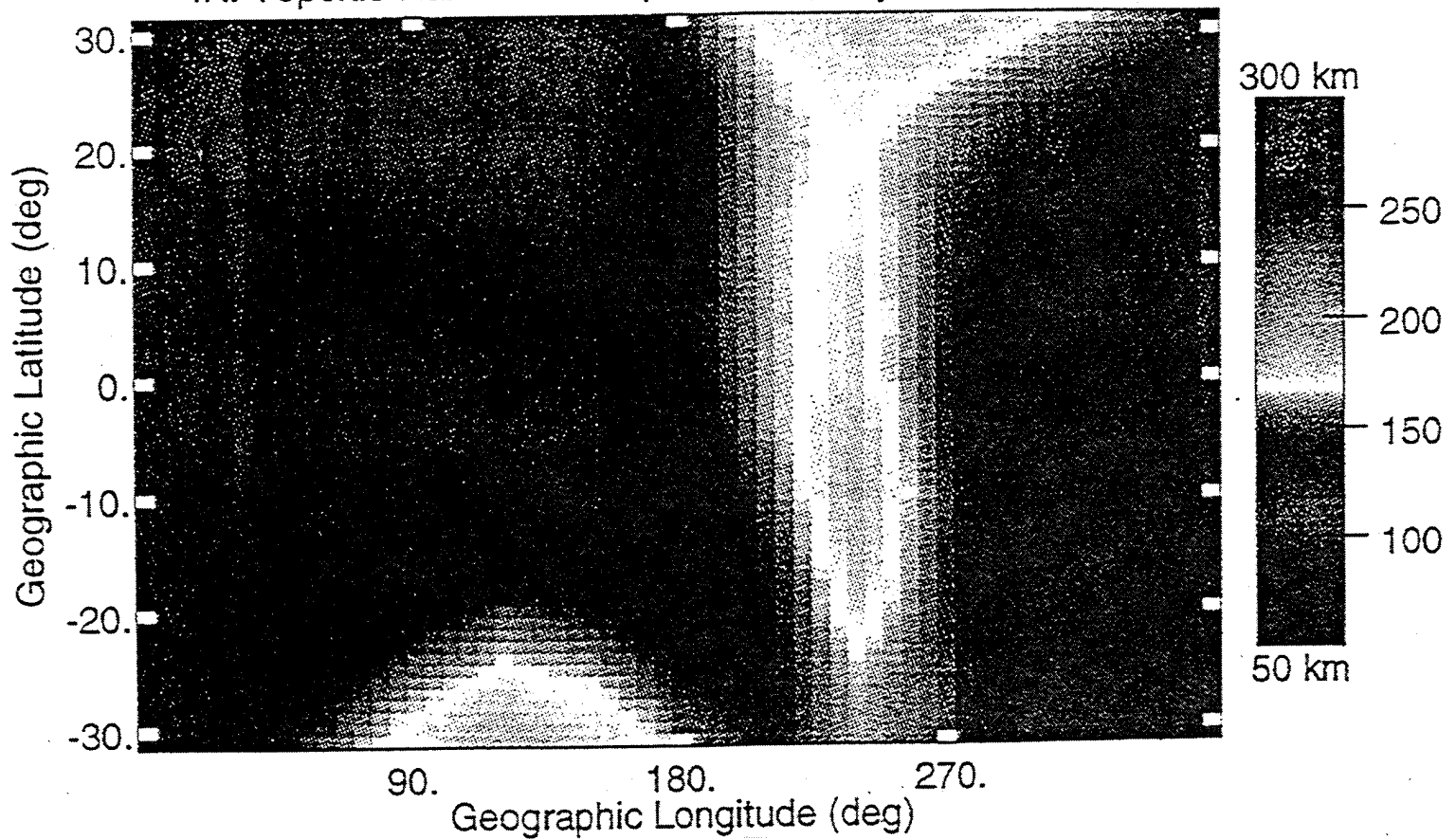
FIGURE 21

27

a reformulation of the topside within IRI or a fitting of Booker functions to PIM topside profiles. Given all this, we have developed and tested for one particular case a PIM option for IRI90.

One of the quantities IRI90 provides is the electron density profile (EDP) from 100 to 1000 km. This profile is made up of six subregions: the topside, the F2-bottomside, the F1 layer, the intermediate region, the E-valley, and the E-bottomside and D-region. The shortcomings described previously have involved the topside and F2-bottomside regions, and it is these regions that the PIM option is designed to modify. The present IRI90 normalizes both the topside and the F2-bottomside to the F2-peak density (NmF2) and altitude (hmF2). The F2 peak density comes from either the CCIR or URSI coefficient sets, which are derived from Fourier and spherical expansions of ionosonde data. Likewise there are CCIR coefficients of M(3000) which are used to infer hmf2. The topside profile shape comes from analytic fits of the Bent sounder data. The fits are done using Epstein functions which can be used to define a Booker function. The Booker function used in IRI90 consists of 3 layers and it takes 8 parameters to define the profile. Five of the parameters are fixed and the other three are given as functions of geomagnetic latitude, solar flux, and foF2. (This profile can be described in terms of the LAY formalism.) The bottomside is given by a fairly simple function which uses a thickness parameter. The present IRI90 either looks up this parameter or calculates it based on a half thickness from Gulyaeva.

As mentioned above, the PIM option would involve using PIM values for NmF2, hmF2 and bottomside half thickness directly in IRI. To use the topside from PIM in IRI will require either fitting Booker functions to PIM or fitting with some other function that would then have to be incorporated into IRI.

Presently, IRI90 allows inputting a NmF2 and hmF2 chosen by the user. To input a bottomside half thickness chosen by the user requires modifications of the IRI driver routine such that a user specified thickness can be accepted and will be substituted for the Gulyaeva thickness. For the topside we have explored one possibility by fitting topside PIM profiles with 2 parameter Chapman profiles. The IRI driver was modified to accept these two parameters and a routine was added to IRI to calculate the topside profile using a Chapman layer rather than a Booker function. Overall, the changes described here required only 20 lines of new code to IRI90. Examples of how well the PIM option can work are given in Figures 22 - 25. The dotted curve is the PIM profile in all the plots. The solid curve is the IRI profile as you go from the default version of IRI90 to the version with the full PIM option.

While the focus in this work was on low latitudes, it would seem that given the fact that high latitude modifications are being considered for IRI it would be best to develop a global PIM option for IRI. This would avoid the problem of attempting to merge a PIM option in one region with standard IRI in other regions. One way to have a global PIM capability for IRI would be to fit the 5 PIM parameters to analytic functions in the same way as was done with the F2 peak parameters derived from ionosonde data (CCIR or URSI coefficients). Whether this is feasible will require further work.

3. GPS OBSERVATIONS

3.1. Limitations in Determining Absolute Electron Content from Dual-Frequency GPS Group Delay Measurements

The greatest problem in determining absolute TEC using GPS is in the calibration of the satellite differential group delay offsets. This value is called Tgd, and can be over 10^{17} el/m^2, or 10 TEC units. Several ionospheric research groups have made estimates of the Tgd values for the various
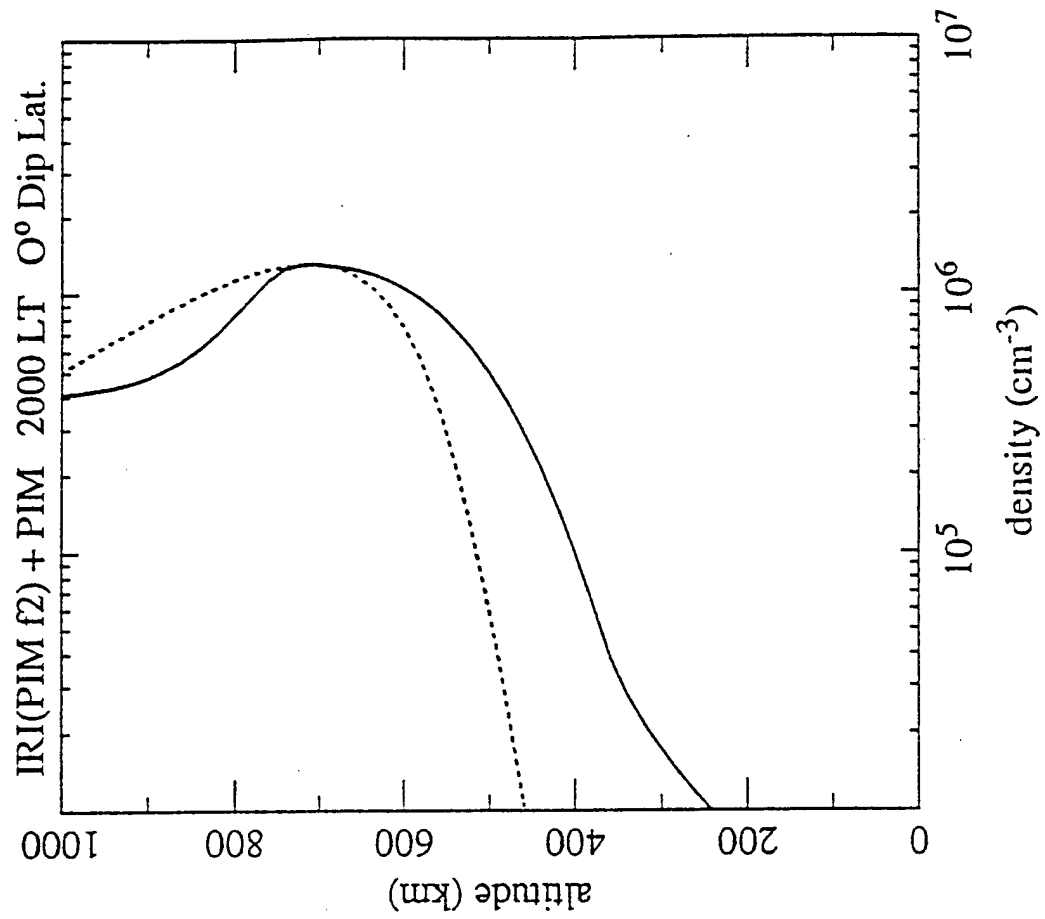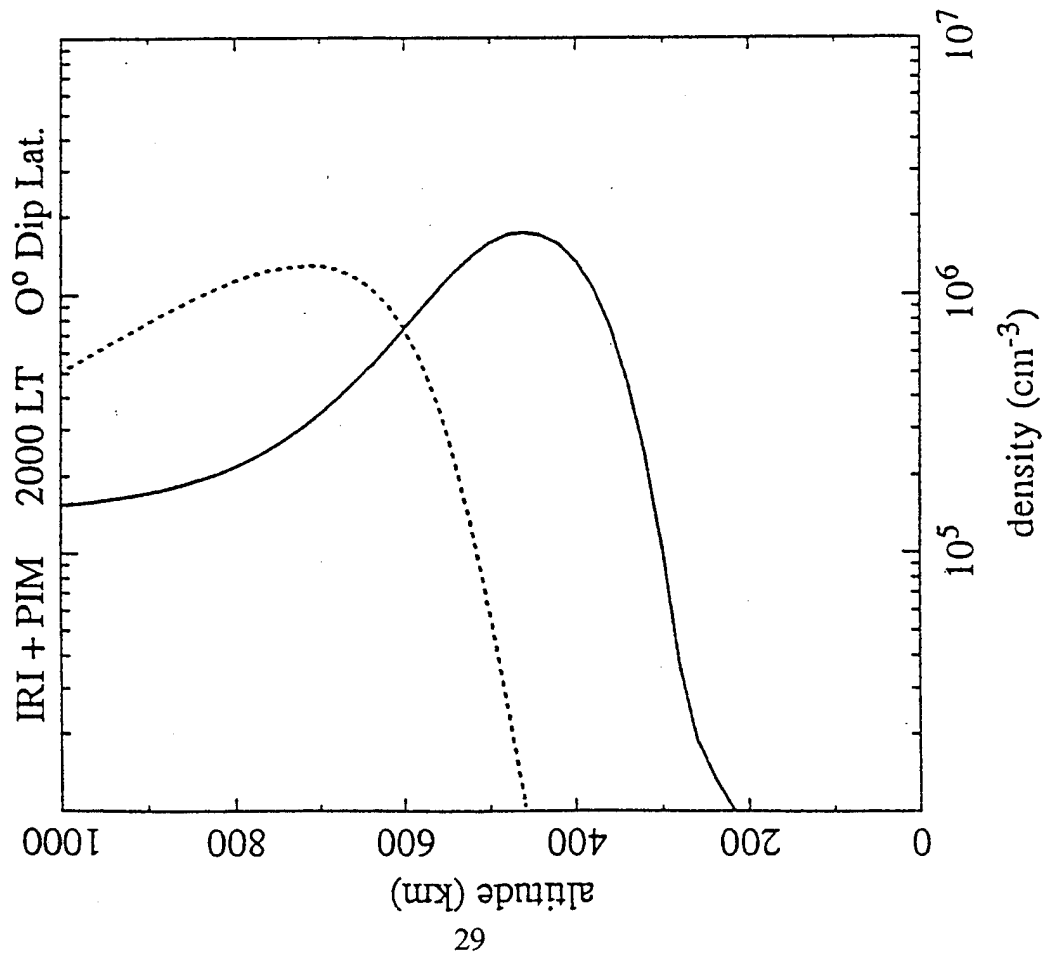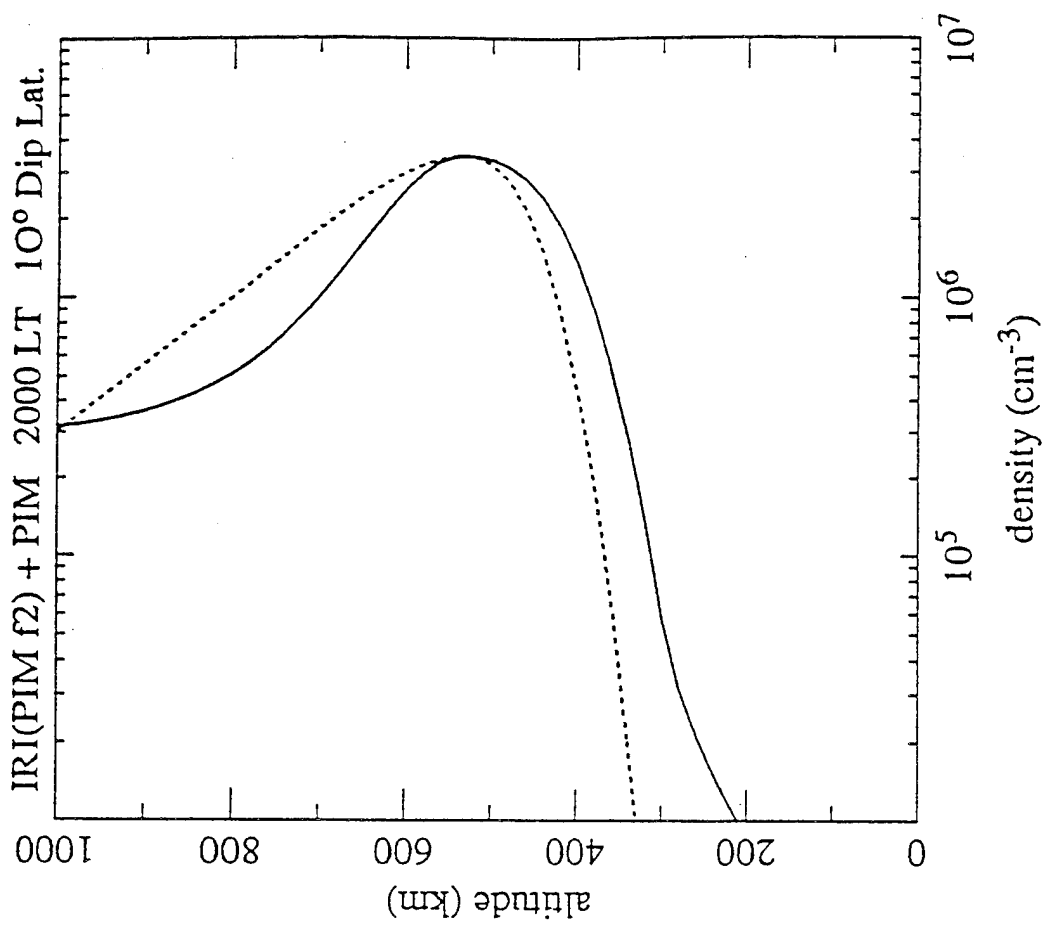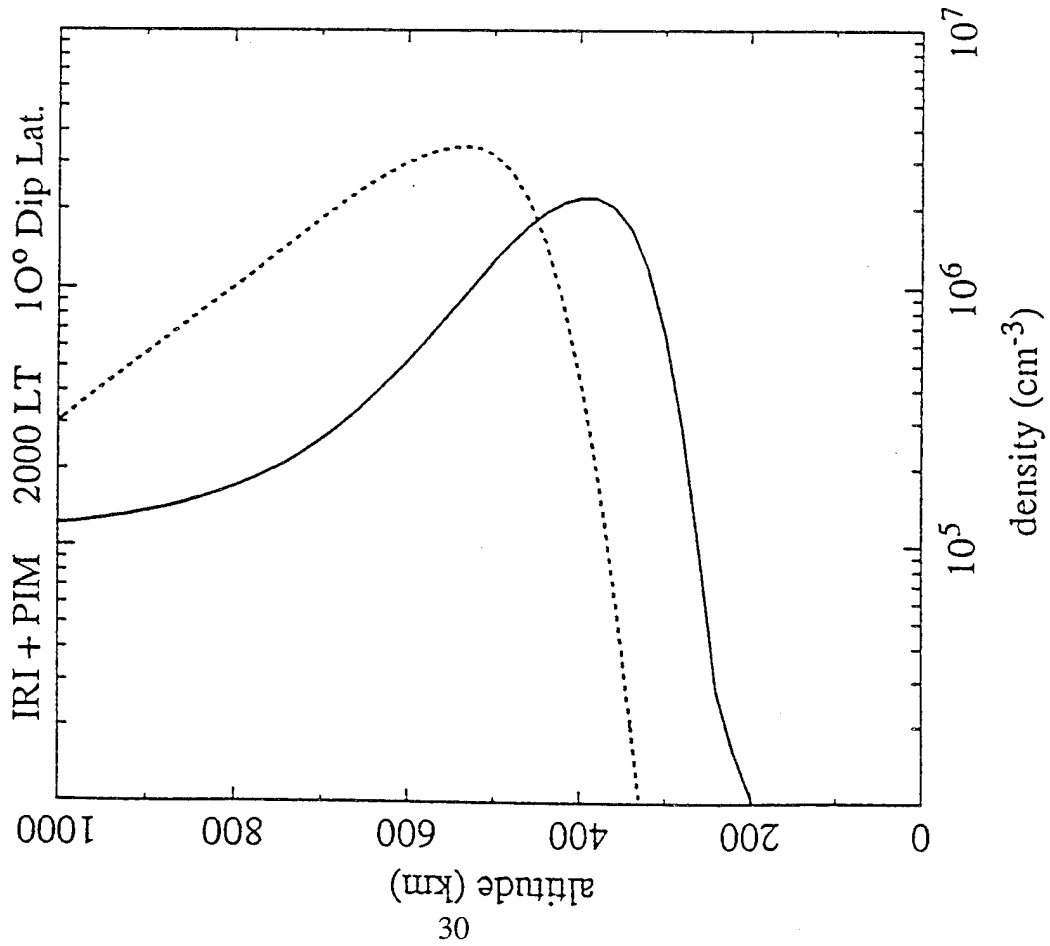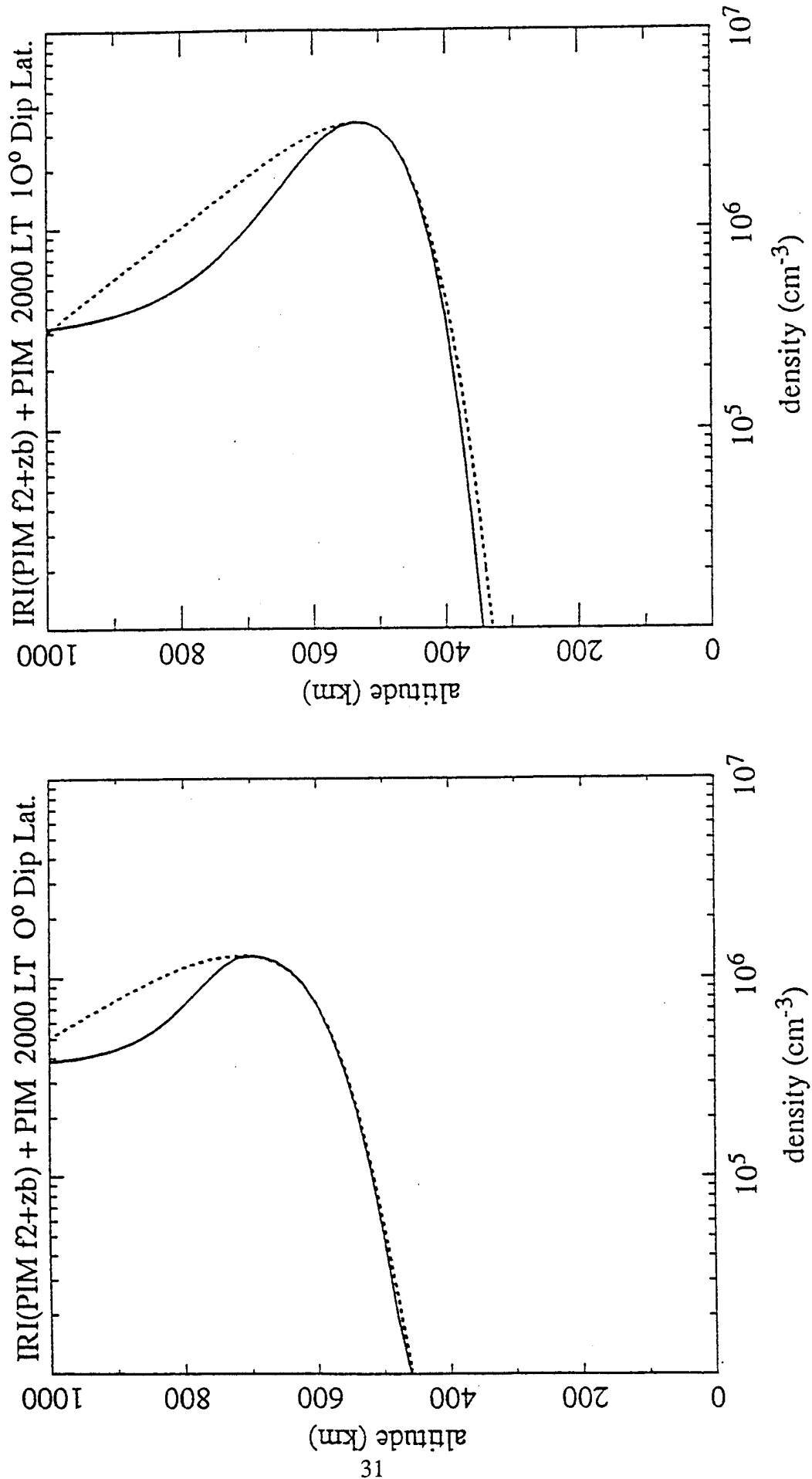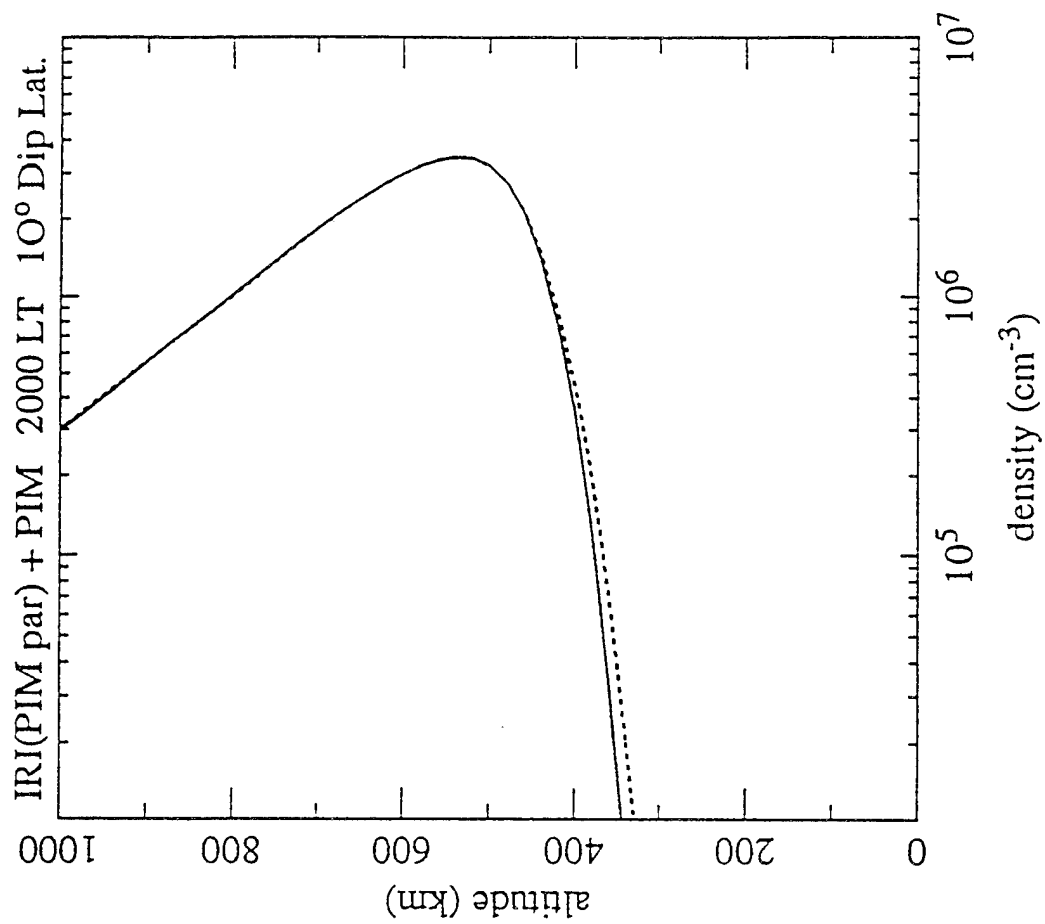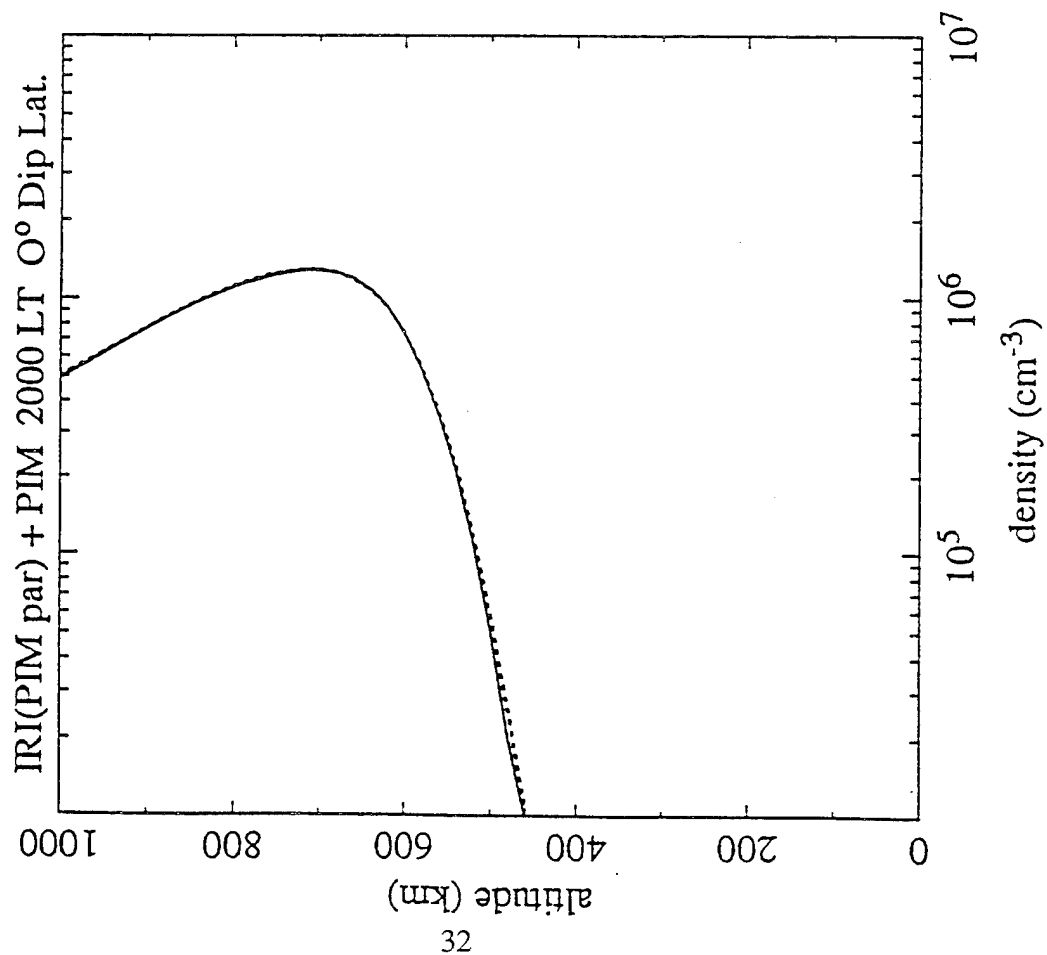
FIGURE 22

29

FIGURE 23

30

FIGURE 24

31

FIGURE 25

32

GPS satellites. All studies have implemented different methods to obtain the Tgd values and there are apparent discrepancies among the results. Over the last year, work has been done to suggest a new method of determining GPS satellite Tgd.

All of the methods of determining Tgd used by workers to date have implicitly neglected the effects of the electrons in the earth's protonosphere in their attempts to determine these values. They have all, in some form or other, used an ionospheric "shell" model, which does not include the contribution to electron content of the earth's protonosphere in different viewing directions during a typical GPS satellite pass. However, it is well known that the relative effects of the electron content of the earth's protonosphere can be up to 50% of the entire TEC during the nighttime, and 10% of the TEC during the day [*Davies*, 1980]. Since a typical GPS satellite observed from a station covers a widely different portion of the protonosphere over the course of its pass, it can be expected that any simple "shell" model of the ionosphere will not be an accurate representation of the actual behavior of TEC over the pass.

Figure 26 illustrates a cutaway view of geomagnetic L shells from the northern mid-latitude station located at Westford, MA. The L shells greater than approximately 4 are considered to be open field lines, and consequently do not contain any electrons. Note from Figure 26 that satellites viewed from Westford, MA to the north, cross only open field lines. Thus, a typical GPS pass, crossing from north to south, would see completely different amounts of protonospheric electron content, ranging from zero in the north, to relatively large values when looking along the closed magnetic L shells less than 4 to the south of the station. The theoretical ionospheric model developed by *Bailey and Sellek* [1990] has been used to calculate the contributions of the O^+, H^+ and He^+ ions to the total TEC observed along various GPS trajectories. A representative sample of relative contributions of each of those ion species is illustrated in Figure 27 for GPS space vehicle 24. The 400 km ionospheric intersection locations from the Westford station are given in the inset in Figure 27. Note that the electron content contribution due to H^+ ions is actually greater than that from O^+ near the end of the pass. The contribution to TEC from the electron content of the H^+ protonospheric ions certainly cannot be neglected. Figure 27 illustrates that a simple "shell" model of the ionosphere, having a constant mean height, is not adequate to model changes in TEC during a GPS satellite pass.

A new method of directly measuring Tgd from the ground, without modeling either the protonosphere or the ionosphere, should be possible by choosing a location on the earth at a time when there is a very low TEC in both the ionosphere and the protonosphere along the path to an individual GPS satellite. Locations viewing GPS satellites above a magnetic L shell of approximately 4 should be high enough in latitude to have no contribution to TEC from the earth's protonosphere. Magnetically quiet winter nighttime in the sub-auroral latitudes can be occasions when the TEC from the F2 region is very small. This can be confirmed by nearby ionosonde measurements of very low values of foF2. At those times, monitoring the relative differential phase and the relative differential group delay from a GPS satellite as it passes over the sky, should yield no changes as a function of satellite elevation angle, simply because there is little, if any, TEC to be measured. At those times, providing the receiver differential delay is known, the satellite Tgd can be determined directly, since there is essentially no ionosphere. For instance, an foF2 value of 2 MHz, corresponding to an N_{max} of 4.9×10^4 el/cm^3 with an assumed slab thickness of 250 km, yields a TEC of only 1.2×10^{16} el/m^2 column, not an unreasonable value for quiet winter nighttime conditions in the ionospheric trough region.

3.2. Statistics of Time Rate of Change of Ionospheric Electron Content

Dual frequency signals from the Global Positioning (GPS) satellites provide an excellent opportunity to study the behavior of ionospheric Total Electron Content. A global network of
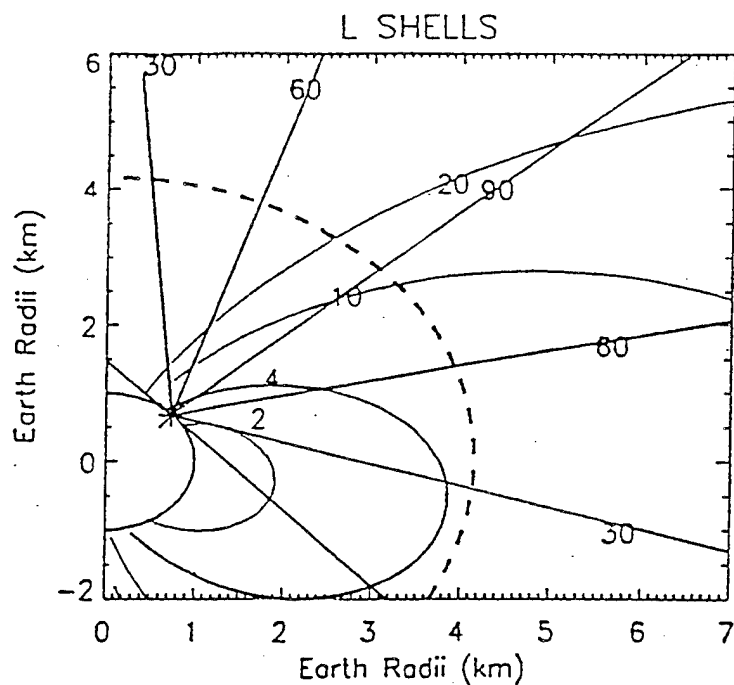
L SHELLS

Cutaway view of the earth along the station meridian, showing the magnetic L shells and the station elevation angles, both north and south of the station. Dashed line represents GPS orbital height.

FIGURE 26
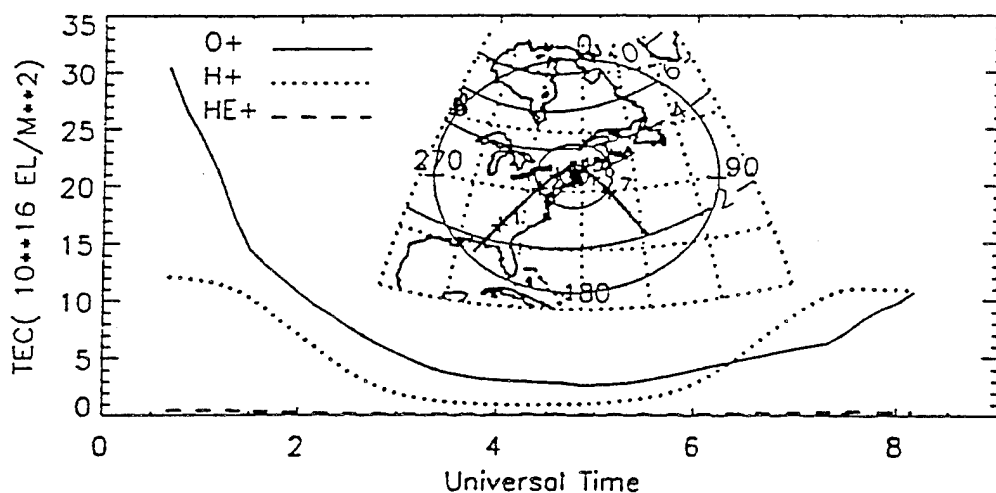
Electron contents of O^+, H^+, and H_e^+ for GPS SV Nr. 24 as viewed from Westford, MA.

FIGURE 27

34

stations recording continuous dual-frequency GPS measurements has been established by the International Geodynamics GPS Service (IGS). The potential use for this data base in ionospheric research is extensive and has been described by *Wanniger* [1993]. The data base has already been utilized to generate global ionospheric maps [*Wilson et al.*, 1992]. In addition, *Wilson and Mannucci* [1993] implemented the data base to estimate the instrumental biases in both the GPS receivers and the individual GPS satellite transmitters.

In this study, a significant portion of recent measurements from the IGS network has been used to observe the magnitude of relative short term changes in TEC as seen from a wide range of locations in the United States and Canada. Statistics of the percent occurrence of changes in TEC will be presented for different times of day, viewing direction and various levels of geomagnetic activity.

Data Processing Procedure

The data used in this study was recorded from December 1993 through May 1994 at the IGS network locations listed below:

Yellowknife, Northwest Territories	62.3°N, 114.5°W
Fairbanks, Alaska	64.8°N, 147.5°W
Albert Head, British Columbia	48.2°N, 123.5°W
St. John's, Newfoundland	47.4°N, 52.7°W
Westford, Massachusetts	42.4°N, 71.5°W
Goldstone, California	35.1°N, 116.9°W
Richmond, Florida	25.0°N, 80.4°W

All stations in the IGS network are equipped with GPS ROGUE receivers that record both differential carrier phase and differential group delay from eight satellites simultaneously. To insure data compatibility, all stations in the network store the data in Receiver Independent Exchange Format (RINEX).

In this study, absolute TEC and it's rate of change were obtained by fitting the highly accurate differential carrier phase to the noisy differential group delay over the portions of the pass where there are minimal multipath effects. In order to isolate short term TEC changes, the absolute TEC measurements were then high pass filtered to remove diurnal changes and changes induced by the changing elevation angle. Finally, relative changes in absolute TEC were computed over time intervals of 1, 2, 5 and 10 minutes.

Statistical Results

Monthly statistics of TEC time rates of change have been produced separately for 4 different times of day for each station named in this study. Time is defined as the local time at the receiver station and is grouped as follows: 05-11 lt, 11-17 lt, 17-23 lt and 23-05 lt.

Figures 28 through 29 illustrate some of these results in the form of arithmetic probability type plots. In this type of plot, changes in TEC are plotted versus their probability of occurrence in order to illustrate the shape of the distribution. A straight line indicates a normal distribution. The slope of the line is a measure of the standard deviation of TEC changes about a mean value.

Figure 28 is a comparison of changes that occur within 1 minute during the local nighttime hours at Yellowknife, Fairbanks, Westford and Albert Head during December 1993. It is evident that these changes occur most frequently at the auroral zone stations of Yellowknife and Fairbanks. Similar results were achieved for the daytime period of 11-17 local time. Figure 29 focuses specifically on data recorded at Yellowknife by showing the probability of one minute rates of change in TEC at 4

different time periods during December 1993. Obviously, rapid changes in TEC induced by auroral activity have a high probability of occurrence throughout the day at Yellowknife. A similar figure (not shown) supports the theory that these fluctuations are very short term by showing much smaller changes in TEC over 5 minute intervals for the same data set illustrated in Figure 29. Figure 30 is a global map showing the locations of the stations used in this study together with a mathematical representation of the Feldstein auroral oval [*Holzworth and Meng*, 1975] at 05 UT under moderate geomagnetic activity conditions. This figure indicates that all the satellite passes recorded at Yellowknife would likely pass through the auroral zone. Similarly, a fair number of passes recorded at Fairbanks would also pass through the auroral zone. Measurements made at Albert Head and St. John's are not likely to be affected by the aurora at these moderate magnetic conditions. During severe magnetic storms, however, auroral effects can be seen at the mid-latitudes. This is illustrated in Figure 31, where local daytime time rates of change recorded at St. John's were split by Kp levels.

Auroral scintillations, as illustrated, can cause high rates of change in TEC. The region of the world with the highest recorded scintillations, however, occur in the near equatorial region. Figure 32 illustrates the probability of 1 minute time rates of change during local nighttime hours recorded at Richmond for three different seasons. During winter and summer, the data is normally distributed with no significant probability of rapid changes in TEC. During equinox, however, rapid changes in TEC are likely to occur 10% of the time. Since the satellite passes to the south of this station cover the tip of Venezuela, it is evident that this effect is a true latitudinal gradient caused by an extended equatorial anomaly.

Figure 33 summarizes the results for 1 minute time rates of change in TEC for all locations for 3 seasons during local nighttime hours. In this figure, the 1%, 5%, 50%, 95% and 99% cumulative probability levels are plotted versus the geomagnetic latitude of each station. In winter and summer, phase scintillation effects become apparent in the auroral zone, at approximately 60° geomagnetic latitude. In equinox, not only are the auroral effects visible but also effects from an extended equatorial anomaly.

Conclusions

The data set made available by the International Geodynamics GPS Service is invaluable to the ionospheric research community.

The results of this paper indicate that the largest short term changes in TEC occur in the auroral zone during the nighttime hours. The largest changes occur within 1 minute, indicating that they are related to auroral phase scintillations. Significant short term changes in TEC are also evident in data recorded south of the Florida station during March. These changes are likely due to an expanded equatorial anomaly region.

3.3. Ionospheric Measurements Using GPS

Global Positioning System (GPS) satellites provide a unique opportunity for ionospheric research. The GPS dual frequency measurements of carrier phase and group delay at both the L1 and L2 GPS frequencies make it possible to measure ionospheric Total Electron Content (TEC) and ionospheric disturbances.

The International GPS Service for Geodynamics (IGS) is a network of GPS tracking stations located worldwide. IGS was established by the International Association of Geodesy (IAG) to support geodetic and geophysical research activities that utilize the GPS technique. Presently, there are approximately 50 data stations that collect and archive daily observations. Figure 34 summarizes the geographic locations of current stations in the IGS network. The general
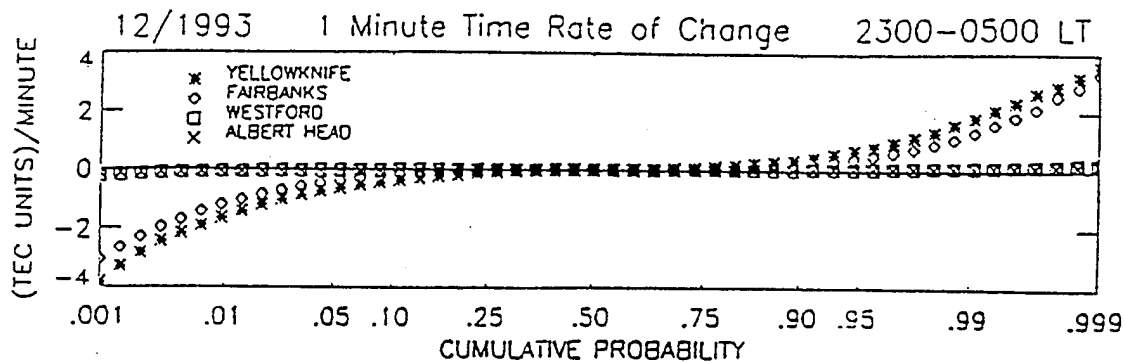
FIGURE 28. 1 minute time rate of change in TEC during local nighttime hours at 4 different locations during December 1993.
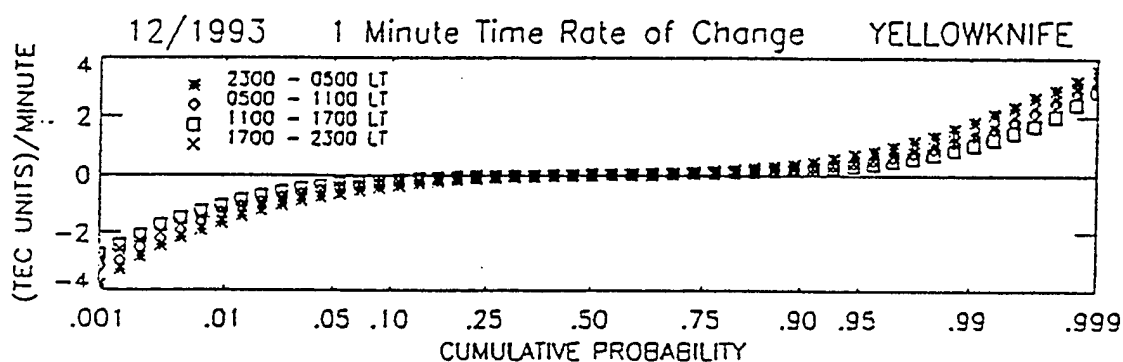
FIGURE 29. 1 minute time rate of change in TEC at Yellowknife for 4 different time periods during December 1993.
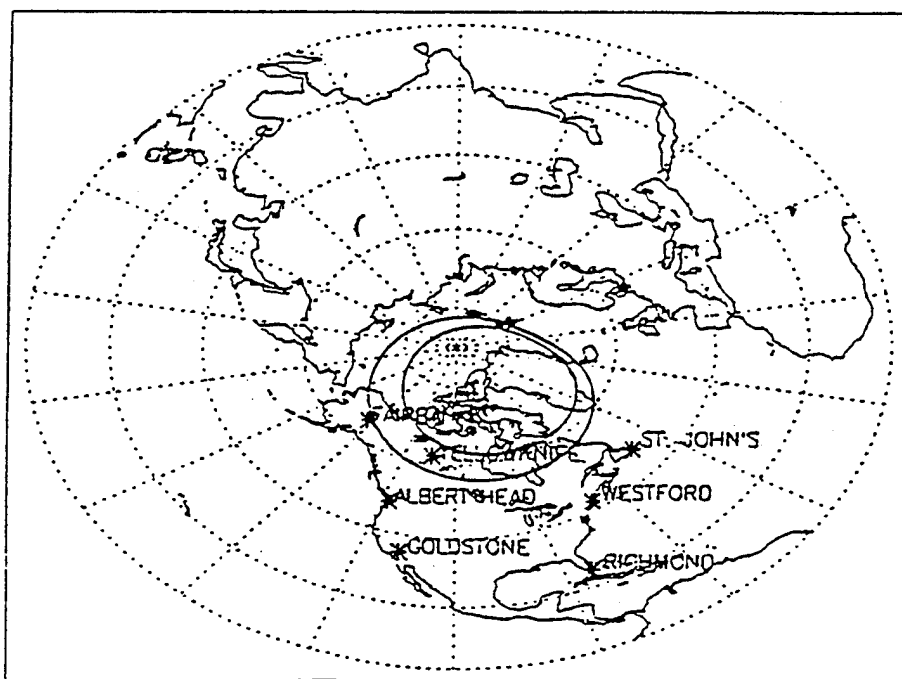
FIGURE 30. Global map of station locations with auroral oval at 05 universal time at Q=3.

37
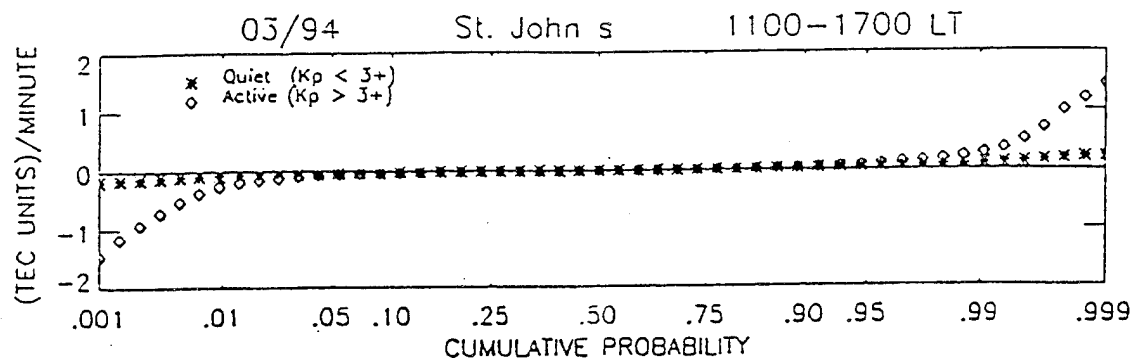
FIGURE 31. 1 minute time rate of change in TEC at St. John's during local daytime hours at different Kp levels during March 1994.
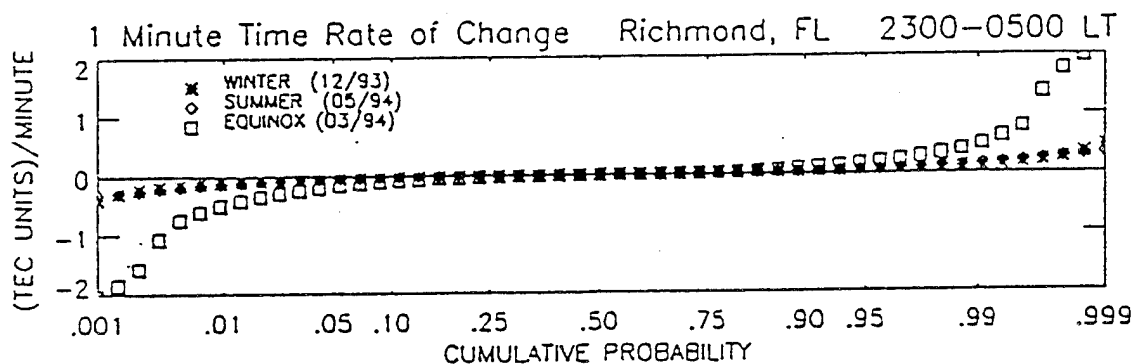
FIGURE 32. 1 minute time rate of change in TEC at Richmond during local nighttime hours for 3 seasons.
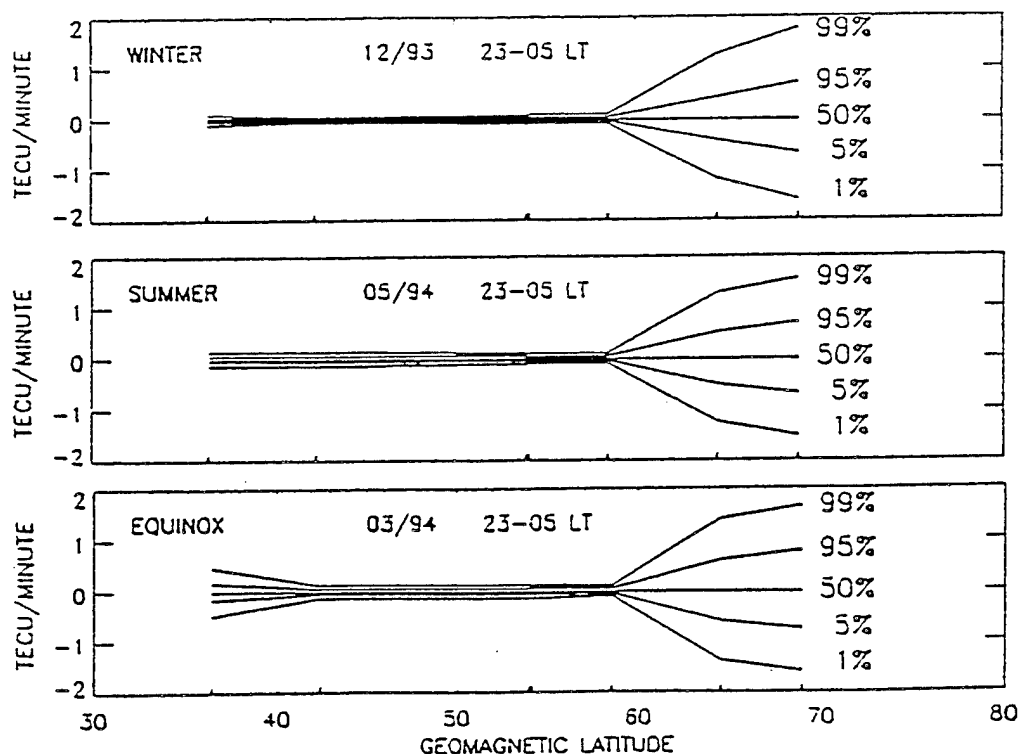
FIGURE 33. 1 minute time rates of change in TEC versus geomagnetic latitude, nighttime hours only.

GPS TRACKING NETWORK OF THE INTERNATIONAL GPS SERVICE FOR GEODYNAMICS OPERATIONAL AND PLANNED STATIONS

FIGURE 34

management of the IGS network is directed by the Central Bureau located at the Telecommunications Science and Engineering Division of the Jet Propulsion Laboratory in Pasadena, CA. Most stations in the IGS network are equipped with GPS Rogue or Turbo Rogue dual frequency receivers that record both differential group delay and differential carrier phase for up to 8 satellites simultaneously. To provide data compatibility, all stations store phase and pseudorange observations in daily Receiver Independent Exchange Format (RINEX). Data sets are available from several networks including the Central Bureau via Internet. Also available from the Central Bureau are RINEX format descriptions, navigation message files, current satellite and station information and software for data compression and decompression.

The potential use of the data base in ionospheric research is extensive and has been described by *Wanniger* [1993]. The data base has also been utilized by *Wilson et al.* [1992] to generate global ionospheric maps. In addition, *Wilson and Mannucci* [1993] used the IGS data base to estimate instrumental biases in the GPS receivers at the various sites, as well as in the individual GPS satellite transmitters. *Doherty et al.* [1994] determined statistics of the time rate of change in ionospheric range delay using six months of data from a wide range of IGS stations in the North American continent. These references are only a sample of the vast potential that the IGS network provides for ionospheric research.

This documentation provides information regarding the acquisition of data from the IGS network and the calculation of TEC using RINEX formatted data. It also describes software developed at the Air Force Phillips Laboratory to process the data. Any questions regarding this package should be addressed to:

Patricia Doherty
Institute for Space Research
Boston College
Newton, MA 02159
Internet address: doherty@plh.af.mil
Telephone: 617-377-4283

TEC Calculations Using RINEX Data

RINEX data contains a well defined set of observables including dual frequency carrier phase, pseudorange (code) and observation time. The ionospheric range error or Total Electron Content can be determined from dual frequency pseudorange or carrier phase measurements. Figure 35 illustrates both of these measurements for a typical satellite pass recorded at Westford, MA.

The pseudorange or group delay measurement, shown in the top panel of Figure 35, represents an absolute measure of the ionospheric range error in meters. These measurements were recorded under anti-spoofing conditions and therefore exhibit excessive variations in receiver noise. This increased receiver noise is due to the low signal to noise ratio that results when a receiver is operated in a codeless mode of tracking. This noise is more evident at low elevation angles, as can easily be seen near both ends of the pass. This measurement is also susceptible to noise induced by multipath. Multipath is strongly dependent on the local environment and is also more evident at low elevation angles. To calculate differential delay (ns) from the dual frequency (or P-code) data:

1) convert P code in meters to ns:

$$p1(ns) = p1(m)/.3$$
$$p2(ns) = p2(m)/.3$$

2) calculate differential code delay(ns):

diff. code delay(ns) = (p2(ns) - p1(ns) - HWCAL(ns))
where HWCAL(ns) = hardware calibration in ns
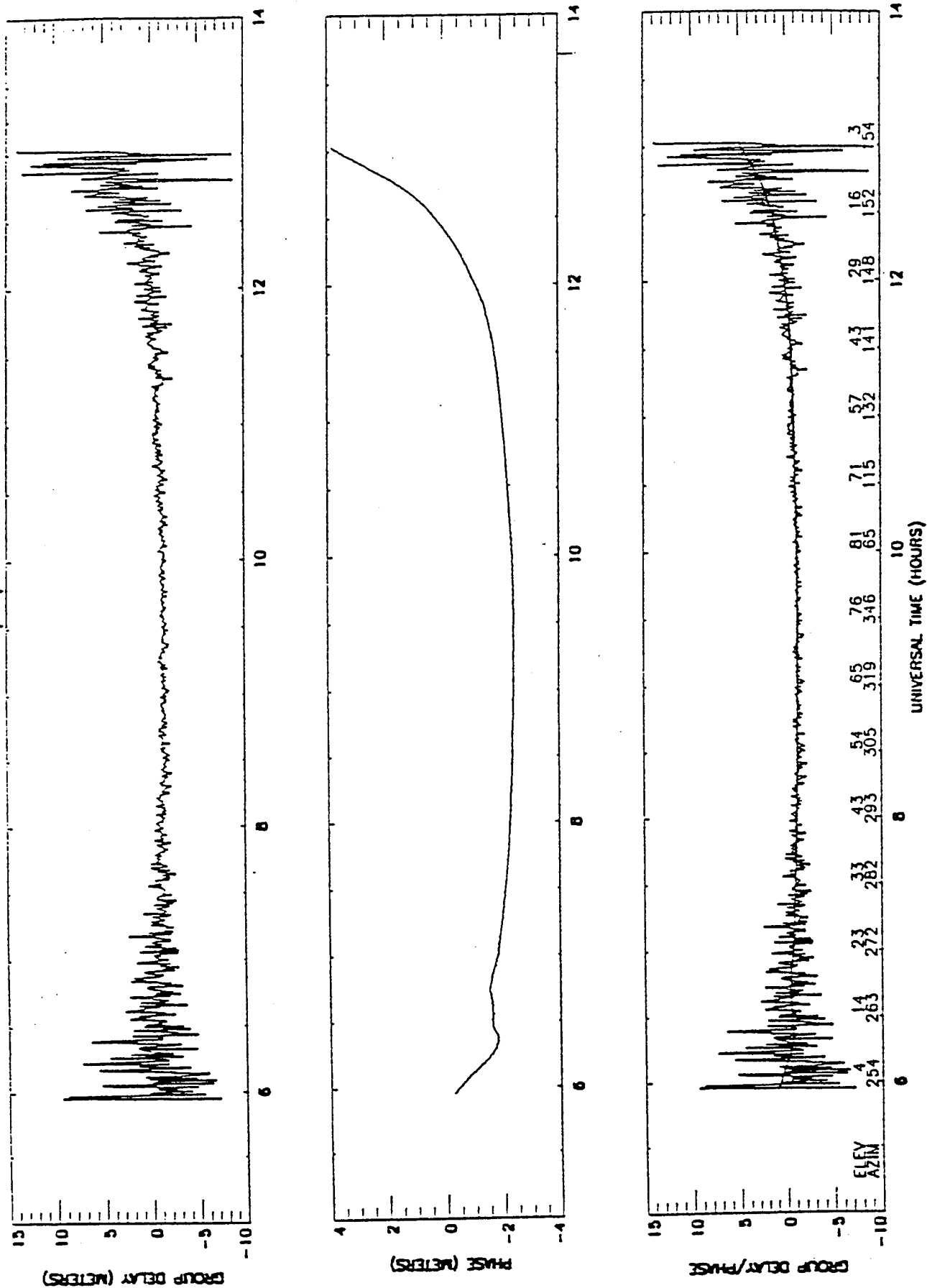
FIGURE 35

The differential carrier phase measurement, shown in the middle panel of Figure 35, provides a much more precise measure of the ionospheric error, but only on a relative scale. This measurement is not as noisy as the group delay and is not susceptible to multipath. It is measured in whole cycles at both L1 and L2. To calculate differential delay (ns) from carrier phase:

1) convert cycles of L1 and L2 to ns:

$$L1(ns) = L1(cycles)/1.57542$$
$$L2(ns) = L2(cycles)/1.22760$$

2) calculate differential phase delay:

$$\text{diff. phase delay(ns)} = L1(ns) - L2(ns)$$

The user can then convert differential delay to other parameters with the following conversion factors provided by *Klobuchar* [private communication, 1994]:

1 nanosecond of differential delay:

$$= \quad 2.852 \times 10^{16} \text{ el/m}^2 \text{ (TEC)}$$
$$= \quad 1.546 \text{ nanoseconds of delay at L1}$$
$$= \quad 0.464 \text{ meters of range error at L1}$$

In processing the data, the accurate phase measurement is fit to the noisy pseudorange measurement to obtain an absolute and precise measurement of TEC. This fit is determined with data collected during the middle of the pass to avoid the noisy data at low elevation angles and multipath interference. Then the pseudorange measurements are discarded and we are left with the differential carrier phase data fit to the absolute scale provided by the pseudorange. The bottom panel of Figure 35 illustrates this process by showing the phase measurements fit to the group delay measurements. The approximate elevation and azimuth of the satellite is printed below the data in the bottom panel.

The IGS network also provides Navigation Message Files in RINEX format. These files contain a subset of clock and ephemeris data for each of the transmitting GPS satellites. The parameters included in this file are for the beginning of the GPS week with the exception of the Mean Anomaly which is referenced at the time of ephemeris. In processing the data, a navigation message file is required to determine elevation and azimuth positions as viewed by the recording station.

Accessing the Data

Access to the RINEX data files is through the IGS data center at JPL. Data is stored in JPL's guest computer "BODHI" in the sub-directory: /pub/rinex. Approximately 180 days of data are stored on line. Data is stored in directories indexed by the Julian day of the year. An underscore "_" after the day number indicates that data is available for that day. Each directory contains data and navigation message files for each station in operation for a single day.

Files can be accessed via anonymous ftp through internet (address: 128.149.70.66). A sample transfer session is described below. In this description, the user commands are in italics and comments regarding the user commands are in parentheses.

SUN [120]: *ftp 128.149.70.66*   (open ftp session with BODHI)
Connected to 128.149.70.66
220 bodhi FTP server (Version 1.7.109.2 Tue Jul 28 23:32:34 GMT 1992) ready.

Name(128.149.70.66:doherty): *anonymous*   (login is anonymous)

42

331 Guest Login ok, send ident as password.
Password:*user@location*   (password is your internet address)

ftp> *cd pub/rinex*   (change directory)
ftp> *binary*   (for binary transfer of data)
ftp> *cd 244_*   (change directory to data stored for day 244)
                                             (the underscore _ indicates that data is available)
ftp> *get 94sep01west____r0.rnx_z*   (get data recorded at Westford on 09/01/94)
                                             (multiple files can be accessed with a macro)
150 Opening BINARY mode for data connection for 94sep01west____r0.rnx_z (612441 bytes).
226 Transfer complete.
local: 94sep01west____r0.rnx_z   remote:94sep01west____r0.rnx_z
612411 bytes received in 42 seconds (14 Kbytes/s)
ftp> *bye*   (end transfer session)

The IGS Central Bureau at JPL also provides information about the network through anonymous ftp at 128.149.70.41. In the directory "igscb", files can be found that outline data format and availability, station information, software and other general information.

Software to Process RINEX Data

Software has been developed at the Air Force Phillips Laboratory to process the RINEX data provided by the IGS network. The software was developed by Boston College under Air Force Contract F19628-93-K-0001. The main programs developed for processing the data are listed below:

RINEX.F -   fortran program that performs all the calculations and generates three
                       output files for further processing
PLTRNX.PRO -   IDL plot routine to plot the results generated in RINEX.F
SLIP.PRO -   IDL plot routine to plot out and correct potential cycle slips in phase that
                       were not automatically corrected in RINEX.F

The fortran program is written in standard fortran and should be portable to any other system. The plot programs are written for a UNIX based system using the Interactive Data Language analysis software. If the IDL package is not available, similar graphics software can be developed to display the results generated by **RINEX.F**.

RINEX.F is the front end of the process. It requires an input file named "rinex.info" containing directives for processing the data. It must include the following information:

line 1: rinex data filename (uncompressed ".rnx" file)
line 2: navigation message filename (uncompressed ".eph" file)*
line 3: month, day, year - (for the rinex data in 2 digit format)
line 4: station name - (where rinex data was collected)
line 5: Julian day - (day of the year corresponding to month, day, yr)
line 6: Hardware calibration(ns) - (receiver hardware calibration)

* When accessing the network, the user will find a navigation message file for each station data file. In the processing described here, it is not necessary to provide a different ephemeris file for each station data file. The **RINEX.F** program converts the ".eph" file to a standard almanac set that can be used for any station location. In fact, the **RINEX.F** program can predict accurate satellite positions using a ".eph" file that is up to three weeks old.

After reading the input file "rinex.info", **RINEX.F** will perform the following:

a) read in the rinex data (.rnx file)
b) calculate the geographic location of the station
c) convert the phase and pseudorange data to TEC units, where 1 TEC unit = $1*10^{16}$ el/m^2.
d) calculate elevation and azimuth angles for each data sample (using the .eph file)
e) search for time gaps that may be related to receiver drop outs
f) search and correct apparent cycle slips in phase for individual satellite passes
g) determine absolute TEC by fitting the smooth, relative phase data to the noisy, absolute pseudorange data using an arithmetic mean fit
h) generate 3 output files for further processing:
> data.file - contains the final output including phase, pseudorange, absolute fitted TEC, elevation, azimuth and time at 1 minute intervals
>
> error.file - contains information on errors found in the data including gaps in time (potential drop outs) and cycle slips
>
> slip.file - contains satellite passes that may contain cycle slips that were not corrected in **RINEX.F**.

PLTRNX.PRO is a plot routine written in IDL (Interactive Data Language). It simply reads the output file "data.file" created in **RINEX.F** and plots the results. Figure 36 illustrates some of these results for data recorded on 10/08/94 at Westford, MA. Each panel exhibits the carrier phase data fit to the absolute scale provided by the pseudorange measurement for separate satellite passes.

SLIP.PRO is a plot routine written in IDL. It reads and plots the "slip.file" data file created in **RINEX.F**. Slip.file contains problem data passes. In general, **RINEX.F** automatically detects and corrects for cycle slips. Passes that are written to "slip.file" are those that **RINEX.F** was not able to correct. **SLIP.PRO** is menu driven allowing options to zoom into problem areas, to correct apparent cycle slips or to accept or reject the data file. Figure 37 illustrates a simple session with **SLIP.PRO**. The top panel is the standard plot with the fitted phase data plotted over the pseudorange data. The middle panel shows the phase data alone with a pointer indicating an apparent cycle slip at 14.50 hours UT. The bottom panel illustrates the resulting phase curve after the cycle slip was corrected by **SLIP.PRO**. **SLIP.PRO** generates an output file containing corrected satellite passes. This file must be concatenated with the "data.file" provided by **RINEX.F**.

Summary

The programs and techniques included in this package together with the data set made available by the International GPS Service for Geodynamics provides and excellent opportunity for ionospheric research. Additional software can be developed by the individual user to further analyze the data for many different applications.

The following list summarizes the steps to obtain and analyze data from the IGS network using these techniques:

1) login to the central network at JPL
2) access data files and navigation message files in binary mode
3) decompress data and navigation message files on your computer
4) create the input file named "rinex.info" required by **RINEX.F**
5) run the **RINEX.F** program
6) run **SLIP.PRO** to look at and correct problem passes in "slip.dat"
7) concatenate the corrected passes from **SLIP.PRO** to "data file" from **RINEX.F**
8) optionally plot the "data.file" with **PLTRNX.PRO**
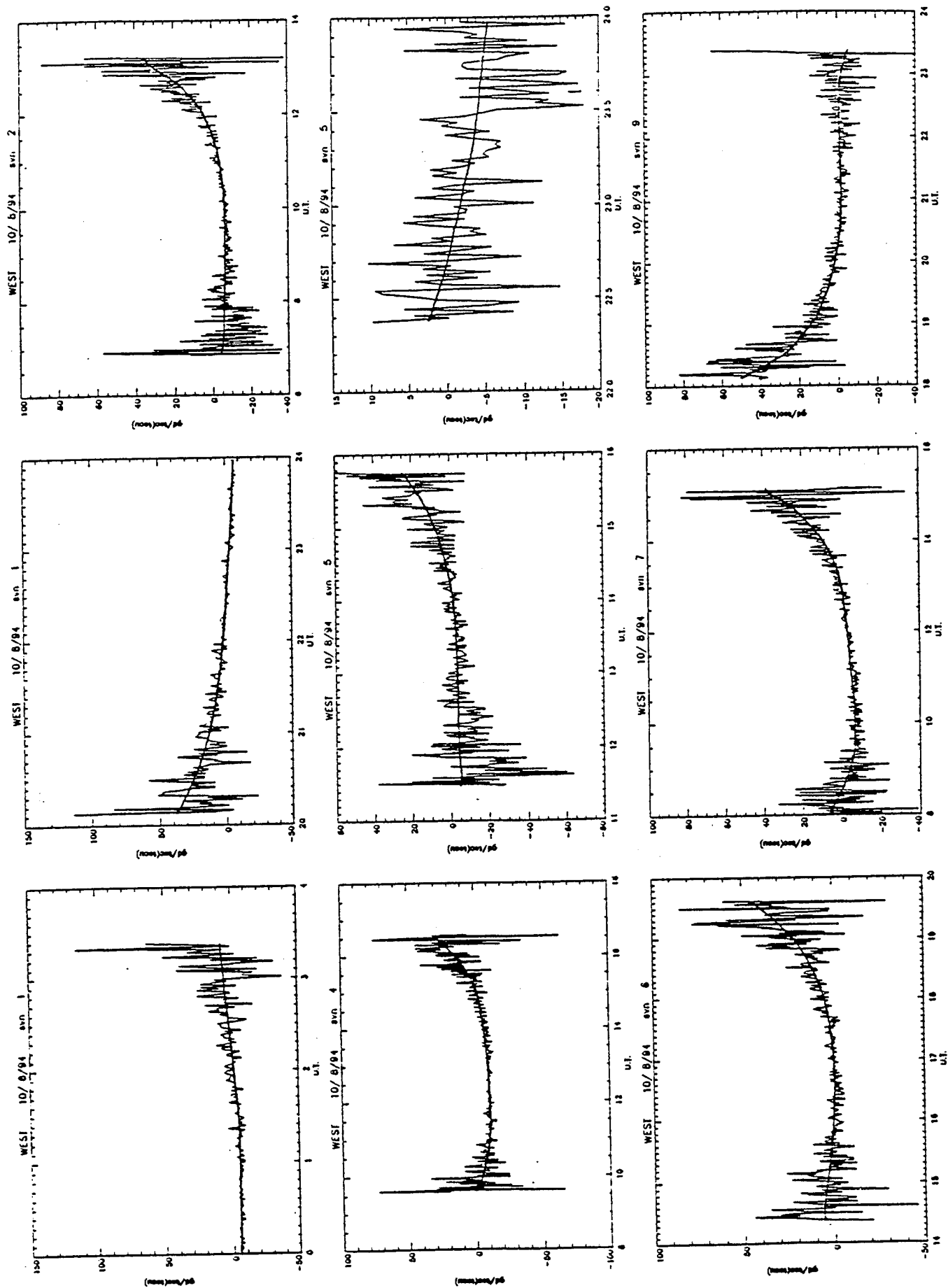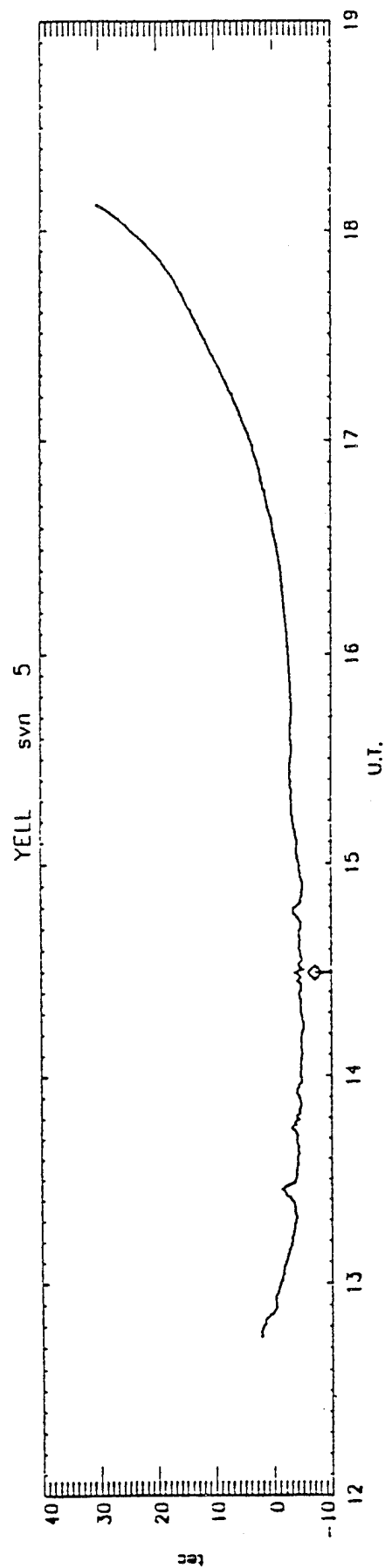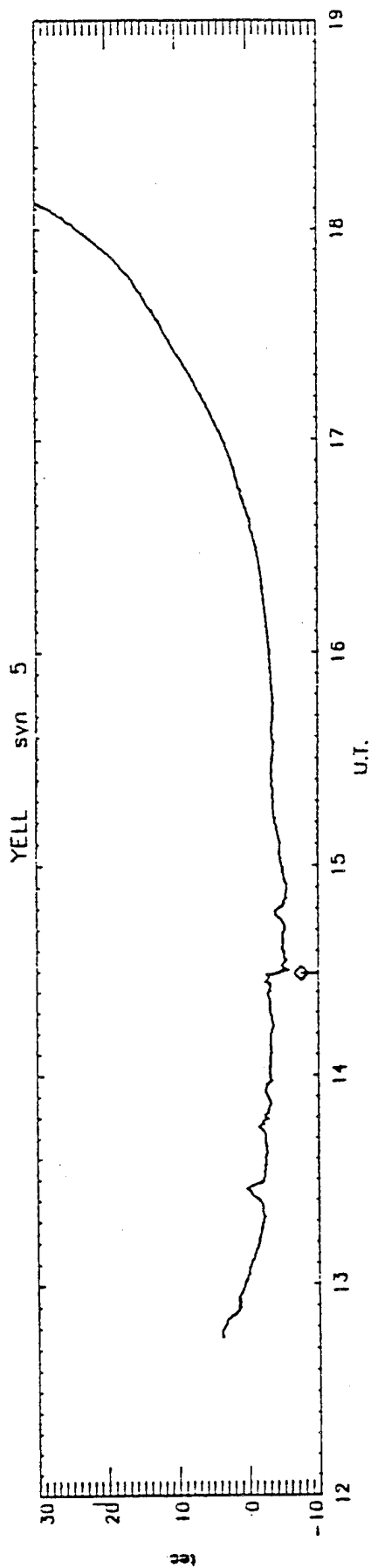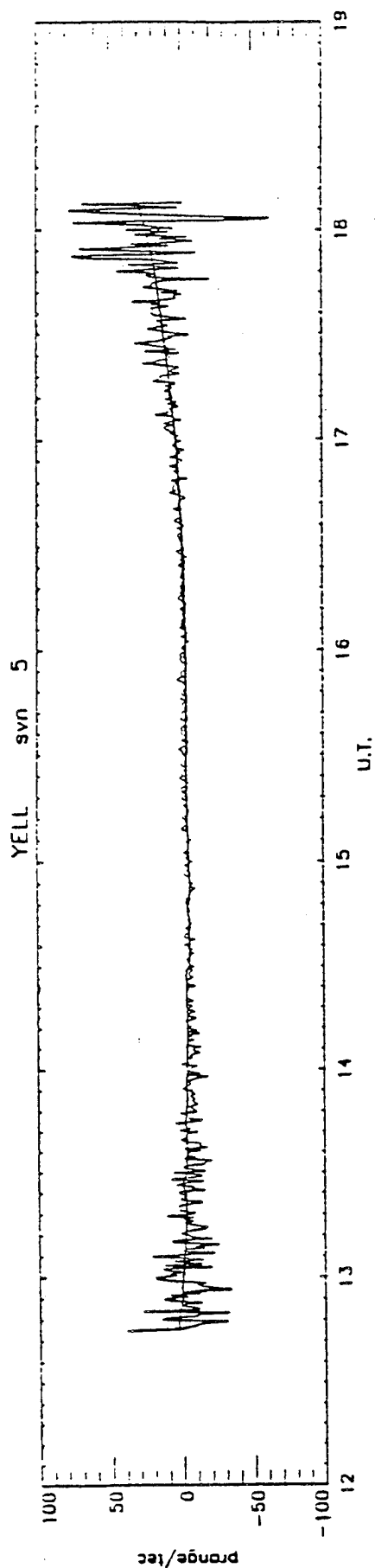9) develop additional software to study the results.

FIGURE 36

45

FIGURE 37

46

4. ELECTRON BACKSCATTER AND PROTON PRECIPITATION

4.1. Proton-H Atom Transport: A Comparison of Theoretical Techniques

Our collaboration with the group in Apatity has continued. They have sent us results from their Monte Carlo (MC) calculations as well as an expanded outline for a collaborative paper. They have also sent a copy of their new Continuous Slowing Down (CSDA) model. The agreement between their MC model and our Proton/H Atom Transport model (PHT) was basically good though there were some differences that needed to be understood. The surprising difference was that while our fluxes essentially agreed, our energy deposition rates showed some differences as well as our eV/ion pair for the case of a 2 keV Maxwellian incident flux. We derived the expressions for the energy deposition rate and surmised that our original definition differed from what the group in Apatity was using. We also suspected that the two groups were using different energy thresholds for the charge exchange process. Both of these suppositions proved to be true and when corrected the energy deposition rates from the two models were found to be in excellent agreement. The redefinition of the energy deposition rate also corrected what appeared to be inconsistent eV/ion pair value for a 2 keV run of the PHT model. When the two models use consistent energy thresholds their eV/ion pair values are about 10% apart. This difference can be traced back to about a 10 percent difference in the peak ionization rates. Again this difference lead us to suspect a difference in definition between the models. The most recent message from Apatity states that there was a difference in definition as well as bug in the Monte Carlo model. They report that their most recent runs now produce values for the eV/ion pair that are in good agreement with the PHT model. Given these successes, we have now written the first drafts of several sections of a paper on this comparison between three different proton transport models.

4.2. Electron-Proton_H Atom Aurora: Comparison With Observations

In the summer, we submitted a paper entitled "Upgoing Electrons Produced in an Electron-Proton-H Atom Aurora" to the Journal of Geophysical Research. After a couple of months, we received two referee's reports. One was satisfied and the other had several criticisms. The basic point was that more discussion was needed in the summary especially concerning the issue of uncertainties.

In response, we have made a series of calculations to assess some of these uncertainties and to improve the quality of our fits to the data. We have also expanded considerably the discussion and summary of the paper. The final piece of information that we need before sending the paper back into JGR is a relative error in the calibration of the LAPI instrument. Unfortunately during their attempts to come up with a firm estimate, our colleagues at SWRI discovered that there were problems in the software that processes the data from counts into units of flux. When we corrected the proton data for these errors, we found that the data was changed by a significant amount. However, before we began redoing all of our calculations, a possible error was discovered involving the data processing of the original telemetry as it came from the satellite. This is still being debated at SWRI and when they are confident that it is resolved we will reprocess the data we are using and repeat our calculations for the paper. We anticipate that, while some of the details may change, the summary given below will be essentially unchanged.

In this paper, we have presented the first comparisons between observations and the results of a fully coupled three component auroral transport model. This model solves for the electron, proton, and H atom differential fluxes as a function of altitude, energy, and pitch angle. Using observed incoming electron and ion fluxes as boundary conditions, we have calculated the resulting upgoing electron flux. In Figure 38, the calculated flux is compared to the observed upgoing flux and they are in excellent agreement. However our ability to produce such agreement was dependent on extrapolating the observed incoming proton flux from 30 to 150 keV using a kappa distribution
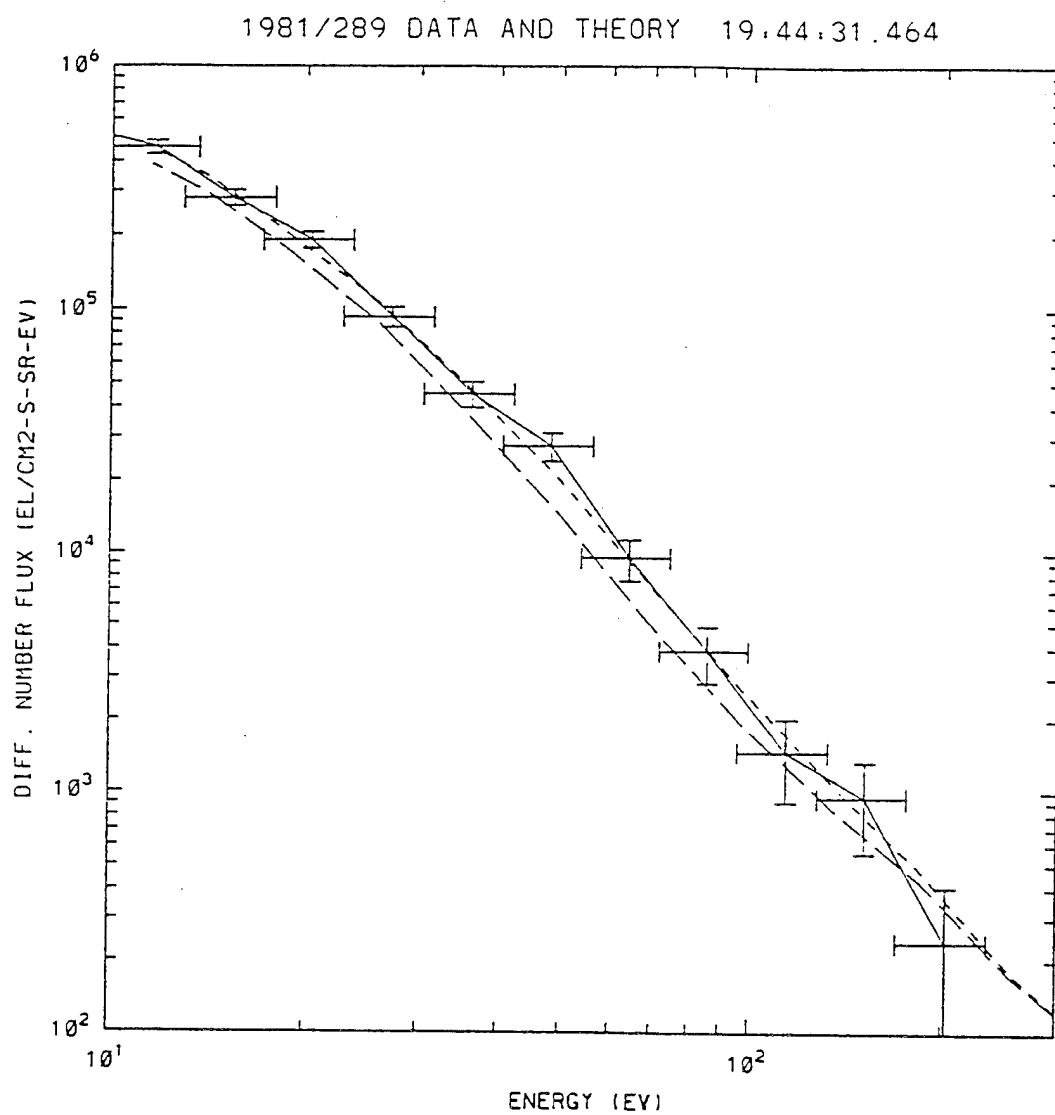
FIGURE 38

48

with $\kappa = 3.0$ and $E_0 = 8.0$ keV. This raises two questions: (1) Is the kappa extrapolation reasonable? and (2) what other uncertainties should we consider in assessing the reliability of the agreement?

In considering which extrapolation to use, we first considered where the observations were made. These are auroral observations made as the satellite is moving equatorward in the pre-midnight sector. Examining the electron data in Plate 1 we see prior to 19:43:52 energetic electron spectra that are indicative of precipitation from the boundary plasma sheet. The subsequent softening of the electron spectra and the fact that the satellite is moving equatorward in the pre-midnight sector suggests that the proton precipitation is coming from the inner regions of the central plasma sheet (CPS). While we have few examples of ionospheric observations of proton spectra at energies above 30 keV, there have been studies of ion populations in the CPS [*Christon et al.*, 1988, 1989, 1991] which have included such energies. Their findings have been that at high energies (E > characteristic or peak energy) there is a non-thermal power-law tail which can be fitted using a kappa distribution. With kappa distributions being normally observed in the plasma sheet, the critical question for us is whether they are still present when the ions reach ionospheric altitudes. As we noted above, we have found little ionospheric proton data at energies above 30 keV. In one paper however, data from various instruments were combined to show that proton distributions at ionospheric altitudes have high energy tails and are the same as those seen for earthward streaming protons in the outer boundary of the plasma sheet [*Lyons and Evans*, 1984]. Another example of the proton differential flux at ionospheric heights over the energies of interest comes from the Particle Environment Monitor (PEM) experiment on board the Upper Atmosphere Research Satellite (UARS) [*Sharber et al.*, 1993]. The spectra that are shown in their Figure 4 were observed in the auroral zone at an altitude of 585 km and the broadly peaked spectra are characteristic of precipitation from the CPS. The observations were made during a magnetic storm and an examination of this ionospheric ion spectrum shows a high energy power-law tail similar to that described by *Christon et al.* [1991] as typical of CPS ion populations. While neither of the two cases we have just described precisely fits our situation (that is ion precipitation from the CPS during periods of magnetically quiet conditions), they indicate that the use of a kappa distribution to extrapolate above 30 keV is perhaps reasonable.

Is the value of $\kappa = 3$ that we have used reasonable? Again turning to *Christon et al.* [1989], they report that during undisturbed periods κ ranges from 3 to 9.5. We have shown that using $\kappa = 3$ gives excellent agreement with the data. If we use $\kappa = 9.5$, the model underestimates the data but does a better job than that with the Maxwellian. While we have used a κ at one extreme of the observed range, we need to remember that the κ one determines depends critically on how the fitting is done. In the *Christon et al.* [1989] work, they were attempting to fit particle spectra over three decades in energy. On the other hand, we extrapolated from around 30 to 150 keV. When we tried fitting a kappa function to the ion spectrum given in *Sharber et al.* [1993] we found that if we wanted to fit from 74 to 500 keV, a $\kappa = 6.5$ does a reasonable job. However, if we fit from 40 to 150 keV, a κ range of 3.5 to 4.5 gives reasonable results. Thus given the data currently available, we conclude that a $\kappa = 3$ is certainly a possibility but questions concerning its probability will have to wait until more observations are available.

We now discuss the other uncertainties we have to deal with. At the top of the list is the question of cross sections. In particular, those cross sections for collisions between energetic protons/H atoms and the neutral species of the atmosphere. We focus on proton/H atom cross sections because typically the various electron cross sections are much better known. In general, the cross sections for proton/H atom collisions with N_2 and O_2 are measured and the quoted accuracy's are typically ± 20-30%. On the other hand, the collisions involving atomic oxygen are not measured and one has to resort to "estimates" based on other cross sections. The one exception is for charge changing collisions for which measurements have been made with quoted accuracy's of 25%, but at present there are still factors of 2 disagreement between some of these measurements. We have not performed a systematic sensitivity study involving all the cross sections. However, we have

49

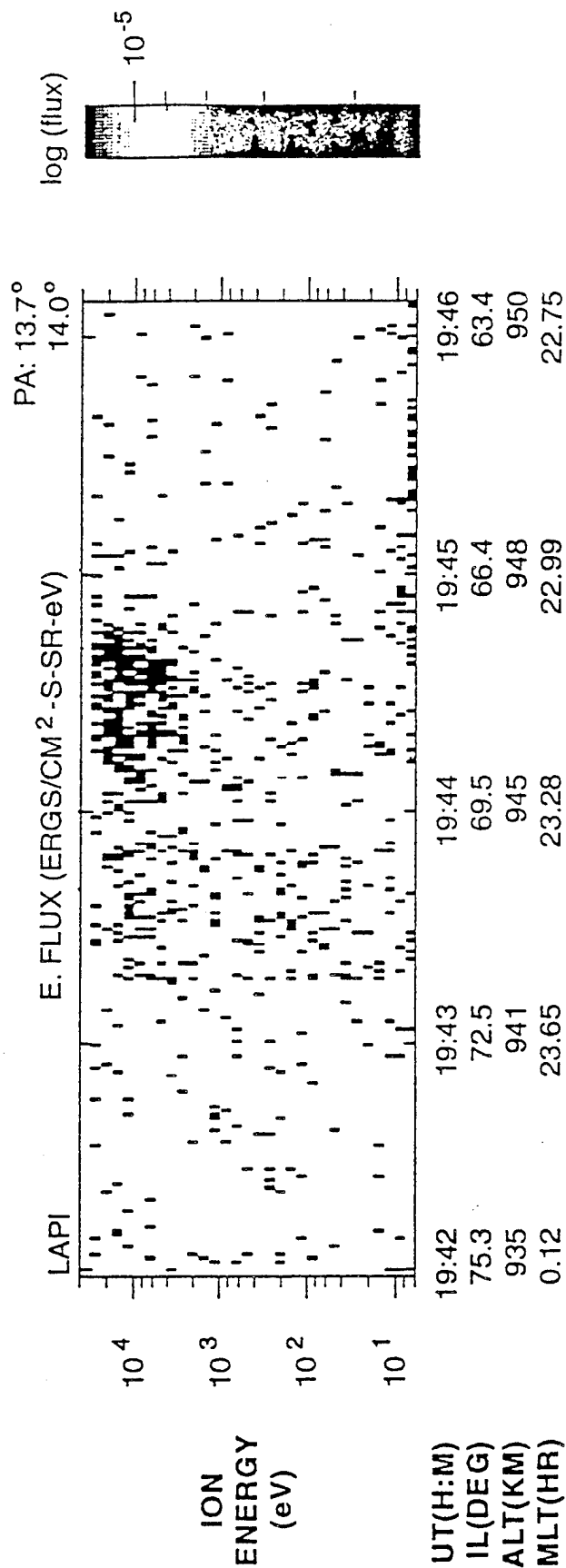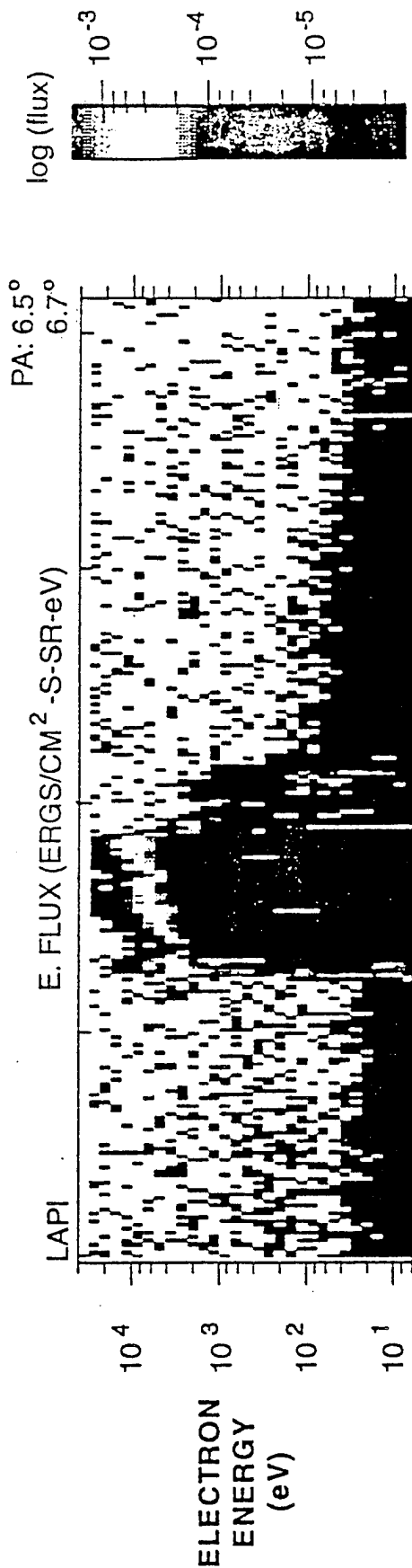DYNAMICS EXPLORER

YR/DAY: 81/289

PLATE 1

looked at the effect of changing the atomic oxygen ionization cross section. The reason for this is that we have found that for energies less than 100 eV over ninety percent of the upgoing electron flux at 950 km originates from above 200 km. Hence collisions with oxygen are playing a dominant role in producing the upgoing electron flux. The variation we considered was to use our O_2 ionization cross section for the O ionization cross section. In the past, various O cross sections have sometimes been estimated to be some fraction of the O_2 cross section and we feel that using the total O_2 cross section represents a maximum upper bound for the O cross section. In the case of ionization of O by proton or H atoms, this represents an increase of around a factor of 2 near the peak (~60 keV) of the cross section. The effect of this change in the κ =3 calculation was to increase the upgoing electron flux below 100 eV by up to 25%. Between 100 and 200 eV the effect drops to less than a percent as the upgoing electron flux becomes dominated by the electron precipitation. Since the protons are responsible for a little less than half of the upgoing flux this means the upgoing flux produced by protons and H atoms increased by up to 60%. Using the enhanced O cross section in the Maxwellian calculation produces a smaller effect of a 12% increase. It is smaller in this case because with the Maxwellian extrapolation the protons contribute only around 20% of the total upgoing electrons. What this then says is that by using a range of O cross sections between our present cross section and our upper bound cross section a range of kappas could be found to fit the data. On the other hand, even using the upper bound cross section is not sufficient to bring the Maxwellian case into agreement with the data.

Two other uncertainties have already been discussed in the previous section; proton beam spreading and mirroring. As discussed, beam spreading would tend to lower the calculated fluxes and would make agreement worse for those extrapolations that already lead to underestimates of the data. For the extrapolation presented here, we estimated its maximum effect might be to cause a 15% reduction in the upgoing flux. The effect of mirroring is much less clear cut. Monte Carlo calculations [*Kozelov*, 1993] have shown that mirroring of the protons tends to reduce the downward proton and H atom flux by something like 5 - 20% but creates an upward flux above 200 km that can be up to 10% of the downgoing flux. Without doing a calculation that includes mirroring it is difficult to determine whether mirroring creates a net increase or decrease to the upgoing electron flux. We would expect that whatever the effect it will be less than 10%.

In Figure 39, we showed that from 10 - 100 eV a little more than half of the upgoing flux is due to electron precipitation with the remainder being produced by the proton/H atom precipitation. This means that any uncertainty in the electron transport calculation is as important as that in the proton/H atom transport calculation. While there have been many more opportunities to test electron transport calculations, we have found few examples where the upgoing electrons due to electron precipitation have been modeled and compared to data. In calculations we have made involving photoelectrons and the polar rain [*Decker et al.*, 1990], we found the low energy upgoing electrons (< 80 eV) were about 25% below LAPI observations. A topic for future study will be to perform a study on upgoing electrons in a pure electron aurora. One issue we have been able to explore is that of the role of electron-electron collisions in determining the low energy upgoing electrons. The electron density profile used was selected precisely to give the fit seen in Figure 37 for the κ = 3 case. We found that turning off the electron-electron collisions had a significant effect at energies below 30 eV. For example at 11.5 eV the upgoing flux increased by over a factor of 2 when the coulomb collisions were turned off. Thus at energies below 30 eV the assumed electron density profile is as critical as the assumed extrapolation for the high energy protons in determining the upgoing electrons.

The final uncertainty we wish to discuss is in the LAPI measurements themselves. Prior to launch the relative error in the instrument calibration was estimated to be ±15-20%. It is the relative calibration rather than the absolute that is critical in this case because both the inputs to (downgoing electrons and protons) and the outputs from (upgoing electrons) the linear transport model are measured by LAPI. Hence any absolute uncertainty will not effect our agreement between model and data. The observations used in this paper were taken within the first few months of the DE-2
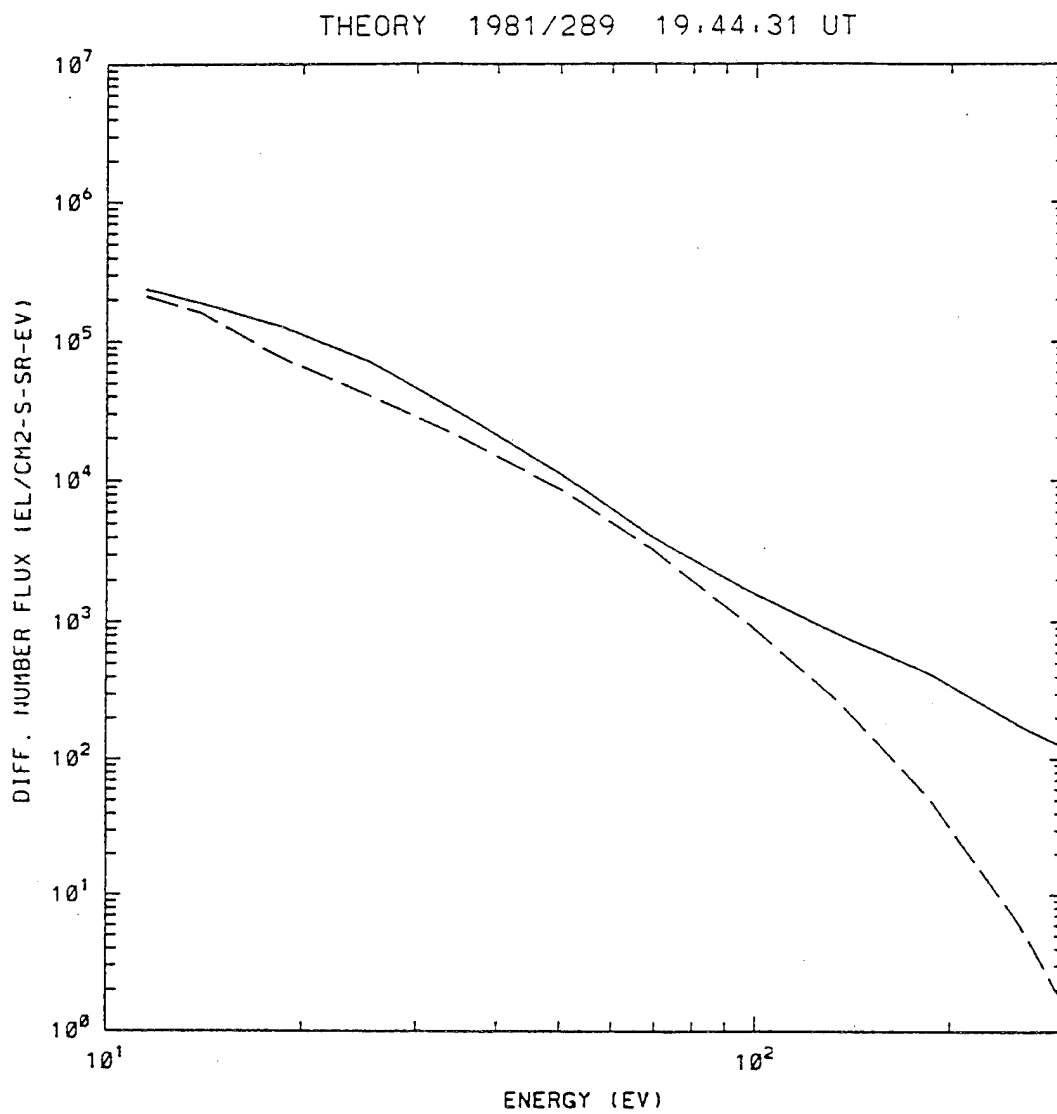
51

THEORY   1981/289   19:44:31 UT

FIGURE 39

52

flight and there was no evidence of any degradation nor was any anticipated at that point in the life of the instrument.

The effect of all the above uncertainties is that there is a range of κ that could easily produce reasonable fits to the data. On the other hand, while not impossible it would require an advantageous combination of adjustments to the model and the data in order to produce a good fit to the data using a Maxwellian extrapolation.

Clearly, more definitive tests of the model will require better known cross sections as well as more comprehensive observations. While PEM on UARS holds some promise for providing ion data over a larger energy range, for the foreseeable future validating proton/H atom transport models will continue to be a difficult task. However, two conclusions regarding the proton aurora can be derived from the present study. First, the observations presented do support the prediction of the model (as discussed in Sections 3 and 4) that the secondary spectra due to protons and H atoms is much softer than that produced by precipitating electrons. The other conclusion of this study is that the incoming proton differential flux at ionospheric altitudes most likely has a power-law behavior at high energies. If this is the typical situation, this implies that determinations of total energy flux from instruments with low-energy cutoffs by assuming a Maxwellian distribution [*Hardy et al.*, 1989] may seriously underestimate the flux. For example, in the case discussed in this paper when we fitted with the Maxwellian we estimated a total energy flux of ~0.22 ergs/cm^{2}sec whereas when fitted with a kappa distribution with $\kappa = 3$ the total energy flux was ~0.7 ergs/cm^{2}sec. A similar point for the plasma sheet is discussed in *Christon et al.* [1991]. Since various ionospheric effects of the proton aurora have been previously calculated [*Strickland et al.*, 1993] by assuming a Maxwellian distribution these calculations should be repeated using kappa distributions in order to fully assess the impact of these high energy power-law tails.

5. MODELING HIGH LATITUDE F REGION BLOBS AND PATCHES

We have continued examining the scenario for producing polar cap patches originally studied by *Anderson et al.*, [1988]. We found that the structure produced was very sensitive to details of the convection pattern. It is not yet clear if this mechanism will work in general or if it is basically an artifact of the Heelis 82 convection pattern that was originally used. We also made some initial attempts to study the formation of Storm Enhanced Densities (SED) that have been observed by the Millstone radar. The first few simulations produced no signs of a SED, but finally we ran a case that produced a SED like feature. What was surprising is that it seemed to have a very sensitive seasonal dependence. At present we do not understand this and will be working on this topic in the future.

We have also used our patch simulations to study the related phenomena of blob formation. High resolution simulations have verified that in both our By and *Anderson et al.* simulations, blobs are produced in the auroral zone as a natural consequence of time dependent convection. A summary of this work can be found in the extended abstract given later in this report.

We have also been working to upgrade the high latitude model. We had received the newest convection software from Rod Heelis, however it would only work for southward Bz. We also began work on a new way to handle the potential pattern in the model. The point of the change is to give us more flexibility in using convection patterns from different sources. In particular, to give us a more efficiency when we use Heppner/Maynard and to allow us to use results from the assimilative mapping of ionospheric electrodynamics (AMIE) procedure.

REFERENCES

Balan, N., G.J. Bailey, and B. Jayachandran, Ionospheric evidence for a non-linear relationship between EUV and 10.7-cm fluxes during an intense solar cycle, *Planet. Space Sci., 41*, 141, 1993.

Balan, N., G.J. Bailey, B. Jenkins, P.B. Rao, and R.J. Moffett, Variations of ionospheric ionization and related solar fluxes during an intense solar cycle, *J. Geophys. Res., 99*, 2243-2253, 1994.

Bailey, G.J. and R. Sellek, A mathematical model of the earth's plasmasphere and its application in a study of He^+ at L=3.0, *Annales Geophysicae*, 171-189, 1990.

Bilitza, D. and K. Rawer, New options for IRI electron density in the middle ionosphere, *Adv. Space Res., 10*, 7-16, 1990.

Davies, K., Recent progress in satellite radio beacon studies with particular emphasis on the ATS-6 radio beacon experiment, *Space Science Reviews, 25*, 357-430, 1980.

Decker, D.T. and P.H. Doherty, Global ionospheric weather, Phillips Laboratory Directorate of Geophysics, *Report PL-TR-94-2147*, Hanscom AFB, Massachusetts, 1994, ADA285520.

Doherty, P.H., E. Raffi, J.A. Klobuchar, and M.B. El-Arini, Statistics of time rate of change of ionospheric range delay, *Proceedings of the 1994 ION-GPS Meeting*, Salt Lake City, Utah, September, 1994.

Holzworth, R.H. and C.I. Meng, Mathematical representation of the auroral oval, *Geophys. Res. Lett., 2*, no. 9, 1975.

Klobuchar, J.A., private communication, 1994.

Llewellyn, S.K. and R.B. Bent, Documentation and description of the Bent ionospheric model, Air Force Geophysics Laboratory, *Report AFCRL-TR-73-0657*, Hanscom AFB, Massachusetts, 1973, AD772733.

Wanniger, L. Ionospheric monitoring using IGS data, presented at the 1993 Berne IGS Workshop, Berne, March 25-26, 1993.

Wilson, B.D., A.J. Mannucci, C.D. Edwards, and T. Roth, Global ionospheric maps using a global network of GPS receivers, *Proceedings of the International Beacon Satellite Symposium*, Cambridge, MA, 1992.

Wilson, B.D. and A.J. Mannucci, Instrumental biases in ionospheric measurements derived from GPS data, *Proceedings of the 1993 ION-GPS Meeting*, Salt Lake City, Utah, 1993.

PRESENTATIONS AND PROCEEDINGS

We were involved in 19 presentations at various scientific meetings of which 8 appeared in published proceedings.

- D.T. Decker, J.R. Jasperse, and B. Basu, "The Status of Electron-Proton-Hydrogen Atom Transport Theory", presented at the Proton Aurora Workshop, CEDAR Meeting, Boulder CO, June 1994.

- D.T. Decker, "GTIM/CTIM Comparisons", presented at the PRIMO Workshop, CEDAR Meeting, Boulder CO, June 1994.

- D.T. Decker, C.E. Valladares, D.N. Anderson, J.J. Sojka, and R.W. Schunk, "Modeling Polar Cap F-Region Patches: A Review of the Last 2 Years", presented at the Second Joint Workshop for CEDAR HLPS / STEP GAPS, Peaceful Valley CO, June 1994.

Extended Abstract

Introduction

Over the last 30 years, observations have shown that the high-latitude F-region contains a variety of large-scale structures. In particular, it has been found that during periods of negative or southward directed B_z enhanced "patches" of ionization drift across the polar cap in an anti-sunward direction. These polar cap patches come in a wide variety of shapes and scale sizes. The typical sizes range from a few 100 to ~1000 km, and the enhancements of plasma densities can be up to an order of magnitude above the surrounding background. Over the years, there have naturally been a variety of suggestions as to how patches might be produced. However, identification of the precise mechanisms of patch creation has remained elusive.

By the end of the 1980s, enough was known that a "descriptive working model" could be constructed [*Tsunoda*, 1988]. This model described a sequence of events where various large scale structures evolved from one to another. The sequence begins at subauroral latitudes in the afternoon sector where a broad wedge of enhanced ionization is observed. At higher latitudes, this wedge thins in longitude to what is typically referred to as a tongue of ionization. Then by some process, that wasn't clearly defined but presumably took place near or within the cusp or throat, the tongue is structured into patches which then drift across the polar cap. The patches in turn are then reconfigured into boundary and subauroral blobs as the enhanced plasma convects out of the polar cap into the auroral zone.

For the most part, this picture was built up from observations with some theoretical support from F-region modeling. But there were many gaps in the details, many uncertainties, and actually very few theoretical studies had explicitly focused on how F region structure might be produced. Thus at the time of the first CEDAR HLPS/STEP GAPS workshop in June 1992, a quantitative demonstration of the definitive mechanism or mechanisms for patch creation was still lacking. Since that workshop, there has been an increased effort to model F region patches. An effort that has lead to significant progress.

In the last two years, modelers have successfully simulated the creation of high-latitude large scale plasma structure using two separate mechanisms (time varying global convection and meso-scale events). Morphological predictions have been made that are currently being tested against data. A study at Sondrestrom has suggested that both mechanisms can be important and may very well operate together in a complex and intertwined manner. Simulations using time-dependent convection have also illustrated how patches can evolve into blobs in much the way predicted in the

work of *Robinson et al.* [1985]. The purpose of this paper is to review this progress in patch modeling. We will discuss the theoretical approaches, simulations involving time varying global convection, simulations involving meso-scale convection (plasma jet, vortices, flow channels, etc.), and future directions.

The Theoretical Approach

The question that we have focused on is if we take a "state of the art" theoretical F-region model can we understand the large scale ionospheric structure in terms of temporal and spatial structure in the geophysical inputs to the model? By F-region models, we are referring to models that solve sets of fluid equations over substantial portions of the globe. In particular, we will discuss two models: (1) the Phillips Laboratory Global Theoretical Ionospheric Model (PL GTIM) which solves continuity and momentum equations for one species, O^+ and (2) the Utah State University Time-Dependent Ionospheric Model (USU TDIM) which solves continuity, momentum and energy equations for multiple species.

Such models require a number of geophysical parameters as inputs and the two inputs that are of special interest for modeling large-scale structures are particle precipitation and the magnetospheric electric field (ionospheric convection). The reason for this is that all the suggested mechanisms for producing patches, that we are aware of, have involved the behavior of one or both of these inputs. For the purposes of modeling, we have found it useful to classify each of the various mechanisms into one of three types: 1) particle precipitation, 2) global **ExB** convection and 3) meso-scale **ExB** convection. In type 1, the focus has been on spatially restricted regions of precipitation associated with such names as the cleft/cusp/dayside aurora/mantle/lower-latitude boundary layer etc. The idea is that "dayside" precipitation produces regions of enhanced ionization which then convect into and across the polar cap. For the type 2 mechanism, it is the spatial structure and time dependence of the global convection pattern that is critical. The idea is to have changes in the pattern that cause changes in the trajectories of the convecting plasma associated with the "tongue of ionization" (TOI). Our third category involves what we're calling meso-scale convection. The focus here is on regions of transient high speed flows that lead to enhanced ion temperatures which in turn create depleted ionization regions via enhanced ion loss rates. By meso-scale, we are considering regions that have scales of hundreds of km. Over the last two years, our efforts have focused on the type 2 and 3 mechanisms. This is not to say that the type 1 mechanism has no role to play. Rather we chose to explore the main thrusts of *Tsunoda's* [1988] "working model" before turning to the other possibilities.

Simulations Using Time Varying Global Convection

In our first study involving the type 2 mechanism, both models simulated the creation of polar cap patches by using time varying convection inputs [*Sojka et al.*, 1993a]. The imposed convection variations were comparable to the type of observed changes in the convection that result from changes in the B_y IMF component during periods of southward B_z. Solar maximum-winter simulations showed that simple changes in the convection pattern lead to significant changes in the polar cap plasma structuring. Specifically, in winter, as enhanced dayside plasma convects into the polar cap to form the classic TOI, the convection changes redirect the TOI producing density structures that are indistinguishable from the observed patches. A follow-on study was performed using the USU TDIM [*Sojka et al.*, 1994] that focused on the seasonal and UT dependence that results from such a scenario. Initial comparisons with data [*Sojka et al.*, 1994; *Sojka et al.*, 1993b; *Basu et al.*, 1993] seem to support the concept of solar produced plasma from lower latitudes playing a critical role in supplying the enhanced plasma for patch formation.

In an attempt to apply mechanism 2 to a specific set of observations, the PL GTIM was used to model the highly structured plasma densities characterized by digisonde observations at Sondrestrom on February 19, 1990 [*Decker et al.*, 1994]. In our initial attempts, we used DMSP F8 ion drift data to infer nine different convection patterns that were then used to construct a crude time-dependent global convection pattern. What we found was that this data alone was inadequate to accurately describe the time evolution of the global convection pattern and thus the observed

density structure. This raised the question as to whether any combination of patterns could reproduce the large scale behavior of the digisonde data. After much experimentation, a judicious combination of Hairston/Heelis and Heppner/Maynard patterns was found that could reproduce the large scale behavior of the observations. As in the previous work, the critical issue again proved to be the manipulation of the trajectories that bring solar produced plasma from lower latitudes into the polar cap.

Most recently, our work on mechanism 2 has brought us back to revisit the work of *Anderson et al.* [1988]. In the original study, the ionosphere over Thule, Greenland was simulated assuming a time-varying convection pattern . The time variation consisted of changing between one pattern characterized by an 80-kV cross-tail potential and a 12° polar cap radius and another with a 100-kV cross-tail potential and a 15° polar cap radius. The result of making this change was a seven-fold enhancement in the F_2 peak density at Thule. This study was not a global simulation of the entire polar cap but rather only trajectories that passed over Thule were considered. We returned to this scenario for a couple of reasons: (1) in early testing of the current version of GTIM, we ran into difficulties in reproducing the original results and (2) we came to suspect that many people were incorrectly interpreting the original results. From global simulations of the scenario, we found that the difficulty in reproducing the original results came from an extreme sensitivity to the precise convection pattern being used. The misinterpretation was that many workers assumed that results came about from the smaller pattern being in darkness and the larger pattern reaching out across the terminator to get enhanced plasma densities. What we verified from the global simulations is that both patterns reach into the daytime, both patterns create TOIs, and the effect of going from one pattern to the other is to simply change the width of the TOI. Thus the large effects produced at Thule did not require large density gradients either on the terminator or near the convection boundary. Rather the effects are essentially of the same type as we have seen in our other studies of mechanism 2.

Simulations Using Meso Scale Convection

Our first attempt at using the type 3 mechanism again focused on modeling the digisonde observations at Sondrestrom for February 19, 1990 [*Decker et al.*, 1994]. The reason for continuing to work with this case was the availability of radar observations that included several transient high-speed plasma flow events that were collocated with regions of low F-region density [*Valladares et al.*, 1994]. Having previously found a time-dependent convection pattern that reproduced the larger scale behavior of the digisonde data, we hoped that including the observed flow events would produce some of the smaller scale structure seen in the digisonde data. What was seen in the radar data were five events that consisted of fast plasma flows in excess of 2 km s^{-1} (requiring electric fields of 100 mV m^{-1}). These flows were collocated with enhanced F-region ion temperatures exceeding, in some cases, 4000°K. The suggestion of *Valladares et al.* [1994] was that the depletions were the result of enhanced ion loss rates due to the large ion temperatures.

While we wanted to include these events in our modeling, they were observed to have quite a complex temporal behavior that is not well understood and that we were not in a position to treat in a detailed manner. So we chose to use just two features of each event: (1) the time of their occurrence and (2) the order of magnitude of their electric fields. The electric fields were approximated by adding to the global potential pattern small circular regions in which the potential varies like a triangular sawtooth across any diameter. These additions were done at the observed times of the five events in the vicinity of Sondrestrom for a period of around 16 minutes each. What was found was that each event created significant depletions whose times and magnitudes were in quite nice agreement with the digisonde observed depletions.

Our next effort focused on just one of the observed flow events [*Valladares et al.*, 1993]. The point here was to improve our representation of an event and to compare to radar observed plasma densities. In this case, the meso scale potential added to the model consisted of two ellipses. This gave us the ability to more closely match the observed velocities within the high speed jet than was possible with a simple circular region. This potential was again added to global

potential pattern near Sondrestrom for a period of 15 minutes. To properly compare the modeled and the measured data, we conducted elevation scans through the simulated volume mimicking the radar scans. We found that the simulated plasma density in and around the flow region is in good agreement with the experimental data.

The most recent improvement to the meso-scale modeling has been to allow the flow event to move. This idea is supported by magnetometer, radar and optical measurements. With this improvement, we find that the meso-scale events still create depletions and the resultant structures are even more suggestive of patch observations than in our earlier simulations.

Future Directions

Clearly, our representations of a time-varying global convection are extremely crude. Likewise our representations of the meso-scale events are at a rudimentary level. To improve on this, we need observations that better define how the global convection pattern behaves in time and what is the behavior and morphology of meso-scale events. Over the last two years, we have also effectively ignored the role of particle precipitation. Simulations are needed that will explore the various scenarios involving particle precipitation, especially within the cusp/cleft/dayside aurora etc. To begin to determine which structuring mechanisms actually occur regularly, we will need a more complete observationally-based understanding of the morphology of large scale structures. Finally, our whole approach has treated the electric field as a free parameter that we can play with, but clearly there are many self-consistency issues that need to be explored. Developing the necessary ionosphere/magnetosphere coupled models to study these issues is going to be long term theoretical and observational challenge.

Anderson, D.N., J. Buchau, and R.A. Heelis, Origin of density enhancements in the winter polar cap ionosphere, *Radio Sci.*, *23*, 513, 1988.

Basu, S., Su. Basu, J.J. Sojka, and R.W. Schunk, Patches and scintillations in the polar ionosphere: UT and seasonal dependence, *EOS Transactions*, *74*, no. 43, 94, 1993.

Decker, D.T., C.E. Valladares, R. Sheehan, Su. Basu, D.N. Anderson, and R.A. Heelis, Modeling daytime F layer patches over Sondrestrom, *Radio Sci.*, *29*, 249, 1994.

Robinson, R.M., R.T. Tsunoda, J.F. Vickrey, and L. Guerin, Sources of F region ionization enhancements in the nighttime auroral zone, *J. Geophys. Res.*, *90*, 7533, 1985.

Sojka, J.J., R.W. Schunk, and J.A. Whalen, The longitude dependence of the dayside F region trough: a detailed model-observation comparison, *J. Geophys. Res.*, *95*, 15,275, 1990.

Sojka, J.J., M.D. Bowline, R.W. Schunk, D.T. Decker, C.E. Valladares, R. Sheehan, D.N. Anderson and R.A. Heelis, Modeling polar cap F region patches using time varying convection, *Geophys. Res. Lett.*, *20*, 1783, 1993a.

Sojka, J.J., R.W. Schunk, M.D. Bowline, and E.J. Weber, Model-observation comparison that show the polar cap patch UT dependence in winter, *EOS Transactions*, *74*, no. 43, 94, 1993b.

Sojka, J.J., M.D. Bowline, and R.W. Schunk, Patches in the polar ionosphere: UT and seasonal dependence, *J. Geophys. Res.*, 1994, in press.

Tsunoda, R.T., High-latitude F region irregularities: a review and synthesis, *Rev. Geophys.*, *26*, 719, 1988.

Valladares, C.E., D.T. Decker, R. Sheehan, Su. Basu, and D.N. Anderson, Observations and workstation modeling of large scale plasma density structures in the cusp/cleft region, *EOS Transactions*, *74*, no. 43, 94, 1993.

Valladares, C.E., Su. Basu, J. Buchau, and E. Friis-Christensen, Experimental evidence for the formation and entry of patches into the polar cap, *Radio Sci.*, *29*, 167, 1994.

- D.N. Anderson, D.T. Decker, and C.E. Valladares, "Modeling Boundary Blobs Using Time Varying Convection", submitted to the Second Joint Workshop for CEDAR HLPS / STEP GAPS, Peaceful Valley CO, June 1994.

Extended Abstract

Introduction

Boundary blobs are F-region electron density enhancements which are observed to be very narrow in the magnetic north-south direction (~2°-3°) and elongated in the east-west direction (several hours in local time). As their name implies they are most often observed on the equatorial edge of the auroral oval (poleward edge of the trough) usually in the pre-midnight sector. Incoherent scatter radar observations at Chatanika using elevation scans have shown unambiguously both the latitude and altitude extent of the blobs [*Rino*, 1983; *Weber et al.*, 1985]. Successive elevations scans have observed blobs over a twelve hour local time period [*Rino*, 1983].

In an excellent review article, *Tsunoda* [1988] has summarized the observations and the mechanisms which are thought to generate boundary blobs. The theory that seems to fit the observations and the ad hoc modeling that has been carried out suggests that the blobs originate as solar-produced "patches" of enhanced F-region plasma which rapidly convect in an anti-sunward direction over the polar cap and then become elongated as they are caught up in the return-flow pattern equatorward of the auroral zone. *Robinson* [1985] modeled this process by assuming an initially circular plasma density enhancement in the polar cap and then tracing the convection of this region as it's shape distorted into a thin, elongated feature stretching from midnight to noon over a 3 hour elapsed time.

In this paper we investigate, quantitatively, the mechanisms which generate the boundary blobs by theoretically calculating F region (O^+) plasma densities as a function of altitude, latitude and local time and compare our results with some of the past observations to determine the degree of agreement. We are especially interested in comparing the latitude and longitude extent of the features as well as the density enhancements. Typically the observed enhanced F-region peak densities are in the neighborhood of 4 to 8 x 10^5 electrons/cm^3 and are two to three times the background density. If reasonable agreement is obtained then the correct physical mechanisms which are incorporated into the calculations and which generate the boundary blobs can be identified and authenticated.

Theoretical Model

The Theoretical Global Ionospheric Model (GTIM) which is used to calculate O^+ density profiles as a function of latitude, longitude, and local time has been described in detail by *Decker et al.* [1994]. It numerically solves the time-dependent, linear, plasma continuity and momentum equations including the effects of production of ionization by solar EUV radiation and energetic particle precipitation, loss through charge exchange with N_2 and O_2, and transport by diffusion, ExB convection drifts and neutral winds. For this simulation, input parameters reflect the conditions appropriate for December solstice, solar maximum conditions for moderate Kp values. This model was used to study the effects of changing B_y in creating polar cap patches, and the same conditions apply to this study [*Sojka et al.*, 1993]. In this paper patches were successfully generated by changing from a $B_y > 0$ condition to a $B_y < 0$ condition, maintaining this orientation for one and a half hours and changing back to $B_y > 0$. The patches that were generated were then caught up in the sunward, pre-midnight convection cell, became elongated, and are responsible for the boundary blob distributions we present in this study.

Results

For specific meridional slices, we have repeated the patch generating calculations using a higher latitude resolution of 0.2° or about 20 km. These slices at specific Universal times reveal altitude and latitude electron density distributions which vary closely resemble the boundary blobs

observed by the Chatanika radar. For example, at 2000 UT an enhancement in electron density occurs between 67 and 69 magnetic latitude with a maximum density of $7.6 \times 10^5 el/cm^3$ compared to a background density of less than $1.6 \times 10^5 el/cm^3$. The enhancement is also extended in altitude in agreement with past observations of boundary blobs. In the talk, we will present a pc-movie of the generation of the patches and how they evolve into boundary blobs. We will also illustrate the enhancements as contours of plasma density as a function of altitude and latitude, simulating an incoherent scatter radar making elevation scans at a number of different local times.

Decker, D.T., C.E. Valladares, R. Sheehan, Su. Basu, D.N. Anderson, and R.A. Heelis, Modeling daytime F layer patches over Sondrestrom, *Radio Sci.*, *29*, 249, 1994.

Rino, C.L., R.C. Livingston, R.T. Tsunoda, R.M. Robinson, J.F. Vickrey, C. Senior, M.D. Cousins, J. Oven, and J.A. Klobuchar, Recent studies of the structure and morphology of auroral zone F region irregularities, *Radio Sci.*, *18*, 1167, 1983.

Robinson, R.M., R.T. Tsunoda, J.F. Vickrey, and L. Guerin, Sources of F region ionization enhancements in the nighttime auroral zone, *J. Geophys. Res.*, *90,* 7533, 1985.

Sojka, J.J., M.D. Bowline, R.W. Schunk, D.T. Decker, C.E. Valladares, R. Sheehan, D.N. Anderson, and R.A. Heelis, Modeling polar cap F region patches using time varying convection, *Geophys. Res. Lett.*, *20*, 1783, 1993.

Tsunoda, R.T., High-latitude F region irregularities: a review and synthesis, *Rev. Geophys.*, *26*, 719, 1988.

Weber, E.J., R.T. Tsunoda, J. Buchau, R.E. Sheehan, D.J. Strickland, W. Whiting and J.G. Moor, Coordinated measurements of auroral zone plasma enhancements, *J. Geophys. Res.*, *90*, 6497, 1985.

- C.E. Valladares, D.T. Decker, R. Sheehan, D.N. Anderson and K. Fukui, Modeling the Formation of Polar Cap Patches Using Convection Elliptical Vortices, submitted to the Second Joint Workshop for CEDAR HLPS / STEP GAPS, Peaceful Valley CO, June 1994.

Extended Abstract

Based on data collected by the Sondrestrom incoherent scatter radar (ISR), the Greenland chain of magnetometers, and digisondes located at Sondrestrom and Qaanaaq, *Valladares et al.* [1994] formulated a mechanism for the formation of polar cap patches. These authors suggested that polar cap patches could be formed if the recombination loss is enhanced in a region that is located close to the tongue of ionization (TOI). Prior to the occurrence of the event discussed by *Valladares et al.* [1994], the ionospheric plasma was observed to be convecting in a poleward direction and formed part of the TOI directed into the polar cap. The event started with the appearance of a fast plasma jet containing eastward directed velocities in excess of 2 km s^{-1}. The plasma jet consisted of a channel extending 300 km in width, where the F-region ion temperature (T_i) reached values in excess of 4000°K. The elevated T_i values inside the plasma jet were observed to be exactly collocated with depleted F-region densities. This was convincing evidence that the recombination loss of O^+ had increased by a factor > 10 due to the dependence of the $O^+ + N_2$ reaction on T_i.

This paper presents the numerical simulation of the event of February 19, 1990. Our simulations show that large plasma jets can indeed form patch-like structures when a plasma jet develops near the throat region. This modeling work also makes predictions of the patch shape and size; these parameters can be compared with observations by imagers currently operating inside the polar cap. We used the time-dependent, one species, F-region high-latitude ionospheric model initially developed by *Anderson et al.* [1988] and later extended by *Decker et al.* [1994]. This model solves the continuity and momentum equations along a magnetic flux tube and accepts a large variety of inputs. In our simulation we have represented the plasma jet by a system of two elliptical vortices that extend 10° in longitude, but have different latitudinal widths. The vortices

width and their peak-to-peak potentials were chosen in order to provide the best fit to the radar line-of-sight velocities. Two different scenarios have been modeled and the results are presented in this paper.

In out first simulation a pair of opposite rotating vortices were maintained stationary for 15 minutes. During this time the voltages applied to each vortex were 20 and -5 kV respectively. After 15 minutes the potential was turned off and the effect was observed to relax. By placing the vortices in the vicinity of the TOI, we produced a distortion of the TOI and regions of plasma depletions. Deep depletions are seen not only between the vortices but also at the poleward edge of the vortices. In this region the flow associated with the vortices has the same direction of the background velocity and the total flow is reinforced. After 15 minutes a narrow and elongated region of high plasma is aligned almost parallel to the dawn-dusk direction and bounded to the north and to the south by plasma of lower density. However, both dawn and dusk ends of the plasma structure are not disconnected from the auroral ionosphere. This scheme fails to produce isolated structures; furthermore the patch orientation becomes aligned with the background plasma flow after the vortex potential is turned off.

In our second simulation, the vortices were allowed to convect with the background plasma. The principal feature in the simulation is the complete separation of the mesoscale structure from the auroral region. The patches remain approximately oriented in the dawn-dusk direction during the simulation. Simulated radar scans of the modeled ionosphere show two patch-like structures drifting poleward. They are separated by regions of low density ($3 \times 10^5 cm^{-3}$). Each of the two poleward moving structures constitute the central part of the vortices which, as we stated before, are moving poleward.

Anderson, D.N., J. Buchau, and R.A. Heelis, Origin of density enhancements in the winter polar cap ionosphere, *Radio Sci.*, *23*, 513, 1988.

Decker, D.T., C.E. Valladares, R. Sheehan, Su. Basu, D.N. Anderson, and R.A. Heelis, Modeling daytime F layer patches over Sondrestrom, *Radio Sci.*, *29*, 249, 1994.

Fukui, K., J. Buchau, and C.E. Valladares, Convection of polar cap patches observed at Qaanaaq, Greenland during the winter of 1989-1990, *Radio Sci.*, *29*, 231,1994.

Valladares, C.E., Su. Basu, J. Buchau, E. Friis-Christensen, Experimental evidence for the formation and entry of patches into the polar cap, *Radio Sci.*, *29*, 167, 1994.

The following 7 presentations also were published in the Proceedings of the International Beacon Satellite Symposium, July 1994.

- P.H. Doherty, E. Raffi, J. Klobuchar, and M.B. EL-Arini, "Statistics of Time Rate of Change of Ionospheric Electron Content", presented at the 1994 Beacon Satellite Symposium, Aberystwyth, Wales, July 1994.

Abstract

The time rate of change of Total Electron Content (TEC) is a potential limitation in precise positioning using radio waves from the Global Positioning System (GPS) in the single frequency C/A mode. Dual frequency GPS users with access to the P code automatically correct for the effects of both the TEC and its rate of change. Single frequency GPS users can use a simple algorithm for TEC to place an absolute scale on their measurements of C/A code minus carrier, to correct for the time rate of change of TEC, but the inherent noisiness of the L1 code data can severely limit the single frequency ionospheric correction capability, especially in removing the effects of the rate of change of TEC.

Dual frequency GPS data from stations representative of different ionospheric conditions were obtained from the International GPS Geodynamics Service (IGS) network. Values of dual frequency differential carrier phase were computed at one-minute intervals and then were high-pass

filtered. Relative TEC changes over time intervals of 1, 2, 5, and 10 minutes duration were then computed and the statistics of these rates of change were computed for different times of day, viewing direction and various conditions of magnetic activity. The largest ionospheric range-rates were observed in the auroral region during period of magnetic activity.

- P.H. Doherty and J.A. Klobuchar, "Solar Cycle Dependencies in Mid-Latitude Total Electron Content", presented at the 1994 Beacon Satellite Symposium, Aberystwyth, Wales, July 1994.

Abstract

Measurements of ionospheric Total Electron Content have been obtained at the mid-latitude station at Hamilton, MA from November 1967 through May 1992. These measurements were made by monitoring the Faraday rotation of VHF signals from geostationary satellites of opportunity. This comprehensive data base has been utilized to study both short and long term dependencies in TEC with respect to solar activity. Data recorded during solar cycle 21 (1976-1986) is the prime focus of this study. The mean daily 10.7 solar radio flux (F10.7) is used as the measure of solar activity.

Poor correlations between day to day changes in mean daytime TEC and daily F10.7 indicate that short term changes in TEC are not dependent on daily changes in solar flux. However, examination of these same two parameters over an entire solar cycle reveals an apparent linear dependence of mean daytime TEC to increases in daily solar flux. This linear dependence is not as apparent under intense solar maximum conditions. However, the appearance of saturation effects at these levels is obscure.

Statistics of the variability of TEC for different seasons, times of day and levels of solar activity are also provided in this study. In general, for any given season, time of day and solar activity level, TEC measurements exhibit a nearly normal distribution about a mean value. The largest deviations from normal behavior occur during periods of intense geomagnetic activity. Information about long and short term solar cycle dependencies in TEC and statistics of normal behavior are important to all branches of radio communication.

- J.A. Klobuchar, P.H. Doherty, and M.B. El-Arini, "Mid-Latitude Differential TEC versus Station Spacing", presented at the 1994 Beacon Satellite Symposium, Aberystwyth, Wales, July 1994.

Abstract

The time delay effect of the earth's ionosphere can impose a significant limitation on precise positioning of civilian aircraft using signals from the Global Positioning System (GPS) satellites. The GPS standard positioning service accuracy is limited to approximately 50 meters, 1 sigma. Wide-area differential operation can greatly reduce that limitation, by monitoring GPS signals from a precisely known reference location, and transmitting correction information, via an auxiliary radio link, to each moving platform within that wide area. The largest potential limitation to differential GPS accuracy is the range delay of the ionosphere. Thus it is important to know the statistics of the behavior of TEC as a function of distance, particularly in the mid-latitudes where wide-area differential GPS is presently under consideration for use.

The results of one year of TEC measurements taken at several stations in the continental United States (CONUS), during the declining phase of the present solar cycle, showed that between 5% and 95% probability, with station spacings less than 1000 km, the differential ionospheric range delay was less than ± 2 meters during the daytime hours, which corresponds to a TEC of $\pm 1.2 \times 10^{17}$ el/m^2 column. The effects of magnetic storms on the statistics of differential TEC behavior during the observation period were not large. This work illustrates how measurements of TEC have been made useful to a practical engineering problem in the precise navigation community.

- J.A. Klobuchar, P.H. Doherty, G. Bailey, and K. Davies, "Limitations in Determining Absolute Total Electron Content from Dual-Frequency GPS Group Delay Measurements", presented at the 1994 Beacon Satellite Symposium, Aberystwyth, Wales, July 1994.

Abstract

The differential group delay of the 10.23 MHz modulation between the 1.227 GHz and the 1.575 GHz carrier frequencies transmitted from the Global Positioning System (GPS) satellites must be known accurately in order to make *absolute* measurements of Total Electron Content (TEC) from dual frequency GPS carriers. Numerous workers have noted that the modulation phase difference, *Tgd*, transmitted in the satellite message differs significantly from independent measurements of this parameter. A *Tgd* of one nanosecond (ns) equals 2.85×10^{16} el/m^2, which can exceed 1/4 of the daytime TEC in the mid-latitudes during solar minimum, and can exceed the complete TEC during nighttime hours. Thus, even a 1-ns uncertainty in the *Tgd* value can be potentially an unacceptably large error in absolute TEC. Present uncertainties in this parameter are likely between 2-3 ns.

Early work in estimating *Tgd* required that the quiet mid-latitude nighttime ionosphere could be represented as a shell having no horizontal gradients. Later work assumed no gradients in the daytime TEC at "high elevation angles", or that ionospheric gradients could be ignored, or would average out. All these efforts failed to take into account the fact that the ionosphere cannot be represented by a simple "shell" with simple gradients, since a significant contribution to TEC occurs due to the electron content of the earth's protonosphere. The protonospheric electron content differs in a major way with viewing angle from each station. Other potential sources of uncertainty in the *Tgd* can occur due to "local" multipath on the complicated antenna structure at each GPS satellite. These sources of error and other methods of estimating *Tgd* will be described.

- R.W. Snow, P. Romanowski, P.H. Doherty, and J.A. Klobuchar, "A Comparison of Ionospheric Total Electron Content Measurements with Code and Codeless GPS Receivers", presented at the 1994 Beacon Satellite Symposium, Aberystwyth, Wales, July 1994.

- W.A. Pakula, D.N. Anderson, M. Beaudet, J. Bendito, P.H. Doherty, J. Eicher, P.F. Fougere, L.F. Hughes, R. Inzirillo, N. Jakowski, M. Kapel, J.A. Klobuchar, H. Kuenzler, H.G. Kugland, C. Lottig, R. Leitinger, R. Maderbacher, J.R. Manzano, T.D. Raymund, V.H. Rios, R. Sheehan, B. Trepanier, C. Valladares, and J. Whitfield, "Initial Total Electron Content Results from the Pan American Ionospheric Tomography Campaign", presented at the 1994 Beacon Satellite Symposium, Aberystwyth, Wales, July 1994.

- M.B. El-Arini, R.S. Conker, T.W. Albertson, J.K. Reagan, J.A. Klobuchar, and P.H. Doherty, "Comparison of Real-Time Ionospheric Algorithms for a GPS Wide-Area Augmentation System (WAAS)", presented at the 1994 Beacon Satellite Symposium, Aberystwyth, Wales, July 1994.

- B.V. Kozelov, V.E. Ivanov, D.T. Decker, B. Basu, and J.R. Jasperse, "Proton-Hydrogen Atom Transport in the Atmosphere: A Comparison of Calculational Techniques", submitted to the 21st Annual European Meeting on Atmospheric Studies by Optical Methods, London, England.

Abstract

This paper compares three methods for calculating the transport of energetic protons and hydrogen atoms in the earth's atmosphere. The methods are: (1) a Monte Carlo (MC) simulation, (2) a discrete energy loss solution to the linear transport (LT) equations, and (3) a continuous slowing down approximation (CSDA). In the calculations performed, all three methods used similar cross sections, the same three component (N_2, O_2, O) neutral atmosphere, and incident isotropic Maxwellian proton fluxes of various characteristic energies (1-20 keV). A variety of results will be presented including energy deposition and ionization rates, eV/ion pair, hemispherically averaged differential fluxes of protons and H atoms, energy integrated differential fluxes, and proton and H atom flux fractions. It was found that the results obtained from the different techniques are in reasonably good agreement. However, the MC simulation can include processes such as beam spreading and magnetic mirroring that are neglected in the other two models. The differences that these processes can cause and the possibility of using specific MC results to improve the results from the LT or CSDA models will be discussed.

- P.H. Doherty, E. Raffi, J. Klobuchar, and M.B. El-Arini, "Statistics of Time Rate of Change of Ionospheric Range Delay", presented at the ION GPS-94 Conference, Salt Lake City UT in September 1994. It also appeared in the *Proceedings of ION GPS-94, Part 2*, 1589, September 1994.

Abstract

The time rate of change of ionospheric range delay is a potential limitation in precise positioning using radio waves from Global Positioning System (GPS) satellites in the single frequency c/a mode. Dual frequency GPS users with access to the p-code automatically correct for the effects of both the ionospheric range delay and its rate of change. Single frequency GPS users can use a simple algorithm for ionospheric range delay to place an absolute scale on their measurements of c/a code minus carrier, to correct for the time rate of change of ionospheric range delay, but the inherent noisiness of the L1 code data can severely limit the signal frequency ionospheric correction capability, especially in removing the effects of the rate of change of ionospheric range delay.

To investigate the statistics of ionospheric range-rate changes, dual frequency GPS data from stations in parts of the world representative of different ionospheric conditions was obtained from the International GPS Geodynamics Service (IGS) network, managed by the Jet Propulsion Laboratory (JPL). Values of dual frequency, differential carrier phase were computed at one minute intervals and then were high pass filtered to remove long term changes. Relative ionospheric range delay changes over time intervals of 1, 2, 5, and 10 minutes duration were then computed and the statistics of these rates of change of ionospheric time delay were compiled for different times of day, viewing direction, and various conditions of magnetic activity. The largest rates of change of ionospheric range delay were observed in the auroral region during periods of high magnetic activity.

- D.T. Decker, D.N. Anderson, and C.E. Valladares, "Modeling Boundary Blobs Using Time Varying Convection", presented at the 1994 Fall AGU meeting, San Francisco CA, December 1994.

Abstract

The Global Theoretical Ionospheric Model (GTIM) has been used to study the mechanisms which generate F-region electron density enhancements known as boundary blobs. The model calculates the O^+ density as a function of altitude, latitude, and local time. It includes the effects of production of ionization by solar extreme ultraviolet radiation and electron precipitation; loss through charge exchange with N_2 and O_2; and transport by diffusion, neutral winds, and **ExB** convection drifts. Using time-dependent convection patterns that previously were used to study polar cap patch formation, it was found that patches can be convected out of the polar cap and swept sunward by the dusk convection cell. The resulting structures had many of the features associated with boundary blobs: extended in local time and altitude, narrow in latitude, located in the return flow region of the aurora, and densities up to a factor of 5 over background. These results are a verification and extension of the trajectory modeling of *Robinson et al.* [1985].

Robinson, R.M., R.T. Tsunoda, J.F. Vickrey, and L. Guerin, Sources of F region ionization enhancements in the nighttime auroral zone, *J. Geophys. Res., 90,* 7533, 1985.

- D.N. Anderson, A.J. Preble, and D.T. Decker, "Improving IRI90 Low Latitude Ionospheric Specification", presented at the 1994 AGU Fall Meeting, San Francisco CA, December 1994; the U.S. National Radio Science Meeting, January 1995; and the IRI Workshop on Equatorial Phenomenon, held in India, January 1995.

Abstract

At low latitudes a number of comparisons between the IRI90 model of F-region electron density profiles with observed profiles measured by the Jicamarca incoherent scatter radar indicate that during the daytime, the observed profile shape is much broader in altitude than that specified by IRI90 while at night, just after sunset, observed H_{max} values are significantly higher. This is especially true during periods of high solar activity. The theoretically-derived ionospheric parameters such as H_{max}, N_{max}, and profile shape which are contained in the Parameterized Ionospheric Model (PIM) have been shown to be in better agreement with Jicamarca observations. This paper describes an attempt to improve IRI90 at low latitudes by calculating three ionospheric parameters: the profile half thickness, N_{max}, and H_{max} from PIM as a function of latitude, longitude, and solar local time for a variety of solar cycle, seasonal and geomagnetic conditions. The generation of electron density profiles using these three parameters will be presented as well as a description of how these expressions might be implemented into the IRI90 model. Finally, we discuss the degree of improvement which has been achieved by comparing these profile parameters with a number of ionospheric observations not only at the magnetic equator but also at higher magnetic latitudes near the crests of the equatorial anomaly.

- D.N. Anderson, J.A. Klobuchar, P. Doherty, P.F. Fougere, T. Raymund, W.A. Pakula, R. Leitinger, and N. Jakowski, "Tomographic Studies at Equatorial Latitudes", submitted to the IRI Workshop on Equatorial Phenomenon, held in India, January 1995.

Abstract

The day-to-day variability of the equatorial anomaly region of the earth's ionosphere is responsible for large day-to-day differences in the ionospheric electron density distribution over a

range of latitudes that extend from at least ±30° in magnetic latitude. It is well known that the strength of the equatorial electrojet on different days closely controls the subsequent development of the ionization peaks, commonly called the equatorial anomaly. However, ground-based measurements of the full latitudinal extent of the anomaly on both sides of the equator, over full diurnal periods, have not been made, with the exception of extensive ground-based ionosonde data available during the IGY period in 1958-1959. Topside sounders, satellite in-situ and dual frequency satellite radar measurements have been made of the anomaly, but only over limited local time periods on any given day. Neither the full diurnal development nor the decay of the ionosphere over the complete anomaly latitudes has been measured in any single longitude sector.

The Pan American Ionospheric Tomographic Campaign 1994 was carried out from late March through mid-April 1994 to make the first measurements of Total Electron Content over a latitude range encompassing both equatorial anomaly regions. In order to study the progressive diurnal development of the anomaly in a single longitude sector, a chain of stations was set up to monitor dual frequency, coherent signals from the U.S. Navy Navigation Satellite System (NNSS) satellites, which yielded relative TEC values over a latitude range from approximately ±50°. The stations were spaced approximately 10 to 15 degrees apart in latitude, so that the overlap between stations would provide a sufficient number of intersecting rays to allow tomographic reconstructions of two-dimensional electron density versus latitude. The initial results of the campaign clearly show differences in the day-to-day behavior of the anomaly ionization peaks in both hemispheres.

- D.N. Anderson, D.T. Decker, and C.E. Valladares, "Modeling F-region Polar Cap Patches and Boundary Blobs", submitted to the 1995 Cambridge Symposium/Workshop on Multiscale Phenomena in Space Plasmas, held in Bermuda, February 1995.

Abstract

The Global Theoretical Ionospheric Model (GTIM) has been used to study the mechanisms which generate F-region plasma density enhancements in the polar cap called patches and their subsequent evolution into smaller-scale features which reside on the equatorial boundary of the auroral region called boundary blobs. The model calculates the O^+ density as a function of altitude, latitude and local time and includes the effects of production of ionization by solar extreme ultraviolet radiation and electron precipitation; loss through charge exchange with N_2 and O_2; and transport by diffusion, neutral wind and **ExB** convection drifts. Using time-dependent convection patterns in which the B_y component of the Interplanetary Magnetic Field (IMF) is initially positive, is then reversed to a negative value for one and a half hours and then switched back to a positive value, it is found that polar cap patches are produced, convected out of the polar cap region and swept sunward by the dusk convection cell. The resulting structures have many of the features associated with boundary blobs: extended in local time, and altitude, narrow in latitude, located in the return flow region with plasma densities up to a factor of 8 over background. Comparisons with high latitude/polar cap observations will be presented.

JOURNAL ARTICLES

- M.B. El-Arini, R.S. Conker, T.W. Albertson, J.K. Reagan, J.A. Klobuchar, and P.H. Doherty, "Comparison of Real-Time Ionospheric Algorithms for a GPS Wide-Area Augmentation System (WAAS)", *Navigation: Journal of The Institute of Navigation, 41, 393*, Winter 1994-1995.

Abstract

The Federal Aviation Administration (FAA) Satellite Program Office is developing a GPS Wide-Area Augmentation System (WAAS) to support a precision approach capability down to or near the lowest Category I (CAT I) decision height (DH) of 200 ft. In one of the candidate architectures under development, a vector of corrections is sent to the user via geostationary communications satellites (e.g., Inmarsat). This correction vector includes components for ionospheric, clock, and ephemeris corrections. The purpose of this paper is to evaluate the performance of the grid-based algorithms and other real-time ionospheric algorithms that could be implemented at the ground ionospheric reference stations, as well as at the airborne receiver. Results show that all of the ionospheric algorithms used in this paper (grid-based, least-squares, and spherical harmonics) provide roughly equivalent performance. Based on an extensive data collection program, the error in estimating ionospheric delay is derived. An analysis of WAAS accuracy performance is also presented.

- J.A. Klobuchar, P.H. Doherty, and M.B. El-Arini, "Potential Ionospheric Limitations to GPS Wide Area Augmentation System (WAAS)", accepted for publication in *Navigation: Journal of The Institute of Navigation.*

Abstract

Navigation and positioning using the GPS Wide-Area Augmentation system (WAAS) with single frequency receivers potentially suffers from the unknown spatial variability of ionospheric range delays (e.g., spatial gradients in ionospheric delays) between locations where dual-frequency measurements from GPS satellites are being made. In a given large region, by deploying a sufficient number of dual frequency GPS code and/or codeless reference receivers, it is possible to correct for most of the ionospheric range delay using Wide-Area Augmentation system (WAAS) real-time algorithms.

Using ionospheric data collected from a number of stations in North America the statistics of differences in range delay over station separations from approximately 350 km to over 1600 km are presented. The results illustrate large ionospheric gradients during periods of high magnetic activity. Fortunately, these events are infrequent. For the mid-latitudes the goal is to keep ionospheric range delays to only a few meters for at least 99% of the time so that WAAS can be used in precision approaches. To illustrate the possibility of achieving this goal, statistics of estimation errors in ionospheric range delay using this data set are also presented.